Design of Multi-aperture Optical Systems based in the Apposition and Superposition Compound Eyes.

by

M.Sc. Anel Garza Rivera

Dissertation

Presented as a requisite to obtain the Degree of Doctor of Philosophy (PhD) in Science in Optics

in

Instituto Nacional de Astrofísica, Óptica y Electrónica

December 2013

Tonantzintla, Puebla

Supervised by:

PhD. Francisco Javier Renero Carrillo.

“I am aware that lens design is a part of a bigger picture”

“The dreams of many

are the reality of others”

“Be afraid not of what you dream,

but of what will happen if your dreams come true”

“I have no special talents.

I am only passionately curious.”

Albert Einstein.

Abstract

The design of multi aperture micro optical systems inspired in compound eyes is the main goal of this work. The designs of simple microlens arrays, micro doublets and micro triplets are presented. The use of these micro optical elements together with the understanding of the working principle of natural Apposition and Superposition Compound Eyes has enabled the existence of their artificial counterparts. The design of an artificial Apposition Compound Eye objective AACE, an artificial Superposition Compound Eye objective ASCE, and a Multi Aperture Compound Eye objective ASCETL with micro tunable liquid lenses are explained. These artificial micro optical models are used to develop applications in imaging optics. Additionally, the designs of a free-space multiplexer, demultiplexer, a switch and a wave division multiplexer that could be used in the field of optical communications are also described. Biological background, equations, simulations, optical performance and some applications are shown.

Resumen

El diseño de micro sistemas ópticos de multi apertura, inspirados en los ojos compuestos de insectos y artrópodos, es el objetivo principal de este trabajo. Se presentan los diseños de arreglos de microlentes sencillas, micro dobletes y micro tripletes. El uso de micro elementos ópticos, asi como el principio de funcionamiento de los ojos compuestos naturales de Aposición y Superposición, han permitido la existencia de sus contrapartes artificiales. Se explican los diseños de un ojo compuesto de Aposición Artificial AACE, de un ojo compuesto de Superposición Artificial ASCE, y de un Ojo Compuesto de Multi Apertura con microlentes sintonizables ASCETL. Estos micro modelos ópticos son usados para desarrollar aplicaciones en sistemas formadores de imágenes. Adicionalmente, los diseños de un multiplexor y demultiplexor no guiados, asi como de un circulador y un divisor de longitud de onda WDM con aplicaciones en comunicaciones ópticas, son descritos. Los antecedentes biológicos, las ecuaciones, simulaciones, desempeño óptico y algunas aplicaciones se muestran también en este trabajo.

Al profesor Ernesto Fernández por motivar en mi, el amor al conocimiento.

A D’Artagnan por ser mi gran inspiración,

y a mis tres mosqueteros:

Ian, Iker y Lars por ser mi razón de hacer las cosas.

Agradecimientos

Gracias a Dios por la oportunidad de existir y por concebirme dentro de su plan maestro.

Gracias a mi padre Federico Guillermo Garza Granja por haberme dado en el breve tiempo que compartimos, la guía hacia el sendero del estudio y el gran interés por hacer preguntas y encontrar respuestas. Siempre fue un reto charlar contigo Papi.

Gracias a mi madre Ana María Rivera Ramírez por plantearme retos tan difíciles, lo cual me ha permitido tener que valerme por mis propios medios para resolverlos.

Gracias a mis hermana Flor por todos los momentos lindos que hemos estado juntas y por su gran apoyo y cariño. Tienes una gran fortaleza y muchas ganas de vivir.

Gracias a mi hermano Luis Felipe por tener confianza en mi y por ayudarme a no darme por vencida.

Gracias a Sylvia por las increíbles conversaciones que hemos tenidos y por ser parte de mi familia.

Gracias a mis niños por ser mi alegría de vivir. Los adoro.

Gracias a mi asesor el Dr. Paco Renero por creer en mi, por sus grandes ideas y conocimientos y por ayudarme a poner los pies en la tierra cuando me urgía echarme a volar y todavia no estaba lista. Gracias!!!!!!

Gracias al Dr. Carlos Treviño por abrir su puerta a mis preguntas y por interesarse en responderlas y aun mas, gracias por compartir sus ideas y ayudarme a hacerlas posibles.

Gracias al Dr. Sergio Vázquez por ser una gran ayuda y por ayudarme a resolver mis dudas en Diseño optico. Le tengo un gran respeto.

Gracias al Dr. Alejandro Cornejo por ser una inspiración para mi,y por ser ademas de un reconocido científico, una persona con un gran espíritu de lucha y un enorme sentido de la justicia.

Gracias al Dr. Luis Raúl Berriel por sus invaluables consejos y por hacer que me enamorara de la Optica de Fourier.

Gracias al Dr. Javier Sánchez Mondragon por su increíble entusiasmo y su gran astucia. Ha sido un placer conversar con usted.

Gracias al Dr. Jaramillo y a la Dra. Arllene Pérez por sus aportaciones a este trabajo y por tomarse el tiempo de revisar esta tesis.

Gracias al Dr. Roberto Zurita por sus comentarios, respuestas y aclaraciones. Es simplemente una persona genial.

Gracias a los profesores del departamento de Optica, al Dr. Baldemar Ibarra, al Dr. David Sanchez, al Dr. Arrizon, al Dr. Ponciano Rodriguez, al Dr. Ruben Ramos, al Dr. Sabino Chavez, al Dr. Kuzin y a todos aquellos que me han compartido su sabiduria y experiencia.

Gracias a Jesus Gomez por todas las cosas buenas y malas que hemos compartido y por ser una persona muy importante para mi. Te quiero mucho. Muchas gracias a tus papas y a tu familia.

Gracias a Juan Pablo Treviño por ser un excelente amigo y por sus grandes consejos.

Gracias a mis compañeros y amigos de óptica: Julio, Karla, Juan Carlos, Omar, Carlos, Adrian, Juan Pablo Padilla, Gaby Molar, Juan Martínez, Eli Vela, Dilia, Sergio, Andrea, Gabriel etc. Por hacer de este tiempo un tiempo inolvidable.

Gracias al SPIE, a la OSA, al INAOE y al MCTEP por su apoyo para las conferencias y cursos que hicieron posible que conociera otros lugares y formas diferentes de pensar.

Gracias al Dr. Donald O'Shea por sus invaluables consejos.

Gracias al Ing. Luis Rios Casas, al Dr. Rene Reyes, al Dr. Rene Lara y a mis profesores y amigos de la UDLA por los conocimemientos adquirido durante la licenciatura y por compartir una de las etapas mas increíbles de mi vida.

Gracias a las religiosas del Colegio Miraflores, en especial a Sor Angeles por la formacion que recibí en el Colegio y porque los principios que tengo, los cuales se los debo en gran medida a ustedes.

Gracias a mis amigas: Tony Wainstein, Isabel Gutierrez, Anja Packebusch, Muriel Quast, Hilda Muñiz, Ivonne Casturera, Alejandra de la Medina, Kenia, Rebeca Valdes, Beatriz Ortiz Monasterio, Carmen Vargas y Monica Espinosa por recordarme que todavia hay gente buena en el mundo y que la amistad es un tesoro invaluable.

Gracias a todos los que han dejado huella en mi vida y se han ido al mas allá, en particular a mi Papá, a Catalina Andrade, Silvia Garza y Ricardo Nava.

Finalmente gracias a Conacyt porque sin su apoyo económico, no hubiera sido posible dedicar tanto tiempo a estudiar una maestría y un doctorado. Espero que este trabajo sólo sea el comienzo de un prolífera carrera en la Ciencia y que pueda retribuirle a mi país las oportunidades que me ha concedido.

Contents

Preface

In the last two centuries, usually big things were a synonym of "the larger the better". In the last decades humankind began to understand that space and resources in our planet are limited and that if we do not begin "saving them for future generations", shortage problems are going to appear soon enough for us in our lifetime to see.

Going micro and nano is going to be a tendency that has to continue in the years to come. Not only because limited resources, but because of functionality. It is a lot easier to carry a camera in a cell phone in your pocket than a huge device. The miniaturization tendency in modern electronics has been increased with the development of Micro-Electro-Mechanical Systems (MEMS) and Micro-Opto-Electro-Mechanical Systems (MOEMS), and these new technologies are willing to accept more efficient micro optical systems.

Light manipulation and image formation mechanisms in Apposition and Superposition compound eyes are described in chapter 2, where the Fundamentals behind compound eyes is presented. A biological explanation and a compilation of data about the different types of natural compound eyes pretend to introduce the reader to the study of how nature has solved the problem of seeing in small animals like insects and arthropods, giving enough information to the brain without saturating it. The design equations are presented in chapter 3. The artificial apposition compound eye and the artificial superposition compound eye with their applications are shown in chapters 4 and 5 respectively. Conclusions can be found in chapter 6.

Foreword

What is science about? Many people would say that it is about research, about curiosity of things related with nature, about experimentation or about trying to find answers and why not, about inventing.

I guess everything begins with observation. Afterwards a question comes in your mind and then a possible answer. A following experiment is purposed to give birth to the proof of facts that will say if the original hypothesis is right or wrong. The scientific method is not gone out of business even though we do not realize we are using it.

Sometimes it does not matter in which step we approach a problem, as long as we are able to find a solution. But it is very important to understand, where are we going and what do we want to achieve as a goal. It is true that sometimes a journey begins without knowing where it is going to take us. In the road to discovery, many accidents or casual facts have played key roles.

Optics has been an instrument used to explain our environment. In the way to improve observation, optical instrumentation has developed and it has become a science by itself, so, it could be said that we have both the scientific and the engineering approach. It is difficult to have one without the other, but I must confess that optical engineering is my passion.

I remember as a kid dreaming of calling my friends with a video phone call. Today this is possible by just having an iPod, iPhone, Smartphone, etc. It is possible to call someone in the other side of the world just by making a click in your tablet or computer and with a good internet connection. There are many dreams that are still fantasy. Like the optical computer, clean energy for all, ultra small optical devices for

early cancer detection, and of course the old dreams of the alchemists: something that will turn rocks into gold and the elixir of the eternal youth.

I do not know if this work is going to help approach any of these dreams move to the stage of a near future reality, but I can truly say that it is the recollection of ideas that tend to point in that direction based on scientific facts and on an intensive research. I hope that in the years to come some of the concepts presented in this Dissertation will be useful to the readers. I specially want to thank all the people that have encouraged me to follow the path of science either with their own example or by taking the effort to share their ideas, dreams, tales and most important of all: Time.

General Objective:

The design of multi-aperture micro optical systems inspired in the apposition and superposition compound eyes of insects and arthropods. The main goal of this work is to have improved optical systems with smaller dimensions, versatility, non-conventional configuration and a better quality of the recovered image or desired signal.

Specific Objectives:

- The use of Biomimetics by means of understanding the natural working principle of compound insect eyes and applying it to develop their artificial counterparts.
- The calculation of mechanical and optical parameters of the different proposals by means of design equations and a ray tracing program.
- The simulation of the systems under different conditions like different sources.
- The evaluation of the system's performance according to the spot size and intensity distribution.
- The introduction of micro-tunable lens that work by electrowetting in a multi-aperture micro optical system.
- The ability to employ the proposed systems in different and useful applications, being the main applications: imaging systems and free-space communications.

1. Introduction

The smart-phone camera module has been a product that has changed the market considerably. The forecast for the next five years is that the demand will increase from 1,340 to 2,393 millions of units per year [1]. This module has been miniaturized in order to be included in the phone, but the next technological advances have been necessary to have this kind of product:

1. An image sensor small enough to fit within a very tight space but with enough sensitivity to produce images of acceptable quality.
2. A workable lens system for manipulating the image.
3. Wafer-level optics and packaging technologies, which enable the construction and assembly of the camera modules, in manufacturing processes compatible with semiconductor mass production, and
4. A flash unit that provides additional illumination and improves image quality.

Many consumers have come to understand and adopt mobile imaging through their phones, as a result of the use of mobile applications and the demand for the capacity to capture and share images directly from the device to Facebook and e-mail.

Optics remains the key for making cutting edge products. Even though picture quality has been improved by more responsive sensors and lenses, designers of mobile devices are eager of having tinier technology. The challenge remains fitting effective camera technology into a mobile handset, so this problem has given birth to true innovations like better Complementary Metal-Oxide Semiconductor (CMOS) technology, liquid lenses that can be reshaped, multi-aperture wafer-level optics that present good optical performance as well as be reflow compatible in order to be mounted onto the main circuit board of the camera, and the incorporation of a Light

Emitting Diode (LED) flash with small dimensions, high mechanical stability and a long life.

The idea of incorporating microlens arrays that resemble the structure of compound eyes found in insects means that a single array could replace the single lens or multiple lens assemblies used in camera modules, enabling the entire module to become considerably thinner, and avoid the risk of incorrect alignment due to multiple optical elements. Another benefit could be having camera modules with a wider field of view in each image.

This work presents in chapter 2, an introduction to morphology and physiology of natural insect eyes. Some general concepts of micro lens and micro optical systems are included in chapter 3 where some equations and microlens array configurations are also shown. These basic concepts are of great help for the design procedures that were performed to develop the artificial apposition compound eye model presented in chapter 4 and the artificial superposition compound eye model presented in chapter 5.

Chapter 5 begins with the artificial superposition compound eye, used in imaging systems. It explains, which are the differences between apposition and superposition compound eyes, and in which cases do we use each one.

In our way to exploring micro imaging systems, we came to a crossroad, where we found that microlens arrays used in certain configurations could have more applications in different fields. The first one was in energy concentration which let us to a mixer of laser beams. The theory presented in chapter 5 also let us figure out some concepts about the way the sources interfere.

Thanks to the idea of mixing the lasers to increase energy, we came to the concept of multiplexation and demultiplexation, which is commonly used in optical communication systems, so using a double Gabor superlens and a diffraction grating,

optical switching and Wave Division Multiplexing (WDM) were achieved. This application could be of great use to improve free space optical interconnects.

The incorporation of liquid lens to our designs of multi-aperture optics has resulted in many hours of research inverted to try to figure out how variable focus could be implemented. This idea is currently developed to achieve auto-focus in micro-imaging systems by some companies, but the “know how” remains a secret. Our own proposal is shown in this Dissertation.

2. Optics behind Compound Eyes

2.1 Evolution of Artificial Multi Aperture Designs based on Natural Models.

An eye is an organ of spatial vision, in which different photoreceptors view different directions in space. All animals share a similar type of visual pigment but the way that the organs specialize in accommodating large amounts of it and the way they use for transducting the information into electrical signals is not alike. They are different solutions to the problems of sensitivity and speed of the visual receptor cells. The common ancestor must have been a very simple organism which used light intensity to control its behavior. In its way to obtain some directionality, more sensitivity and to response with a higher speed may have resulted in different receptor types and visual organs. If eyes would have not evolved, life in Earth would have been very different. Eyes have given shape to the evolution of animals and ecosystems since the Cambrian explosion. The result of evolution is a big range of eye types which use pin-holes, lenses, mirrors and scanning devices in various combinations to acquire information about the surrounding environment.

Invertebrates, like molluscs, arthropods, and annelids have very unusual types of eyes. Some of them are not even placed in the head. Some eyes are spread over shells, tentacles or mantle. Creatures without brain have camera type eyes.

The major optical types of eye found in multicellular animals are refracting or reflector devices. The main types are: (a) Pit eye, antecessor of single-chambered eyes, (b) Basic compound eye, in which the receptor is separated from its neighbor by

a simple pigment tube, (c) Aquatic lens eye, found in fish and cephalopod molluscs, (d) Corneal lens eye, found in terrestrial verterbrates and spiders and some insect larvae, (e) Apposition compound eye, found in diurnal insects and crustaceans, (f) Refracting superposition compound eye, found in animals that live in dim environments (g) Single chambered eye where the image is produced by a concave mirror and (h) Reflecting superposition compound eye similar to the refracting type except that the lenses are replaced by mirrors. They are found in decapod shrimps and lobsters. In (Fig. 2.1) the different eye types could be seen [2].

Compound eyes employ a large number of extremely small vision systems. The whole optical system is formed by independent units that act together to perform the formation of an image. It presents different mechanisms for each different type of compound eye. The structure of compound eyes has a lot to do with the processing of information that the neural system of an insect has to deal with, without saturating it's capacity according to its' size and its' energy consumption. The fact that the small individual eyelets (which name is "Ommatidia"), are placed on a curved basis allows the eye to have a large field of view (FOV). Although each ommatidia has a small FOV, the sum of all of them in the compound eye gives a larger FOV. This configuration keeps a small volume and the information capacity of the whole eye is increased to fulfill the requirements of the animal. It makes possible for the insect or arthropod an accurate and fast navigation through its environment. So, the main volume of the brain is available for signal processing and other biological functions [3].

Insect eyes are ten time faster than human eyes. They have a very fast sampling frequency, about 250 Hz, and even though the angular resolution is very poor, it is counterbalanced with the high speed. The focal length of the primary lenslet of the ommatidias is very short, but this allows the compound eye to have a large depth of focus. Thanks to all these characteristics, Compound eyes have become and inspiration to artificial models that try to give this benefits to miniature imaging

systems, and to implement them in new applications like energy concentration, communications, etc.

The two main groups of compound eyes are divided in: (1) apposition compound eyes and (2) superposition compound eyes, which present other subgroups [2]. The goal of this chapter is to present the main structures of the natural compound eyes, and to show the way they work, so that it could be later understood how their artificial countertypes have been designed.

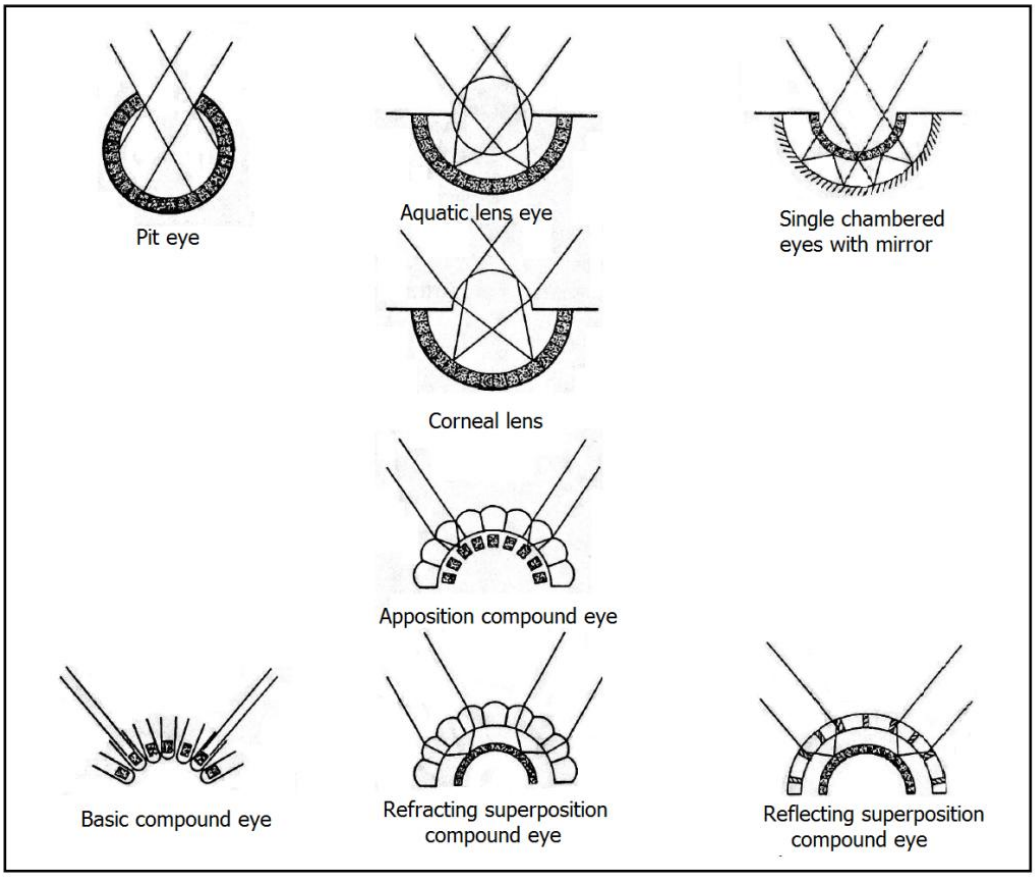

Figure 2.1 Different optical types of eye found in multicellular animals.

2.1.1 Apposition Compound Eyes

The facets of compound eyes are too small to be resolved with the eye, so the first one to take a look at them was Antoni van Leeuwenhoek with his microscope in the seventeenth century. But it was Sigmund Exner in 1891 who actually found how this type of compound eye worked. Compound eyes are different in comparison with single aperture eyes, in that they capture the information coming from the surroundings with multiple lenslets that are placed in a convex surface (Fig. 2.2a). The most important problem at the time when compound eyes were first discovered was that image formation in many animals with these eyes was not very easy to understand in comparison to conventional spherical surface refraction, which is what a simple lens does. Exner proposed that the optical elements behaved as lens cylinders, this means that they have a graded refractive index, densest along the axis and decreasing in a parabolic manner in direction towards the outside. The most important property of these structures is that non-axial rays, striking the end of the cylinder normally, will be refracted continuously towards the axis, this means that an inhomogeneous cylinder would behave a lot like an ordinary converging lens in its image-forming properties [4]. Histological studies have shown that an "ommatidium" is the unit of a compound eye, and it consists of the lens, receptors, and associated structures (Fig. 2.2b). These individual units are Exner's lens cylinders.

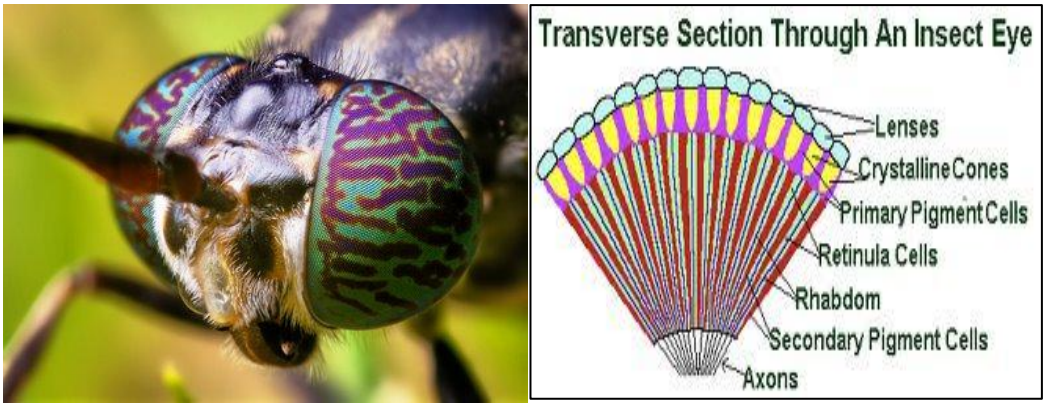

(a) (b)

Figure 2.2 (a) View of the apposition compound eyes of the *Hermetia illucens* [5].
(b) Main parts of a natural apposition compound eye: lens, receptors, and associated structures [6].

Apposition eyes are found mostly in diurnal insects, and they need a great amount of light to resolve an object, because their sensitivity is very limited. It is commonly believed that compound eyes form multiple images. However in apposition eyes each of the lenses forms a tiny image, which is not what the animal sees at the end. The final image formed at the retina, is a mosaic of different tiny images pasted together in such a way that each one seems to be a specific piece of the puzzle. In most apposition eyes, eight receptor cells can be found, and they contribute in each individual unit to a single radial structure called rhabdom which is the structure sensitive to light. The rhabdom behaves like a light guide, so the light that enters the distal tip travels down the structure, making the rhabdom act as a photocell that averages the light that enters it [7].

The resolution of the image seen by the brain is determined by the sampling frequency of the eye (ν_s). The visual surroundings are sampled by the rhabdom in each single ommatidium, and each of the lenslet's optical axis points in a different direction due to the curvature of the eye. The interommatidial angle determines how the overall image is sampled ($\Delta\Phi$). This angle gives the angular offset between the optical axes of two adjacent ommatidia with a microlens diameter *D* [2,4]

$$\Delta\Phi_{nat} \approx \frac{D}{R_{eye}}, \tag{2.1}$$

where R_{eye} is the Radius of curvature.

The optical quality is represented by the spatial cut-off frequency (ν_{co}), and the sampling frequency that could be resolved according to the Nyquist criterion is defined as:

$$\nu_{co} = \frac{1}{2\Delta\Phi}, \tag{2.2}$$

In hexagonal arrays, the definition for ΔΦ can become quite complicate, but it is usually the average of the angle measured along each of the three axes of the array.

The photoreceptor of each ommatidia accepts light from a finite angular interval centered on the corresponding optical axis. The full width at half maximum (FWHM) of the angular sensitivity is the acceptance angle $\Delta\varphi_{nat}$ [2]. This measurement could be considered as the most important parameter of a compound eye because it determines the trade-off between sensitivity and resolution. The geometrical contribution of the acceptance angle ($\Delta\rho$) is defined as:

$$\Delta\rho = \frac{d}{f}, \tag{2.3}$$

where the relation between the photoreceptor diameter d projected into the object space as the focal length f is shown. The geometrical contribution is the angle subtended by the rhabdom tip at the nodal point of the facet lens. There is a second contribution given by the Airy diffraction pattern which originates from the diffraction at the microlens aperture for the wavelength λ. This is because the photoreceptor diameter is approximately the same size as that of the diffraction spot of the cornea lens, and their angular acceptances can be described by a Gaussian function. So the final value of the acceptance angle is defined as:

$$\Delta\varphi_{nat} = \sqrt{\left(\frac{d}{f}\right)^2 + \left(\frac{\lambda}{D}\right)^2}, \tag{2.4}$$

In Fig. 2.3 we have sketched the geometrical optics parameters of the apposition compound eye, described above.

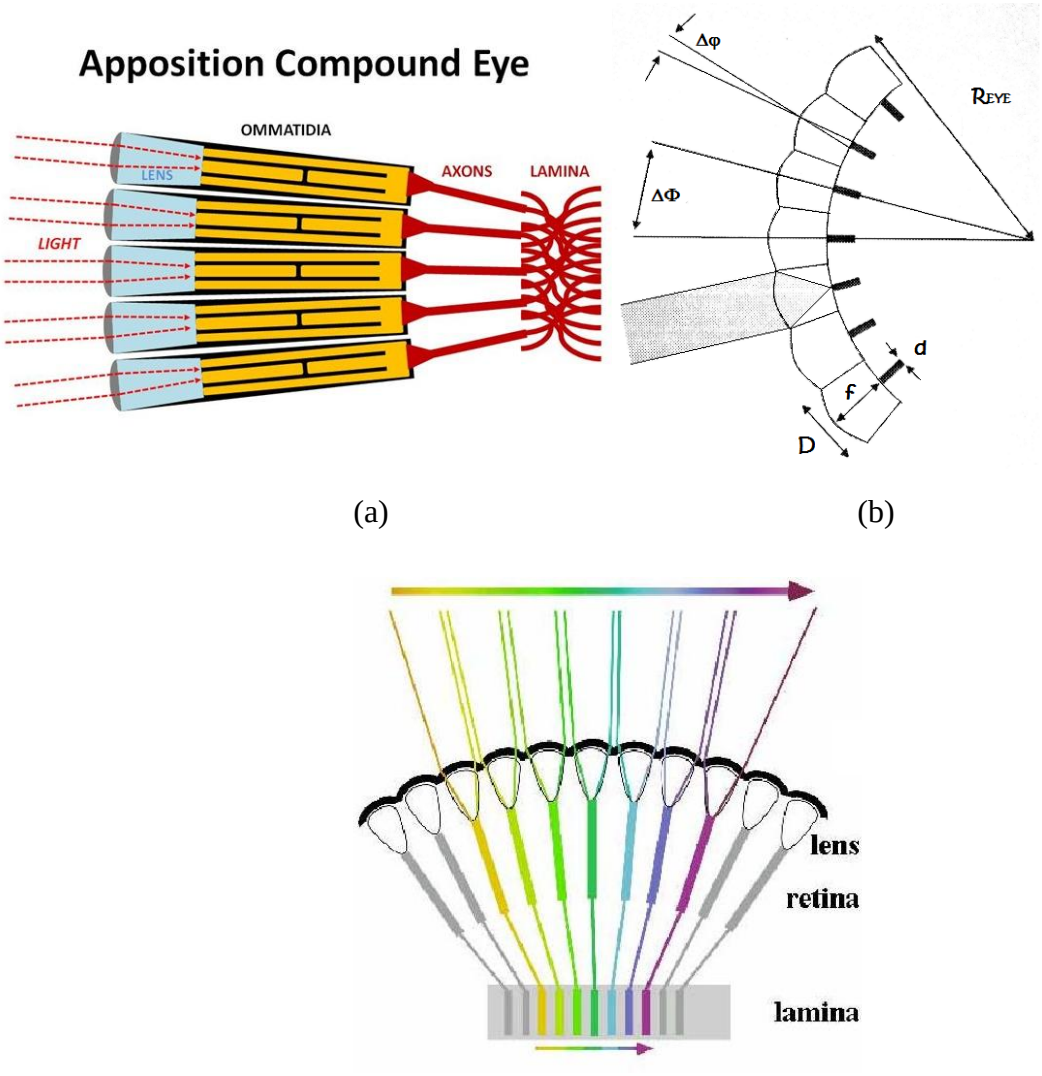

Figure 2.3 (a) Working principle of the Apposition Compound Eye [8]. (b) Parameters of the apposition compound eye, where ΔΦ is the interommatidial angle, Δφ is the acceptance angle, *f* is the focal length, *d* is the photoreceptor diameter, R_{eye} is the radius of curvature and *D* is the lenslet diameter [2]. (c) Image formation mechanism of the Apposition Compound Eye [2].

2.1.2 Neural Superposition Compound Eyes

In neural superposition eyes, light from a single direction is imaged onto different rhabdomeres in adjacent ommatidia, and the related signals are fused in the first synaptic layer of the eye so the image has the same structure as in an ordinary apposition eye [2-4]. This kind of eye could be found in different species of flies, and the simultaneous sampling of the same part of the FOV allows this eye to have more light sensitivity than a normal apposition compound eye (Fig. 2.4).

Apposition compound eyes are very limited in sensitivity, so they need a very big amount of light to achieve an acceptable quality of the image.

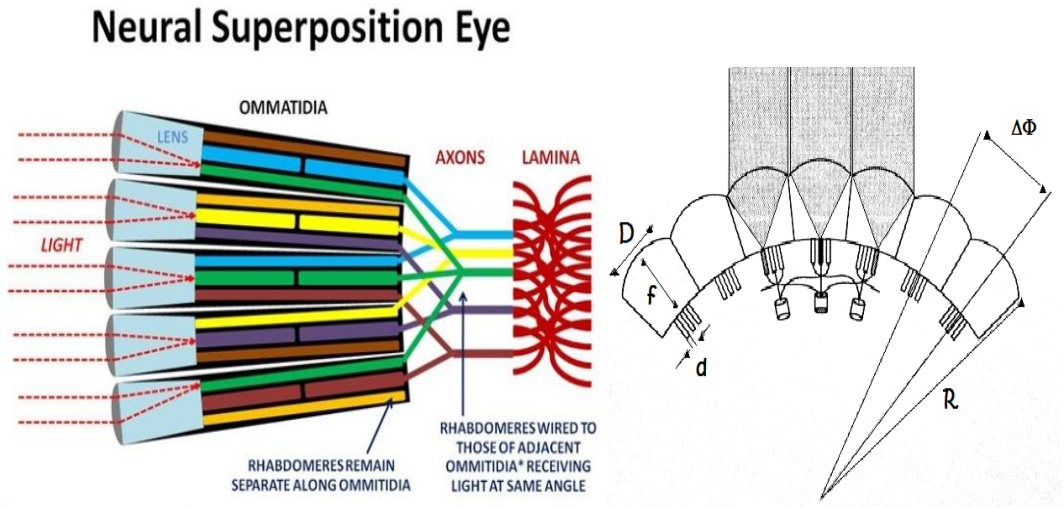

(a) (b)

Figure 2.4 (a) Neural superposition compound eye's working principle, where the same object is sampled by different photosensors of different adyacent ommatidias. The image is formed in a way that it behaves like an apposition compound eye with increased sensitivity [8]. (b) The parameters are *D* diameter of the ommatidia, *f* focal length, *d* diameter of the photoreceptor, *R* radius of curvature and $\Delta\Phi$ interommatidial angle [2].

2.1.3 Superposition Compound Eyes

Superposition compound eyes are also convex structures with facets of similar dimensions. They resemble the apposition compound eyes from the outside, but internally they present anatomical differences: the retina is a single sheet, not like in apposition eyes where it is broken in discrete ommatidial units, and it lies deep in the eye, about halfway between the centre of curvature and the cornea. There is a zone called the clear zone, which is between the retina and the optical structures beneath the cornea. There are different kinds of superposition compound eyes according to the optical devices that compose them. There are eyes with refracting telescopes, mirrors, or a combination of both. These eyes produce a single deep-lying erect image in the vicinity of the retina [2]. The image forming mechanism is very different in comparison with conventional lens, and Exner described it, by supposing that light is redirected by the optical elements across the axis, and in this way they form an image. The optical elements that had a similar structure were two-lens telescopes. Fig. 2.5a shows an insect with superposition compound eyes. Fig. 2.5b is a diagram of the different parts of the superposition compound eye, where the clear zone, cornea, crystalline cones and photoreceptors are shown.

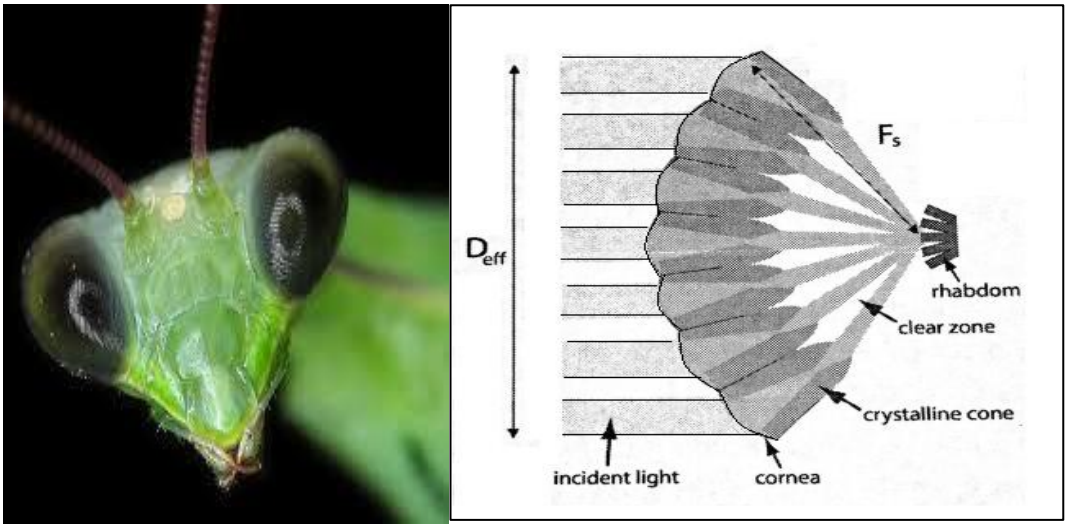

(a) (b)

Figure 2.5 (a) Insect with superposition compound eyes [6]. (b) Anatomy of the natural superposition compound eye where the main parts can be distinguished [2].

These eyes had evolved in nocturnal insects and crustaceans. They are more sensitive than apposition compound eyes because the effective collecting aperture stop D_{eff} is increased to a size which is a lot larger than the diameter of a single lenslet [8]. The volume is larger than apposition compound eyes, due to the clear zone, which is needed to fusion the light bundles to form the final image.

Refractive superposition compound eyes are lens based, and the optical elements need to act as inverting telescopes which redirect light entering the aperture stop across the optical axis. The easiest way to achieve this function is to have two lenses separated by the sum of their individual focal lengths, with a virtual image plane between them. In nature, the curvatures of the lens do not have enough ray-bending power, so Exner concluded that the structures have a radial parabolic refractive index gradient. He called these structures "lens cylinders" [2].

The geometrical optics concepts for superposition compound eyes are shown in Fig. 2.6. The nodal point of the eye is at the center of curvature, and the focal length is the distance out from the center to the image. The focal length is defined as [2]:

$$f = \frac{O_b}{s_o} = \frac{I}{\alpha}, \tag{2.5}$$

Where O_b and I are object and image size respectively, s_o is the object distance, and α is the angle in radians subtended by object of image at the nodal point.

The inter rhabdom angle $\Delta\phi$ is defined by:

$$\Delta\phi = \frac{s_r}{f}, \tag{2.6}$$

Where s_r is the rhabdom's separation and f is the focal length. The rhabdom acceptance angle is the combination of the geometrical contribution of the rhabdom, and the contribution of the diffraction pattern of the Airy disk. Eq. (2.4) defines this angle.

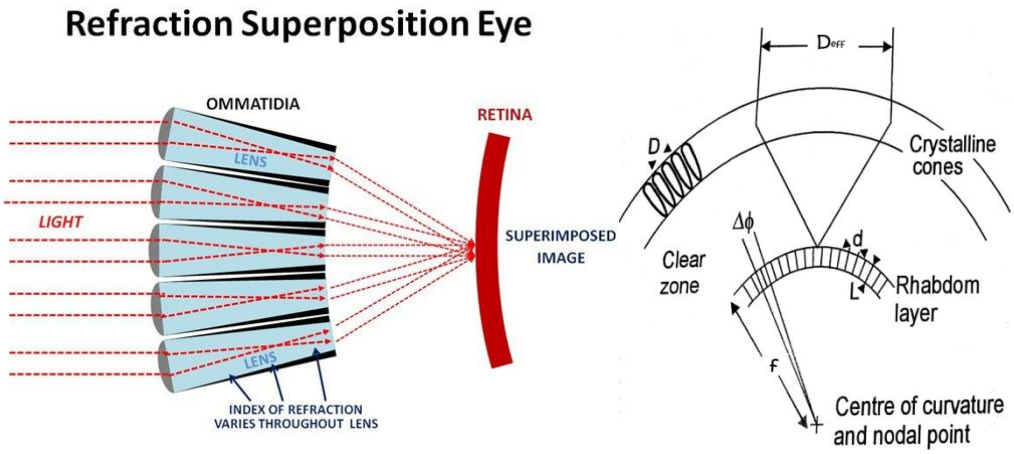

(a) (b)

Figure 2.6: (a) Working principle of the Refractive Superposition compound eye [8]. (b) Optical parameters of the superposition compound eye. D_{eff} is the diameter of the effective aperture pupil, f is the focal length, d is the rhabdom diameter, L is the rhabdom length, $\Delta\phi$ is the inter rhabdom angle and D is the the lenslet diameter [2].

The resolution of the superposition compound eye is not very high because there is a blur caused by the imperfect combination of light beams from the several ommatidia that conforms this eye [9].

2.1.4 Reflecting Superposition Compound Eyes

Decapod crustaceans and shrimps have very different structures in comparison with the ones found in the refractive superposition compound eyes. The image forming mechanism was similar but the optics was completely different. In 1975 Vogt [10] purposed radial arrangements of orthogonal reflecting planes which are formed by the sides of crystalline cones and the purine layers surrounding them. The optical units are flat-faced, four sided truncated pyramids of relatively low refractive index which act as plane mirrors that direct light to a common focus. The ray-bending mechanism is almost identical to the refractive superposition compound eye. The facets of the animals with these eyes are square faced, rather than hexagonal, and this let us to the principle of corner reflector, which explains optically what happens to the rays that are in oblique planes [11]. A ray reflected from two mirrors must be rotated through a total of two right angles, which mean that it will return parallel to its original direction. Apart from a slight lateral displacement of the reflected ray, a corner mirror behaves as though it were a single mirror, but one that is always at right angles to the incoming ray. This property makes reflecting superposition possible. Fig. 2.7a shows the reflecting superposition compound eye and Fig 2.7b shows how the square facet array works using the principle of the corner reflector.

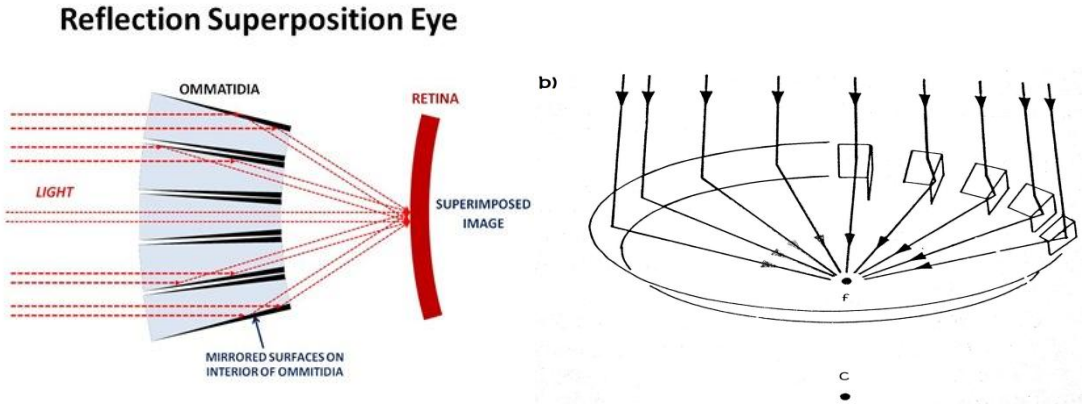

(a) (b)

Figure 2.7: (a) Reflecting superposition compound eye working principle [8] (b) The mirror boxes act as ‘corner reflectors’. Whatever the angle of incidence, the incoming rays are reflected through two right angles, and they emerge parallel to their original path until they reach a common focus at *f*. *C* is the eye’s centre of curvature [2,4].

2.1.5 Parabolic Superposition Compound Eyes

This eye has characteristics of apposition and superposition compound eyes. It was first described by Nilsson in 1988 [2] and it was observed in a swimming crab. Each element consists of a corneal lens, which on its own focuses light close to the proximal tip of the crystalline cone, the way that it is done in the apposition eye. Rays parallel to the cone's axis enter a light guiding structure that links the cone to the deep-lying rhabdom. Oblique rays, encounter the reflecting coating with a parabolic profile that is in the side of the cone. The effect of this mirror surface it to recollimate the partially focused rays, so that they change their direction in such a way that a parallel beam that crosses the eye's clear zone is generated in a similar way that other superposition eyes do.

The rays in the orthogonal plane find other optics. The cone behaves like a cylindrical lens that creates a focus on the surface of the parabolic mirror. The same lens, recollimate the rays on their reverse passage through the cone. This mechanism is the only one known that combines lens and mirrors in insect eyes. A shrimp's eye is shown in Fig. 2.8a, in Fig. 2.8b the working principle of the parabolic superposition optics could be seen. Fig. 2.8c is the top view of the parabolic reflecting ommatidia.

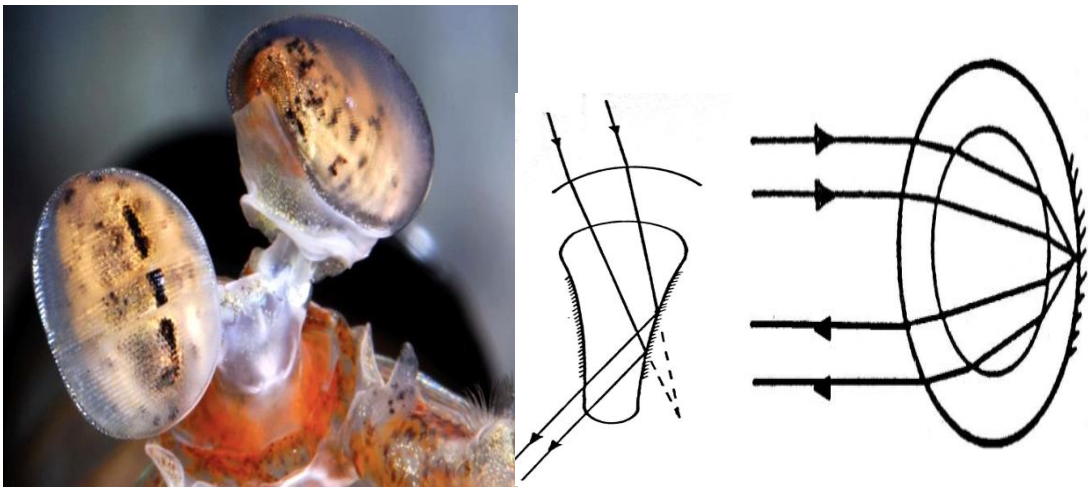

(a) (b) (c)

Figure 2.8: a) Shrimp's eyes [12]. B) Parabolic reflecting eye ommatidia: Rays are focused by the corneal lens in a point near the crystalline cone. Oblique rays are intercepted by the parabolic reflective surface on the walls of the cone, and they are again redirected back across the axis to form a beam that has a contribution to the final image. C) Parabolic superposition mechanism's top view [2].

2.1.6 Strepsiptera's Compound Eyes

The eye of a wasp parasite called *Xenos peckii* has very large cornea lenses. It presents an extended retina at the image plane of each cornea lens and a photoreceptor bundle that is rotated 180^{o} on its way into the lamina. Each lenslet forms an inverted image. There is a relationship between the individual retina blocks of adjacent lenslets in order to improve the spatial resolution. This eye presents interesting possibilities for technical counterparts (Fig. 2.9).

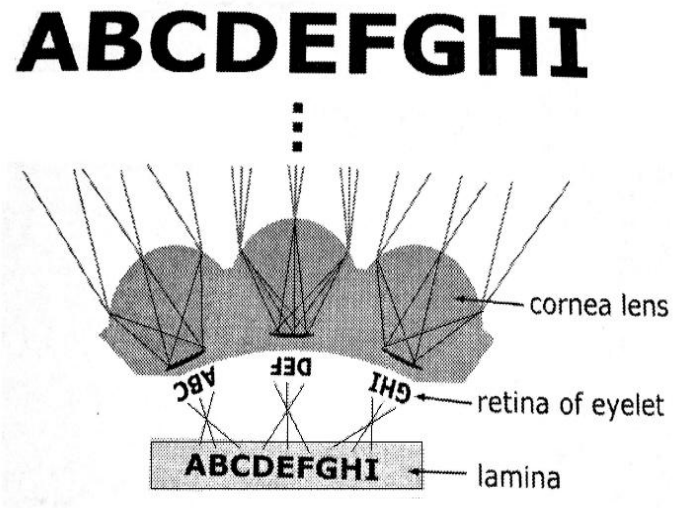

Figure 2.9: Anatomy and working principle of the Strepsiptera's compound eye. The final image is erect, and it works like an improved model of the apposition compound eye [4].

3. Micro and Multi-Aperture Imaging Systems

Micro-optics is a special branch in optics that refers to optical elements which have dimensions of a millimeter of smaller. This means lenses, or structures that act as lenses, as structures that redirect, polarize or alter some state or direction or light [13]. Micro-optics is strongly related to micro-electronics and if it includes optical waveguide structures it is called integrated optics. The speed of light and the enormous bandwidth make optics very attractive for information processing. Light can propagate in space without interfering, so the whole space in its three dimensions can be used as an interconnection system [14].

Micro-imaging optical systems have become popular in the last two decades. The main applications have been in compact optical devices requiring imaging optics to be confined to a small space. These devices are mainly document readers, bar code readers and scanners. The need of low-priced micro-lenses with good optical performance has been increasing. The Electronic sensors are very thin in comparison with the optics and the main reason is that if a lens diameter is getting smaller, the image quality becomes very poor. Conventional one aperture imaging systems present big limitations to miniaturization. The alternative ways to solve this problem have become the search of novel optical designs based on multi-aperture optics inspired mainly in insect's compound eyes.

The maximum resolving power of a lens is given by $R_p = 116/D$, where D is lens diameter in millimeters and R_p is the resolving power in arcseconds [15]. In order to capture enough amount of light and to achieve good angular resolution, a lens should be able to cover multiple pixels. For a diffraction-limited lens system, the number of transported image pixels scales with the square of the lens diameter [16].

Thanks to the evolution of microfabrication technologies, there are three main categories of miniaturized lenses that are available: refractive, diffractive and graded index microlenses.

There are many fabrication techniques used to manufacture refractive microlenses. The most popular ones are: molding, hot pressing, photoresist based, microjet fabrication, photosensitive glass and laser heating.

Diffractive micro-lenses are made by a similar method to the one for making micro-Fresnel lenses which is based on being able to provide a gray scale of exposure. The second method of fabrication is called binary optics.
In order to manufacture graded index microlenses, a method of ion-exchange process in glass was developed [13].

In this chapter, some basic concepts that are used in other sections are described.

3.1 Scaling behavior of lenses

What happens when optical components are shrinked? If we want to image an extended object through a spatial filter, the imaging can be performed either by a macro-lens with a field of view which covers the entire object, or by a set of micro-lenses providing a separate channel for each area of each object point [14].

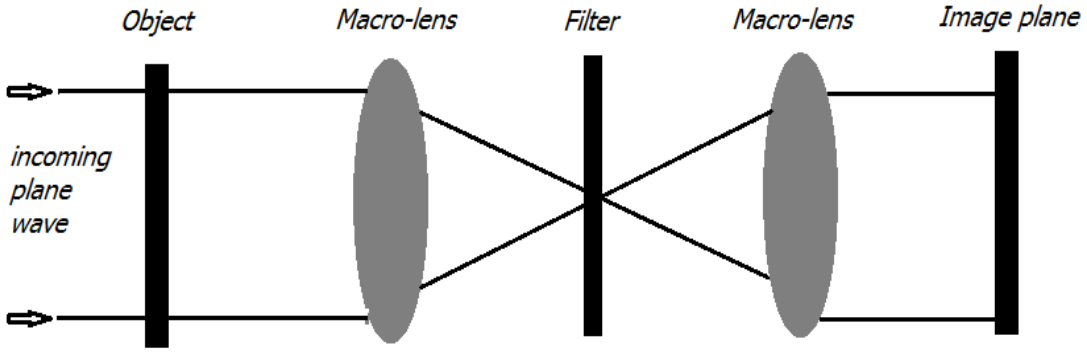

Figure 3.1 An extended object imaged through a spatial filter by a macro-system [14].

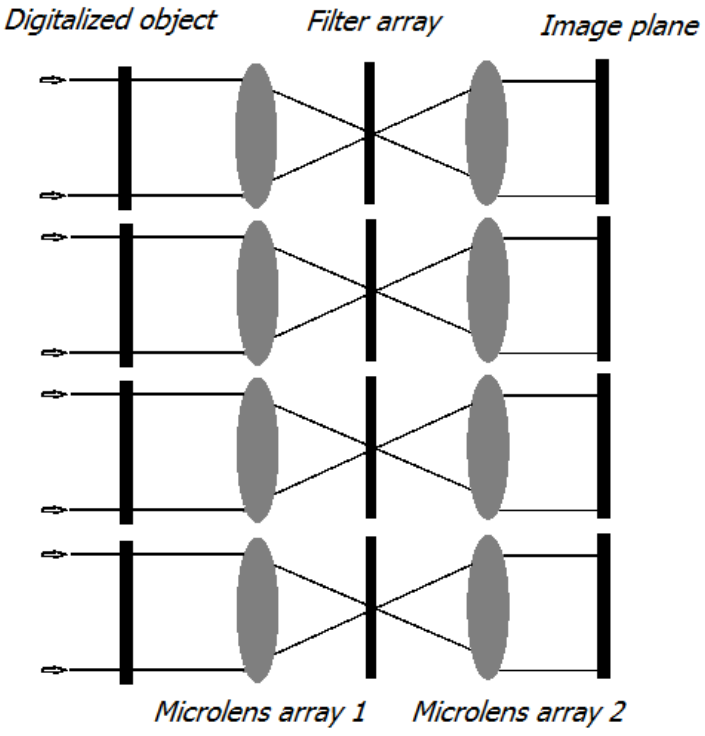

Figure 3.2 A digitalized object imaged through a filter array by a micro-system [14].

If we want to transform the system shown in Fig. 3.1 to the system shown in Fig. 3.2 by scaling the diameter and the focal length of the lenses by a factor S_c, all the angles are invariant. Resolution and depth of focus are also invariant. Distances scale linearly with the factor S_c. Surfaces such as the image field size scale as S_c^2, and the system volume and weight scale as S_c^3. Due to the fact that for the micro-system there are separate filters for each position, the space variant filtering appears.

Table 3.1 Scaling of micro systems parameters [14].

Parameter	Scales to	Equation number
Lens diameter d	$d = S_c * d$	(3.1)
Focal length f	$f = S_c * f$	(3.2)
All angles	invariant	
Resolution $\delta x = \lambda F$	invariant	
Depth of focus $\delta z = 4\lambda F^2$	invariant	
Lateral aberrations ξ	$\xi = S_c * \xi$	(3.3)
Travel time of light Δt	$\Delta t = S_c * \Delta t$	(3.4)
Image field size $A_F = \Delta x \Delta y$	$\Delta x \Delta y = S_c^2 * \Delta x \Delta y$	(3.5)
System volume Vol	$Vol = S_c^3 * Vol$	(3.6)
System weigth W	$W = S_c^3 * W$	(3.7)

Where λ is the wavelength, F is the stop number and Δx and Δy are the lateral dimensions of the image field.

The space-bandwidth product is an important measure for information processing. It represents the number of resolvable points in the image plane or respectively the number of data channels which can be handled in parallel. It is defined by:

$$SW = \frac{A_F}{A_P}, \tag{3.8}$$

Where, SW is the space-bandwith-product, A_F the field size and A_P the area of one pixel. The scaling of the space-bandwith-product is defined by:

$$SW = \frac{A_F}{A_P} = \frac{S^2 * \Delta x \Delta y}{(\delta x)^2 + S^2 * (\delta \xi)^2} \tag{3.9}$$

For a lens system without any aberration ($\delta\xi$ =0) the space-bandwith-product scales with S^2 and for a system where the diffraction effects are neglible compared to aberrations ($\delta x \ll \delta \xi$) the space-bandwith-product rests unchanged. For the transition from macro to microlenses there are important changes in the scaling laws as soon as

the diffraction effects become significant, this means that the aberrations become less important in comparison to the larger Airy disc resulting from diffraction at the aperture stop.

3.2 Plano-Convex Refractive Microlenses

Microlenses are small three-dimensional (3D), transparent, refractive structures with dimensions ranging from centimeters to micrometers, that are made of different materials like different types of glasses, different polymers and plastics.

Multi-aperture imaging optical systems are usually made of different arrays of microlenses, which may have similar or different dimensions, and that have a special configuration which emulate natural compound insect eyes by means of having properties that are alike thanks to the use of new designs of artificial optical devices.

The main physical and optical parameters of plano-convex refractive microlenses are calculated with the following equations [17-18]:

Radius of Curvature

$$R_c = \frac{h(K+1)}{2} + \frac{r^2}{2h}, \tag{3.10}$$

where *h* is the lens sag, K is the conic constant, and *r* is the lens radius.

Lens sag

$$h = f_{E,f}\,(n-1) - \sqrt{f_{E,f}^2(n-1)^2 - r^2}, \tag{3.11}$$

$$h = R_c - \sqrt{R_c^2 - r^2}, \tag{3.12}$$

where $f_{E,f}$ effective front focal length, R_c Radius of curvature, *r* is the lens radius, and *n* is the refractive index of the material of the microlenses.

Effective front focal length

$$f_{E,f} = \frac{R_c}{n-1} = \frac{\left(h + \frac{r^2}{h}\right)}{2(n-1)} \approx \frac{r^2}{h}, \tag{3.13}$$

Focal length in glass

$$f_{glass} = \frac{R_c}{n-1}\, n, \tag{3.14}$$

Imaging Equation

$$\frac{1}{f_{E,f}} = \frac{1}{s_i} - \frac{1}{s_o}, \tag{3.15}$$

where s_o is the object distance and s_i is the image distance.

3.3 Limitations for miniaturization

There are physical and technological constraints for miniaturization, the two main concepts are lithographic resolution and Gaussian beam shape.

The maximum possible deflection angle α of a grating depends of the minimum feature size of the fabrication process.

$$\alpha < arcsin\frac{\lambda}{p_{min}} < \arcsin\frac{\lambda}{ir_s}, \qquad (3.16)$$

where, λ is the wavelength, p_{min} is the minimum grating period, i is a i-level etched grating and r_s is the best resolution.

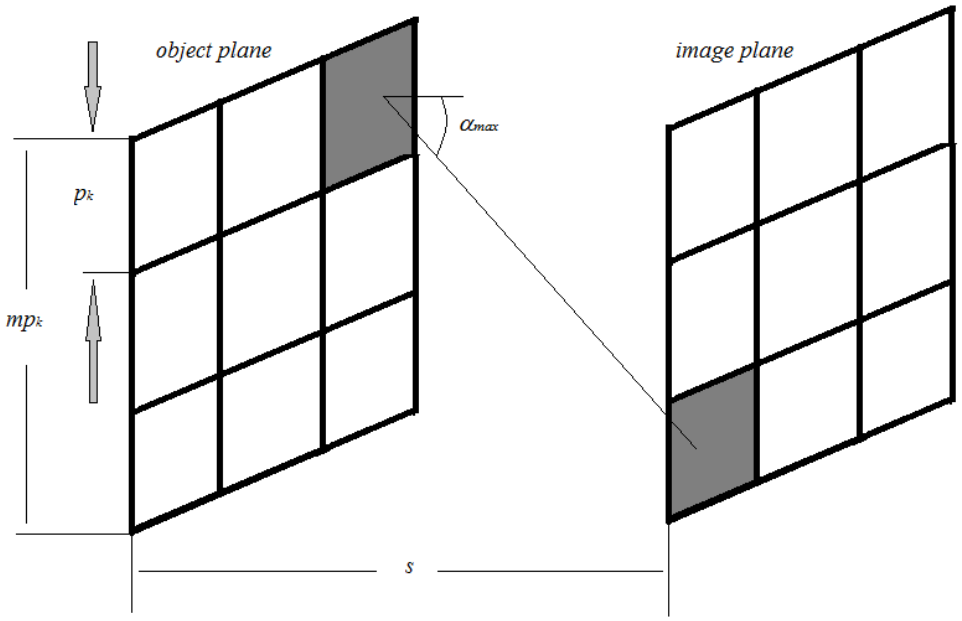

Figure 3.3 Visualization of the basic parameters which characterize the FOV of multi aperture optics. [14].

If we have a system configuration where an input array has to be connected in an arbitrary permutation to an output array, the miniaturization of the whole system is limited by an angular constrain. The maximum deflection angle α_{max} required to connect the two channels which are the furthest away from each other may not exceed the maximum possible deflection angle α of the grating. For a quadratic array of m x m elements with a pixel pitch of p_k, for a diagonal connection the α_{max} is:

$$\alpha_{max} = \arctan\frac{\sqrt{2}(m-1)p_k}{S}, \tag{3.17}$$

with S denoting the system length, which is the distance between input and output array. For a given number of elements and a given resolution the system length cannot be arbitrarily small. Fig. 3.3 shows the minimum system length caused by a maximum deflection angle and the basic parameters used in multi aperture optics.

The following equation constrains the system length:

$$S \geqq \frac{\sqrt{2}(m-1)p_k j r_s}{\lambda}, \tag{3.18}$$

A physical constraint that limits a micro system's size is the fact that a collimated beam of light cannot propagate in free space without increasing in width. There is a limitation on the distance the light can travel in between two lenses without exceeding a given width. The overall system length S can be calculated by:

$$S = I_1 + I_2 = \frac{\pi}{\lambda}\omega_0'\left(\sqrt{\omega_{in}^2 - \omega_0'^2} + \sqrt{a^2\omega_{in}^2 - \omega_0'^2}\right), \tag{3.19}$$

Where ω_{in} is the input beam radius, $\omega_0'$is the beam waist, I_1 is the distance from the input lens to the beam waist and I_2 is the distance from the beam waist to the output lens. In Fig. 3.4 it is possible to see how a beam of light with a Gaussian profile inputs and outputs a lens system.

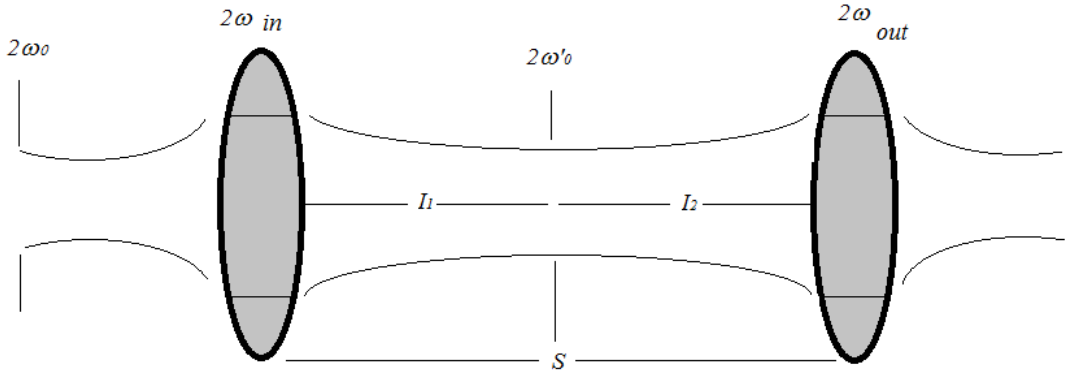

Figure 3.4 Maximum system length caused by the beam size. $2\omega_0$ is the incident beam waist [14].

3.4 Applications of Microlenses

Document readers, scanners and bar code readers have reduced their size in the last years, they require erect one-to-one imaging. The advantage over a conventional lens is the shortness of the working distance that can be achieved. One-to-one image is achieved by means of micro-optical devices that have arrays of microlenses designed to produce collectively a single image. The overlap of all the individual image fields constitutes a single image. Fig.3.5 shows how one point is imaged by a microlenses array.

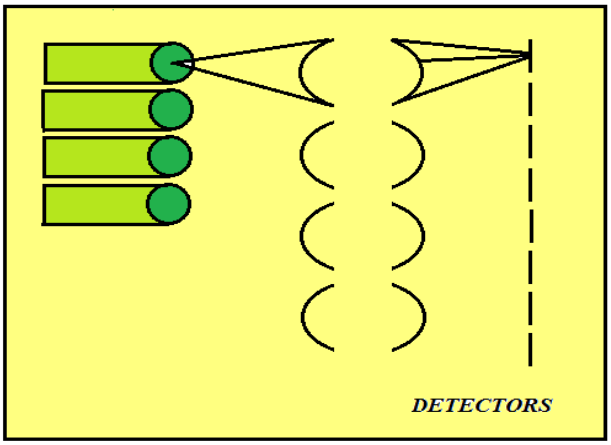

Figure 3.5 Microlens array imaging a point into a detector array [13].

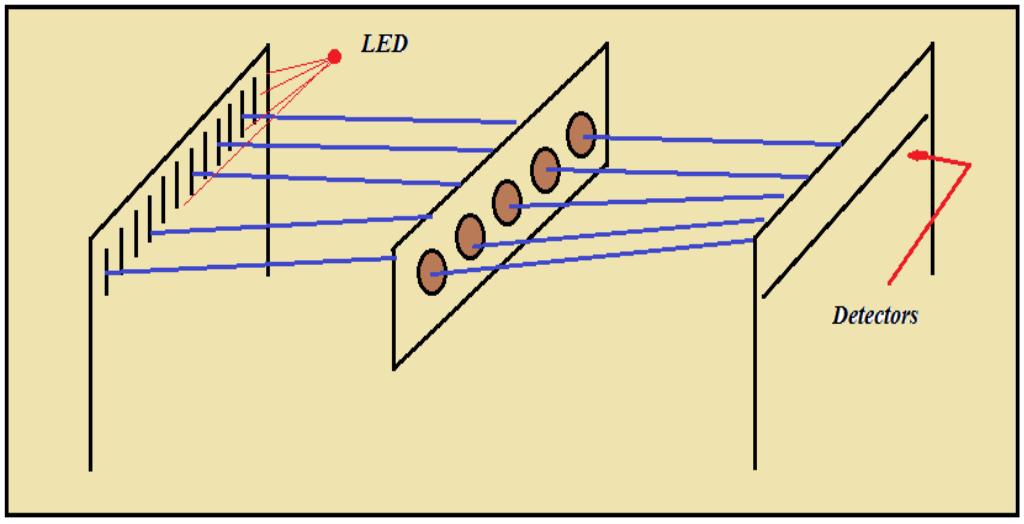

Figure 3.6 One-to-one imaging, application where a document is imaged in a detector array [13].

Another group of applications are optical device interfaces with microelectronic structures which require small closely spaced lenses. One example is a LED printer bar where each pixel is imaged onto the detector. See Fig. 3.6, where a document that is imaged by a microlens array is shown.

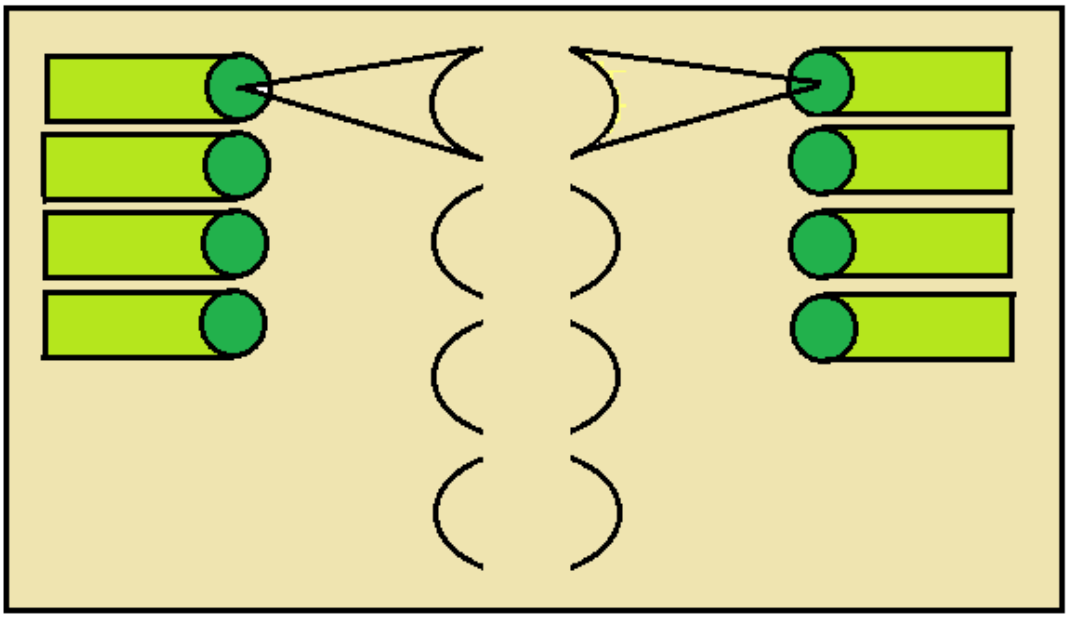

Figure 3.7 Microlens array collimating light from an optical fiber array, and then reimaging it into an output fiber array.

Optical waveguide devices: lens to input and output light from single mode fibers, or arrays are also an important application. The most important use of waveguides is in the efficient coupling of light from a laser diode to a single mode fiber. There are also devices that are part of a WDM (wavelength division multiplexing) system. In Fig. 3.7 it could be seen how light that comes from an optical fiber array is imaged by a microlenses array, and then it is placed in another optical fiber array in the output of the system.

3.5 Micro-Cylindrical Doublets (MCD)

A micro-doublet is the combination of two microlenses, usually a positive and a negative one, that are used together as a single element to reduce aberrations and to improve the imaging properties of the system [19]. The Optics Software for Layout and Optimization (OSLO) was used to perform the calculations and simulations of the MCD.

Table 3.2 Optical design parameters calculated for three different designs of the Micro-Cylindrical Doublets (MCD).

	MCD1	MCD2	MCD3
Refractive index of the first lens (n_1)	1.4370	1.4370	1.5638
Refractive index of the second lens (n_2)	1.5168	1.5168	1.5168
Radius of curvature R_i (μm)	102.04	94.47	119.4
Diameter *Di* (μm)	70	65.5	68.5
Thickness of the first microlens t_i(μm)	30	30	30
Total thickness T_i(μm)	340	320	320

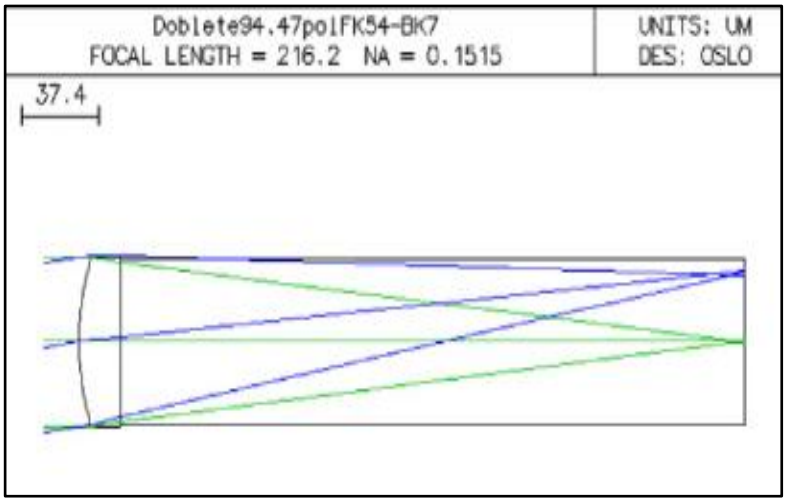

(a)

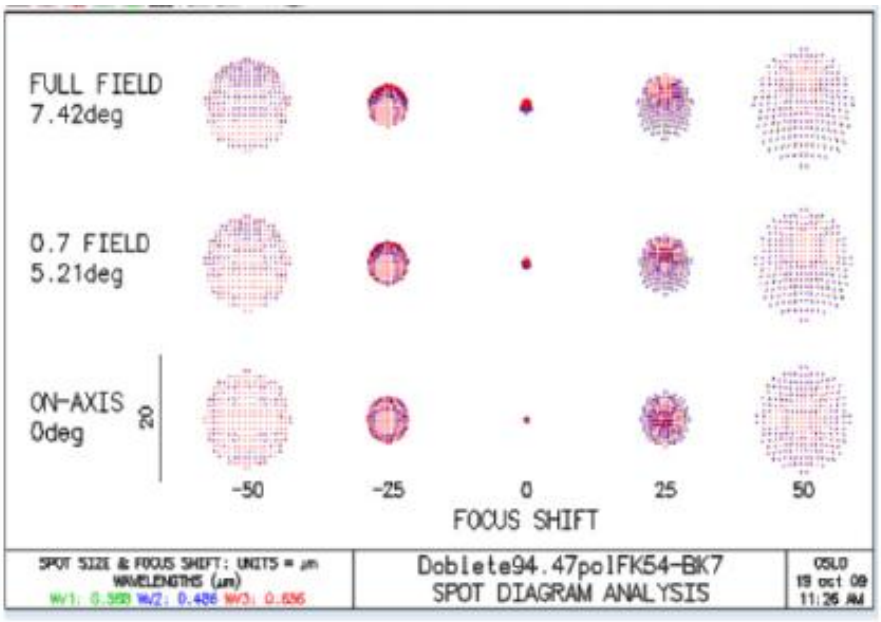

(b)

Figure 3.8 (a) View of the simulation in OSLO Premium of the Micro cylindrical-doublet MCD2. (b)Spot Diagrams of the MCD2 [19].

The general concept of aberration in an Optical system is defined as the failure of the system to conform to the mode of ideal image formation. Aberrations could be a function of pupil position and field angle, and they could be computed to show their value. There are different aberrations like coma, spherical aberration, distorsion, astigmatism, etc.

A Spot Diagram gives a useful impression of the geometrical image quality. It is generated by plotting isolated points for the individual ray intersections at the image plane.

In Fig. 3.8a it is possible to see a side view of the MCD. Fig. 3.8 b shows the Spot diagram of the MCD on axis and off-axis. The size of the larger spot that is off-axis is smaller than 20 microns.

3.6 Micro-Keplerian Telescopes

There are three types of Optical Instruments based on conjugated distances: The telescopes (∞ to finite), microscopes (finite to ∞) and cameras (finite to finite). A telescope is a device used to enlarge the scope of a distance object. This is done by means of increasing the angular size of the object. Telescopes are afocal instruments. Light from the object is collimated on entering and exiting the telescope. The power of a telescope *M* is the ratio of the angle subtended by the image ω' to the ratio of the angle subtended by the object ω [20].

$$M = \frac{\tan \omega\prime}{\tan \omega} = \frac{\omega\prime}{\omega} \tag{3.20}$$

Telescopes consist of an objective (which is the component nearer the object), which may be a refractive or reflective element and an ocular lens. The length of a simple afocal telescope D_t is equal to the sum of the focal lengths of the objective f_o and the eyelens f_e:

$$D_t = f_o + f_e, \tag{3.21}$$

There are three main kinds of refractive telescopes:

a) Keplerian or astronomical: It is composed of two positive components spaced in such a way that the second focal point of the first component coincides with the first focal point of the second. The objective forms an inverted image at its focal point; the ocular reimages the object at infinity where an inverted image may be comfortably viewed by a relaxed eye. The angular magnification of the astronomical telescope is:

$$M = -\frac{f_1}{f_2}, \tag{3.22}$$

b) Galilean or Dutch: The positive lens of the ocular is replaced by a negative eyelens: the focal points of the objective and the eyelens coincide, however the internal image is never formed. The object for the eyelens is a "virtual" object, no inversion occurs, and the final image presented to the eye is erect. The length of a Galilean telescope is calculated by:

$$D_t = f_o - f_e, \tag{3.23}$$

c) Terrestrial: Consists of positive objective and ocular lenses with an erecting lens between both. The erector re-images the image formed by the objective into the focal plane of the eyelens. The final image presented to the eye is erect. The final magnification of the terrestrial telescope is the product of the magnification of the telescope without the erector, and the linear magnification of the erector system:

$$M = -\frac{f_o}{f_e}.\frac{s_{e2}}{s_{e1}}, \qquad (3.24)$$

where s_{e1} is the distance from the back focal length $f_1$of the objective to the erector, and s_{e2} is the distance from the erector to the front focal length f_2 of the ocular.

If a field lens is placed exactly at the internal image of a telescope, it has no effect on the power, but it bends the ray bundles back toward the axis so that they pass through the eye lens. In this way the (FOV) may be increased without increasing the diameter of the ocular. The exit pupil is shifted to the left by the introduction of a positive field lens [21].

In an off-axis telescope, a beam of light entering it would be deviated by an angle that depended upon the focal length of the lenses and their relative displacement. If we have an array of many of these telescopes, the collimated incident beam could be divided in an array of smaller beams which would converge to a common focus, depending on the parameters of the lenses of the array.

3.7 Multi Aperture Imaging Optics

There are some parameters that are specific for multi aperture setups and others that apply for every single channel.

Optical channels

The structure of a two-dimensional array of K_x times K_y individual optical channels conforms a multi aperture optical system.

An optical channel is defined as the axial assemblage of at least one aperture stop together with at least one focusing element, usually a lens or a set of them, and a spacer for the related propagation length to the image plane. Each channel is associated with a two-dimensional partial image of n_x x n_y pixels. In case of a square partial image, the number of pixels is $n_x = n_y = n_g$. The physical edge length of the square partial image is [21]:

$$l_p = n_g \,.\, p_{px}, \tag{3.25}$$

Where, p_{px} is the pixel pitch of the image sensor.

The number of pixels in the final image is defined by N_x and N_y along the *x*- and *y*-direction, Respectively, these concepts could be better understood by looking at Fig. 2.9a. The number of object sampling intervals is related to the number of optical channels in x and y and to the ratio of the total pixel number and the number of pixels per partial image with the following equation:

$$K_{x,y} = \frac{N_{x,y}}{n_{x,y}}, \tag{3.26}$$

Conventionally, The K_x x K_y partial images are arranged in a regular Cartesian array with equal pitch p_k along the *x*- and *y*- direction (see Fig.2.9b). So, the 1D optical fill factor in the image plane is defined as:

$$\Gamma = \frac{l_p}{p_k}, \tag{3.27}$$

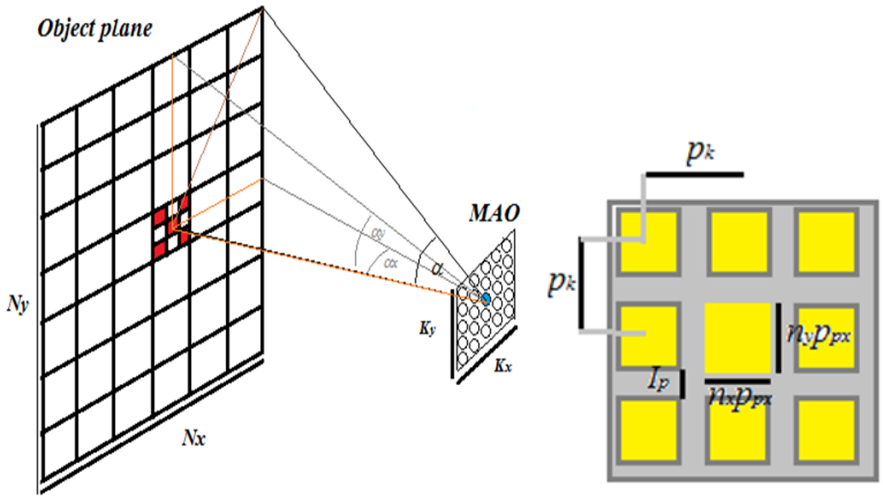

(a) (b)

Figure 3.9: (a) Parameters of multi aperture optical systems, relationship between the optical channels, object sampling intervals and the total number of pixels. (b) Parameters in the image plane.

Field of view

The half cone angles of the field of view along the horizontal α_x and vertical direction $\alpha_{y,}$ define α according to trigonometric relations:

$$tan^2\alpha = tan^2\alpha_x + tan^2\alpha_y, \tag{3.28}$$

The relationship between the horizontal to the vertical edge length of the image can also be calculated with the number of pixels:

$$\frac{N_x}{N_y} = \frac{tan\,\alpha_x}{tan\,\alpha_y}, \tag{3.29}$$

Using Eq. (3.30) and Eq. (3.31) we can calculate:

$$\alpha_x = \arctan\left[\frac{\tan(\alpha)}{\sqrt{1+\left(\frac{N_y}{N_x}\right)^2}}\right]; \qquad \alpha_y = \arctan\left[\frac{\tan(\alpha)}{\sqrt{1+\left(\frac{N_x}{N_y}\right)^2}}\right], \tag{3.30}$$

The segmentation of the FOV by multiple optical channels can be made in different ways, which led to different types of multi aperture optical systems. The different systems are: Apposition type, Electronic stitching of segments, Optical stitching of segments and Multi aperture super-resolution.

Sampling angles

The interommatidial angle $\Delta\Phi$ that is found in artificial compound eyes represents the angular offset between the optical axes of adjacent channels:

$$\Delta\Phi = \arctan\left(\frac{\Delta p_k}{f}\right), \tag{3.31}$$

where:

$$\Delta p_k = p_L - p_k, \tag{3.32}$$

and p_L is the pitch of the microlenses and p_k is the pixel pitch.

The interpixel angle $\Delta\Phi_{px}$ is the offset angle between two adjacent pixels of a single channel when projected in object space, it is defined by:

$$\Delta\Phi_{px} = arctan\left(\frac{p_{px}}{f}\right), \tag{3.33}$$

The effective sampling angle $\Delta\Phi_{eff}$, is the smallest angular sampling interval in object space, and it could be created by the effect of a pair of different optical channels with an effective pitch difference Δp_{eff}. It is defined by:

$$\Delta\Phi_{eff} = \arctan\left(\frac{\Delta p_{eff}}{f}\right), \tag{3.34}$$

4 Artificial Apposition Compound Eye used as an Imaging System

Technological advances in manufacturing and material science have allowed the development of micro-optical systems. Many of them are already incorporated in common use devices such as micro cameras, spy cameras, micro-scanners [1,22-25]. In this miniaturizing trend, non-conventional optical systems offer an alternative to build very compact size imaging systems with a reliable quality that could be used in many applications like chip cards, clocks, automobile industry, etc. [26]. Herein, we present the designs of an ultra-thin planar apposition compound eye used as a camera objective based in the concept of micro cylindrical doublets (MCD). The MCD can be considered as the optical unit of apposition compound eyes [24-25]. We based our work in the anatomy and function of the natural apposition compound eye that some insects have, and in previous papers from Duparré and coworkers [23-27] and Tanida and coworkers [28-30].

We present here the basic concepts of the apposition compound eye, we evaluate the optical performances of the MCD for three different refractive indexes for the first lens element, and finally we show the parameters for the optical design of the objectives. For the design process, we calculated the dimensions of the elements of the MCD, like aperture diameter D, Radius of curvature R_c, and refractive indexes n_1 and n_2. We evaluated the optical performance of the element and we observed the aberrations and the spot diagram produced by the MCD.

Following the OSLO design parameters, we introduced opaque walls between channels, and we considered their thickness to be able to calculate the final number of units N that would integrate the objective. We had to take in consideration the detector size. We used a small piece of detector that consisted of 500 pixels, each of 5 μm. and for a second case we used 5000 pixels. We continued, with the calculation of the pinhole diameter d, the acceptance angle $\Delta\varphi$, the FOV, the pinhole pitch P_p, the pitch difference ΔP, the interommatidial angle $\Delta\Phi$, the sampling frequency ν_s, and the pinhole position X_N. The parameters that give more information about the optical performance of the system are $\Delta\varphi$, $\Delta\Phi$ and ν_s.

4.1 Apposition Compound Eye Visual Unit

Apposition eyes consist of an array of lenses and photoreceptors. The combination of one lens and one photoreceptor forms a unit called ommatidium. Fig.4.1 shows pattern diagrams for illustrative purposes of how a natural apposition compound eye works. Each small lens focuses light from a small solid angle $\Delta\varphi$ of object space onto a single photoreceptor. The angular object space is sampled with the interommatidial angle $\Delta\Phi$. The field of view (FOV) of this imaging system is determined by the radius of curvature R_c and size of the eye [25].

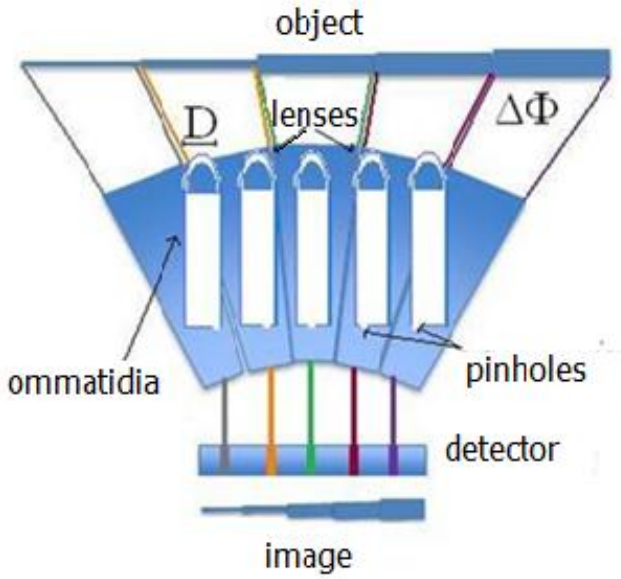

Figure 4.1 Diagram of object sampling and image formation by the natural and artificial apposition compound eyes, where: $\Delta\Phi$ interommatidial angle, and *D* diameter of the microlenses. The planar array with MCD with pinholes that act as "Ommatidias" in the AACE is shown [31].

4.2 Artificial Apposition Compound Eye with Spherical Micro-Cylindrical doublets (MCD)

We have designed three artificial apposition compound eyes (AACE), composed by multiple MCD units, with a thickness of the system that will not be more than 350 μm. The objective consists of a polymer microlens array over a glass substrate

(between the channels are opaque walls), and on the edge, a metallic plate with a pinhole array [25]. The image is recorded by a photodetector just after the pinhole array.

The most important use of the AACE is to form an ultrathin objective with very low volume, high sensitivity and that gives images with acceptable resolution.

4.2.1 **Description of the system and designing issues**

To design the AACE we considered [24-26], the angular resolution (ΔΦ), which is defined by the interommatidial angle;

$$\Delta\Phi = \arctan\left(\frac{\Delta P}{f}\right) \tag{4.1}$$

where ΔP is the pitch difference, and f is the microlens focal length (see Fig. 4.2).

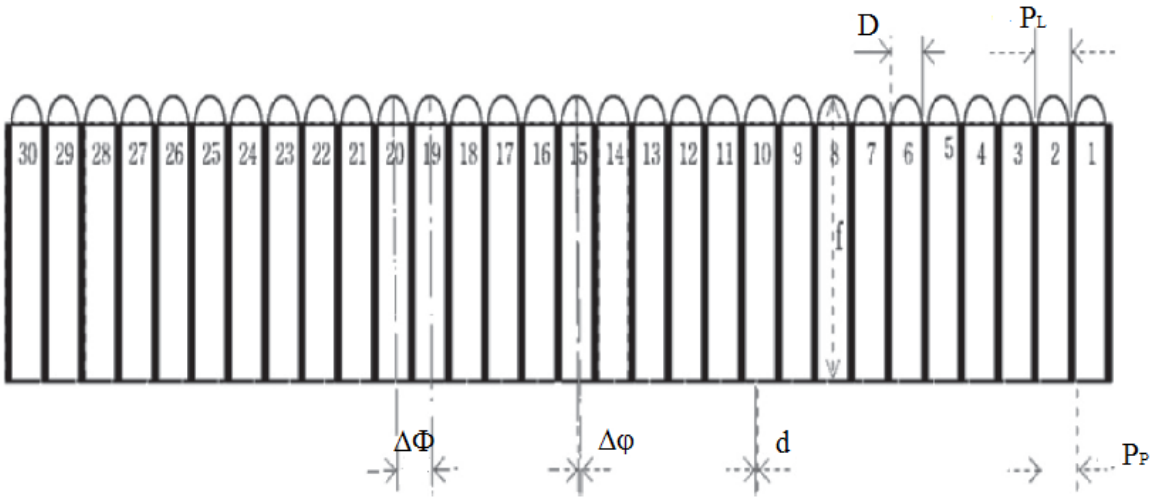

Figure 4.2 Planar artificial apposition compound eye objective in one dimension, where: ΔΦ interommatidial angle, Δφ acceptance angle, D diameter of the microlens, f focal length, d pinhole diameter, P_P pinhole pitch and P_L microlens pitch [31].

The acceptance angle ($\Delta\varphi$) of one ommatidia is calculated using Eq. (3.4), where $\Delta\varphi$ corresponds to $\Delta\varphi_{nat}$., where λ is the wavelength of light coming from the source, d is the pinhole diameter, and D is the microlens diameter .

The pinhole diameter d is calculated by means of Airy disk

$$d_{Airy} = 2.44\frac{\lambda f}{D}, \tag{4.2}$$

the pitch difference is given by

$$\Delta P = P_L - P_P, \tag{4.3}$$

the pinhole array for an objective with N channels in one dimension is calculated with

$$P_P = a\left\{1 - \left[\frac{N}{(N+1)}\right]\right\}, \tag{4.4}$$

where a is the detector length. We based our calculations in a detector unit of 500 pixels with a pixel size of 5 μm. The position of the pinholes can be calculated according to the position of the lens [9].

a) Measuring from the left side:

$$X_N = N_L \Delta P, \tag{4.5}$$

where X_N is the position of the N pinhole measured from the left side, N_L is the corresponding MCD unit and ΔP is the pitch difference.

b) Measuring from the right side:

$$Y_N = N_L P_p, \tag{4.6}$$

where Y_N is the position of the N pinhole measured from the right side, N_L is the corresponding MCD unit and P_p is the pinhole pitch.

4.2.2 **AACE Parameters with Microlens and Pinhole Arrays with a planar configuration**

The most important equations used for the design of the AACE objectives, are the ones presented above. The pinhole's position depends on the area that is not covered by the opaque walls used to avoid crosstalk between channels. Table 4.1 presents the design parameters of three different objectives. The optical performance of the AACE can be estimated by the values of the interommatidial and acceptance angles, using the Nyquist criterion, and the image's quality depends of the value of the sampling frequency.

Table 4.1 Parameters of the Artificial Apposition Compound Eye AACE objectives [31].

Design Parameters	AACE1	AACE2	AACE3
f-number F#	3.3	3.3	3.3
Number of channels N	25 x 25	30 x 30	30 x 30
(for a detector with 5000 pixels)	250 x 250	300 x 300	300 x 300
Aperture diameter D (μm)	70	65.5	68.5
Radius of Curvature R (μm)	102.4	94.5	119.4
Focal length f (μm)	340	320	320
Microlens pitch P_L (μm)	100	84	84
Pinhole diameter d (μm)	2.8	2.7	2.7
Refractive Index microlens (n_1)	1.4370	1.4370	1.5638
Refractive Index spacing structure (n_2)	1.5168	1.5168	1.5168
Field of View FOV (deg)	19	14.71	14.71
Thickness of opaque walls w_{th} (μm)	30	18.5	15.5
Interommatidial angle ΔΦ (deg)	0.4718	0.4834	0.4834
Acceptance angle Δφ (deg)	0.673	0.937	0.937
Sampling frequency ν_s (cycle/rad)	44.27	59.26	59.26

4.3 Artificial Apposition Compound Eye with Aspherical Micro-Cylindrical doublets (AMCD)

Spherical aberration could decrease its value by aspherizing the first surface of the MCD. By means of ALSIE (Automatic Lens design by Solving InEqualities) [32], the numerical value of the aspherical coefficients of the surface general equation could be calculated.
The aspherical surface general equation is given by [33]:

$$x = \frac{cs^2}{1+\sqrt{1-c^2(k+1)}} + h_2 s^2 + h_4 s^4 + h_6 s^6 + \cdots, \qquad (4.7)$$

where c is the curvature, $s^2=y^2+z^2$, k is the conic constant, and h_i are the aspherical coefficients.

During the automatic design, all aspherical coefficients h_i were allowed to vary one by one, but only a solution for h_4 was found. The value of h_4 is -0.40978E-07. Table 4.2 shows the parameters of the initial micro cylindrical doublets used for the aspherization performed by ALSIE.

The first surface is of the microlens, the second surface is the planar second surface of the microlens and the first surface of the glass substrate of the cylindrical microlens. The third surface is the last surface of the glass substrate. The focal length of the third surface is the back focal length before the image plane.

Table 4.2 Parameters of the initial MCD before aspherization by ALSIE, where (*F*/ = 2.8) [34].

Surface #	1	2	3
Radius of Curvature *R* (μm)	118	∞	∞
Focal length *f* (μm)	20	300	25.7
Refractive index *(n*) (d-line)	1.50013	1.52341	1.00000

Fig. 4.3 shows the spot size diagram with the spherical and aspherical MCD respectively. The spot size is reduced considerably with the aspherical MCD. If we take a look in the aberration error merit function, we could see an improvement of more than 200%.

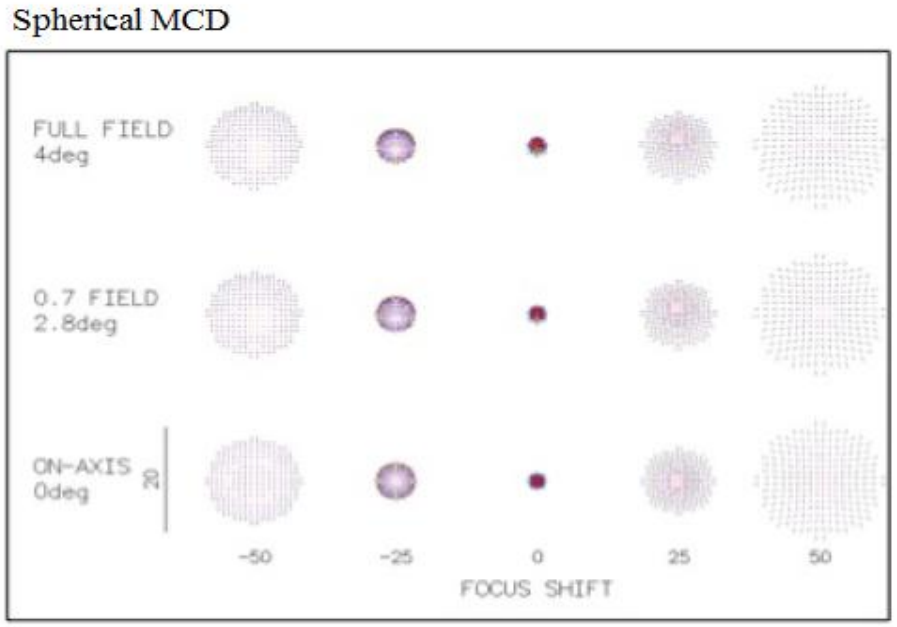

(a)

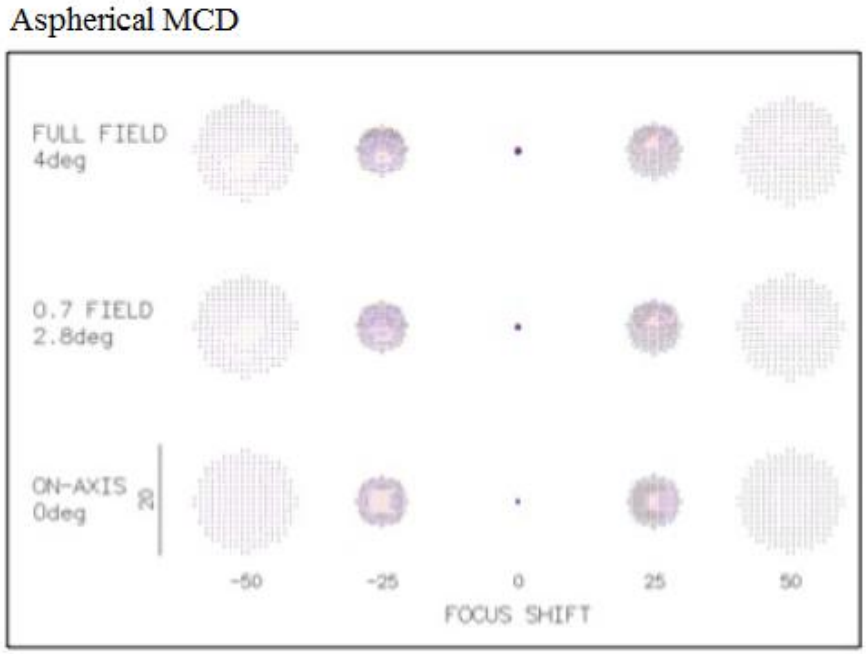

(b)

Figure 4.3 Spot diagram for the a) spherical and b) aspherical MCD respectively. It is possible to see how the spot size is drastically reduced [34].

In Fig. 4.4 the spherical aberration is plotted against the entrance pupil's height. It could be clearly seen how the spherical aberration reduces its value. The optical aberrations are highly improved.

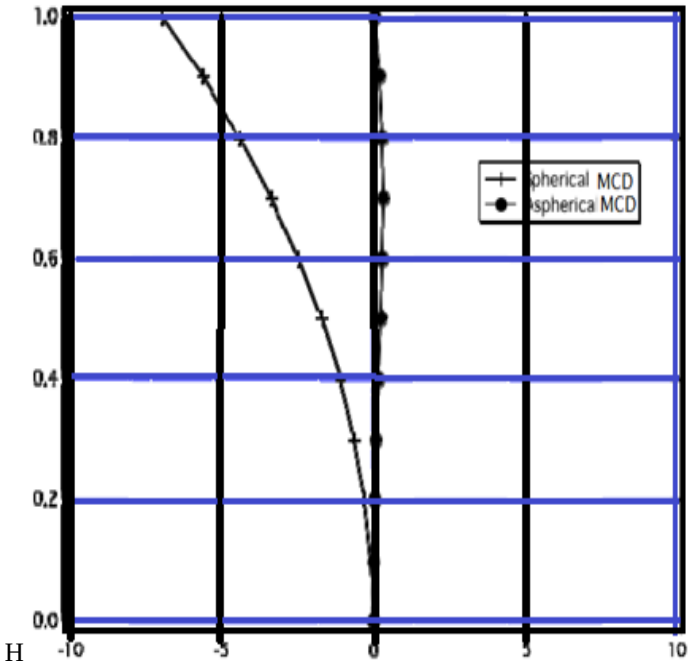

Figure 4.4. Spherical aberration for the a) spherical MCD and b) aspherical AMCD respectively [34].

4.4 Simulation of the Artificial Apposition Compound Eye complete system.

The quality of the image formed by the AACE objective with spherical micro cylindrical doublets was simulated in Zemax©, using a 2D array. The simulation was performed in the non-sequential mode, and the MCD were placed in a square array where twenty five units were distributed in the x and y axis. Fig. 4.5a shows the shaded model of the AACE objective seen in a side view from the z axis. Fig. 4.5b shows the image displayed in the detector without using the pinhole array.

The source used for the simulation is non-coherent. Light coming from an object point at infinity was collimated by a lens to achieve a planar wave, and it was propagated through the spherical MCD2 array. Each micro cylindrical doublet imaged a point. The pinhole array was not introduced in the first simulation.

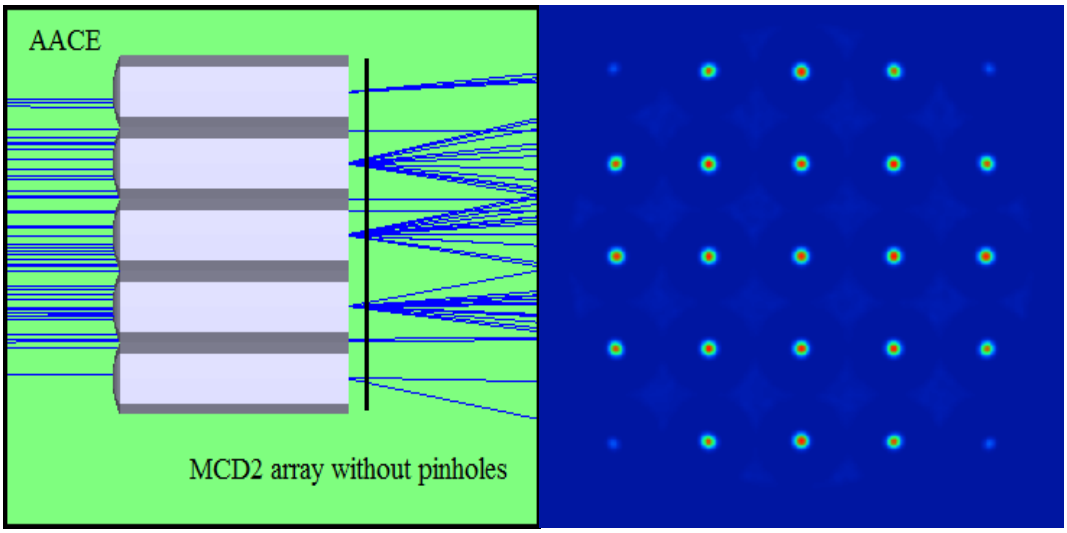

Figure 4.5. (a) Shaded model side view of the MCD2 array used in the AACE objective without introducing the pinhole array. (b) Detector view of the object point source placed at infinity.

A simulation of the AACE with the aspherical MCD2 and with pinholes was done. The results are shown in Fig. 4.6a and Fig. 4.6b. If the position of the pinholes were displaced according to[19], the image presented in the Fig. 4.6b. would resemble a unique image composed of many points pasted together like a mosaic.

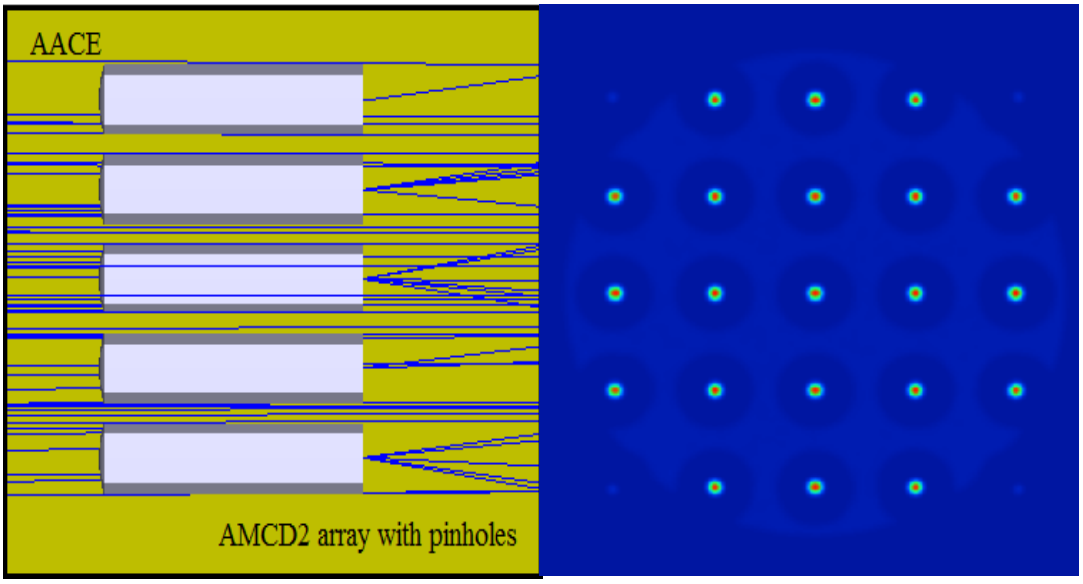

Figure 4.6. (a) Shaded model side view of the aspherical MCD2 array used in the AACE objective with the pinhole array. (b) Detector view of the object point source placed at infinity and a restricted FOV.

5 Artificial Superposition Compound Eye as an Image Forming Objective and as a Free-space Optical Interconnector

5.1 Artificial Compound eye based on the Refractive Superposition Compound Eye.

5.1.1 Working Principle of the Superposition Compound Eye (SCE)

Superposition compound eyes (SCE) consist of multiple off-axis optical elements that operate together to form a single deep-lying image. This kind of eyes present an array of individual units that work like micro telescopes, which are placed one next to the other. Each one of these units images a small section of a large field of view (FOV) in a single point. The partial images formed by the multiple channels will superimpose at the image plane [12,14]. In order to achieve this, a clear zone is needed, which makes the system longer in comparison with apposition, but it has the benefits that is much more light-sensitive due to a larger effective pupil, and the resolution in the case of aberration-free "*ommatidia*" could be about ten times higher. See (Fig. 5.1).

Dennis Gabor proposed an optical system that simulated a natural (SCE) [35]. The working principle consists in the formation of an erect unique image by a special arrangement of microlenses arrays. This optical configuration is known as Gabor Superlens (GSL), and it is described in Fig. 5.2.

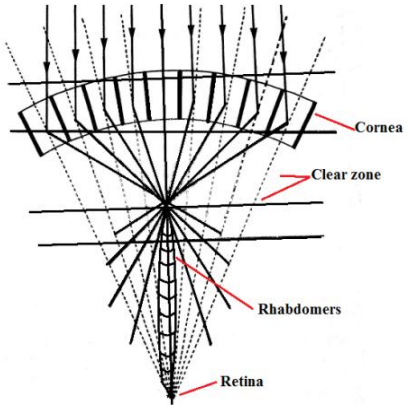

Figure. 5.1 Light coming from an object is focused at the different focal points of the first lenslets which are located after the Cornea. The information at these points will be transferred by the crystalline cones, so that light will be redirected to be focused in one Global Point that is located after the Clear zone [14].

5.1.2 Gabor Superlens (GSL)

Gabor Superlens (GSL) is an optical system consisting of a pair of microlens arrays in which there is a slight difference in pitch. The displacement of one lens with respect to its partner causes the bundle of light passing through a pair of lenses to be deviated in such way that all bundles converge to a common point and the system behaves like a Superlens (which is a device that has resolution capabilities that go substantially beyond the diffraction limit). Gabor used this configuration with a pair of microlens arrays separated by the sum of their focal lengths. The GSL is formed by an array of off-axis micro telescopes in which a beam of light entering the system would be deviated by an angle that depended upon the focal lengths of the lenses and their relative displacement. The deviation varied in such a way that a collimated incident beam would be divided into an array of smaller beams which would converge to a common point or position of minimum confusion. The image formed is erect and its position depends of the object distance.

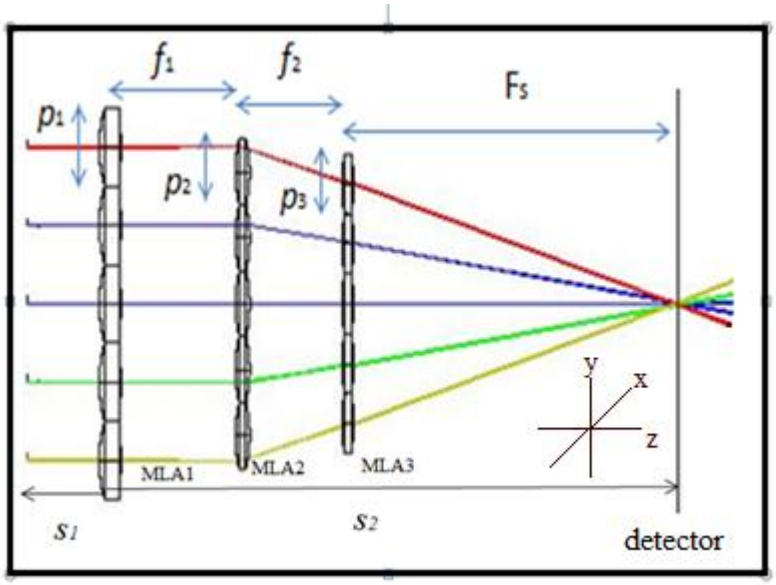

Figure. 5.2 Configuration of a Gabor Superlens. The pitches (p_1, p_2, p_3) and focal lengths (f_1, f_2) are shown for each microlens array.

In Fig.5.2 a Gabor Superlens configuration using microlens arrays is shown. Three microlens arrays (MLA1, MLA2 and MLA3) are used to superimpose the image. MLA2 is located at the focal length of MLA1, and MLA2 is related to the focal length of MLA3, (f_1 and f_2 respectively). In this configuration, p_1 is the pitch of the microlens array MLA1, p_2 is the pitch of the microlens array MLA2 and p_3 is the pitch of the microlens array MLA3, f_1 is the focal length of the MLA1, f_2 is the focal

length of the microlens array MLA3, and F_S is the back focal length of the complete system [36]. The microlens array MLA2 could be used as a relay array.

A GSL has to fulfill the following rules:

a) **Back focus (F_s) for an object at infinity**: All rays from the same object point superpose in a common point in the image plane [36]:

$$\frac{1}{Fs} = \left(\frac{f1}{f2}\right)\left[\frac{1}{(f1+s1)}\right] + \left(\frac{p3}{p1}\right)\left[\frac{1}{(f2-s2)}\right], \quad (5.1)$$

where s_1 and s_2 are the object and image distance respectively.

b) **Back focus (F_s) for a finite object**: The back focal length F_s for a finite object distance can be calculated, the height of a ray in the image plane must be independent of the channel through which it passed [36-38].

$$F_s = f_2 \frac{p_1}{p_1 - p_3}, \quad (5.2)$$

5.2 Design of an artificial superposition compound Eye objective (ASCE).

There have been some previous models of artificial superposition compound eyes. [29,37-42]. In these proposals numerous channels of the whole array contribute to the formation of one erect image in the image plane. These systems are formed basically by an arrangement of micro-lenses that allow the optical superposition of micro-images transferred by the different channels. The devices have a collective bandwidth product.

The optical design procedure of the ASCE consisted in the calculation, simulation and optimization of individual units that worked as *"ommatidias",* with the configuration of off-axis Micro Keplerian Telescopes MKT. Afterwards the ASCE complete system was simulated using the GSL configuration. For an alternative model, the introduction of a Micro triplet lens array in the relay array was made to improve the image quality.

In order to fulfill the Gabor conditions for the simulation of the global system Eq. (5.1) and Eq. (5.2) were used. Fig. 5.3a shows a side view of a MKT with two lenses. The plots of some of the optical aberrations are shown. Fig. 5.3b shows a side view of a MKT with three lenses. The plots of the optical aberrations are also shown. The simulations were done using OSLO Premium and the Optimization was done using the Slider Wheel.

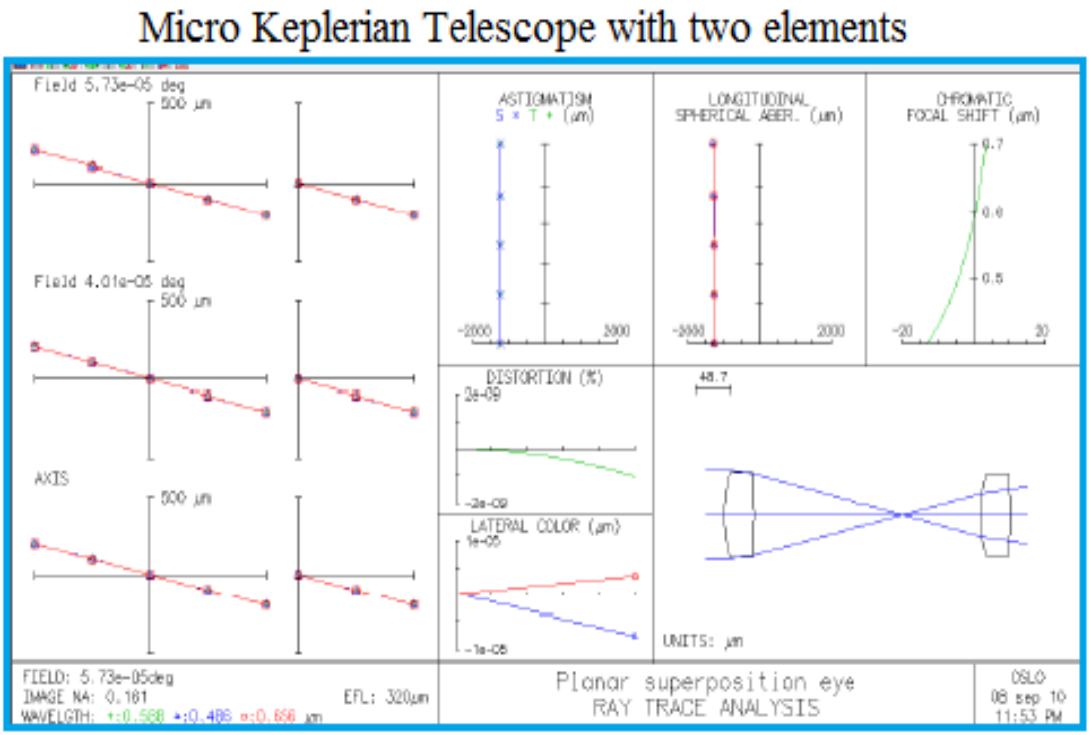

(a)

Figure 5.3 (a) Simulation of the MKT using OSLO Premium with two lenses and plots of the main optical aberrations.

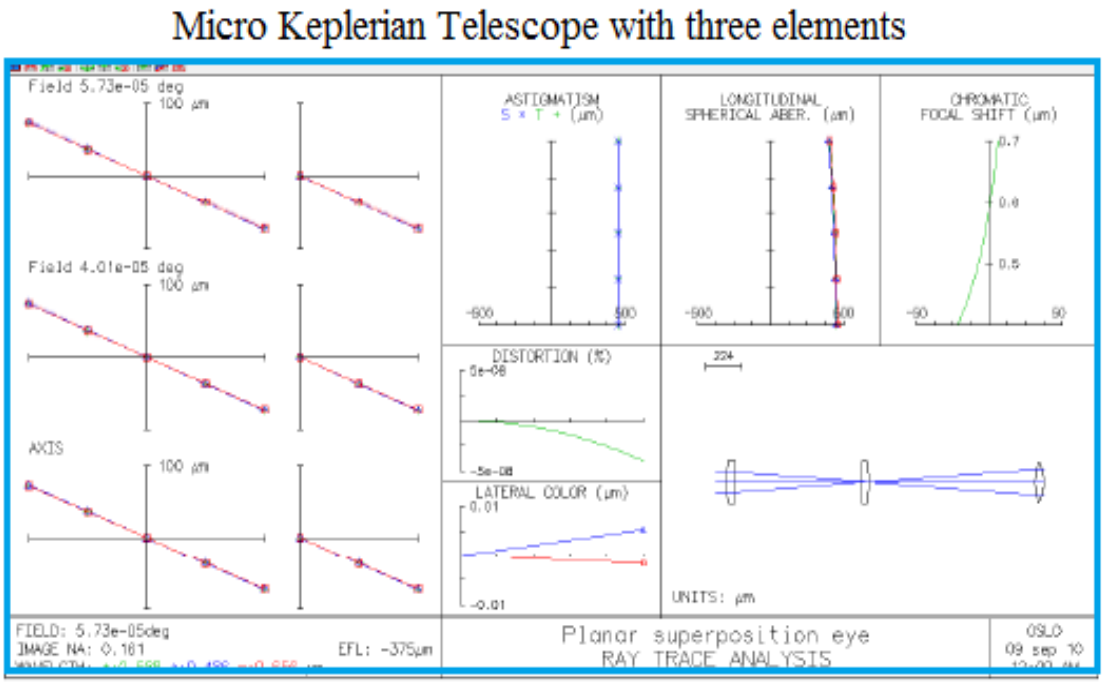

(b)

Figure 5.3 (b) Simulation of the MKT using OSLO Premium with three lenses and plots of the main optical aberrations.

5.2.1 **Simulation of the ASCE Objective**

The simulation of the ASCE objective was done using the non-sequential mode of Zemax. The pitch calculation of the three microlens arrays is extremely important to achieve the GSL configuration. The placement of the individual microlenses in the "x", "y" and "z" axis must be carefully done (see Fig. 5.2) .The simulation was performed with different object points for each channel.
Table 5.1 shows the optical parameters used for the simulation with the three microlenses arrays (MLA1, MLA2 and MLA3).

Table 5.1 Optical Parameters of the Microlenses arrays used in the ASCE [43].

Corresponding lens	Surface #	Radius of Curvature R_c [μm]	Thickness t [μm]	Refractive Index $[n_i]$	Pitch $[p_i]$	Focal length $[f_i]$
Object	1					
MLA1	2	162	30	1.563840	100	190
	3	-650		1.000000		
MLA2	4	165	20	1.7847 20	84	
	5	-164		1.000000		
MLA3	6	386	15	1.952500	66	422
	7	-282		1.000000		

In Fig. 5.4 and Fig. 5.5 it is possible to see the performance and the image quality of the ASCE simulated with simple MKT. There is only one erect image formed at image plane.

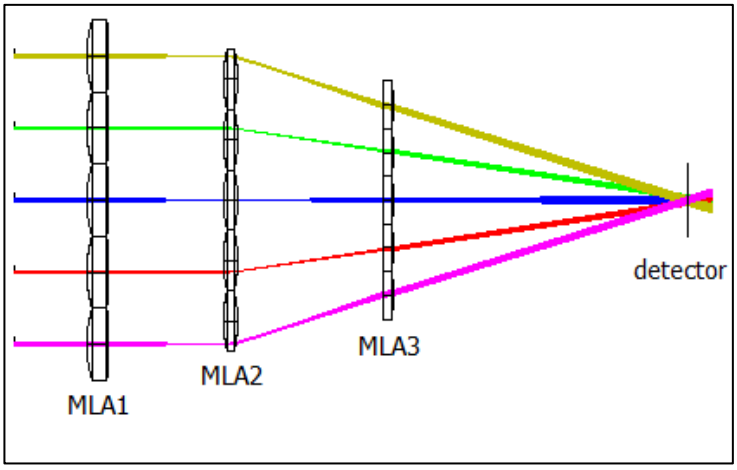

Figure. 5.4 ASCE Simulation with the three simple Microlens arrays. Raytrace performed with Zemax [44].

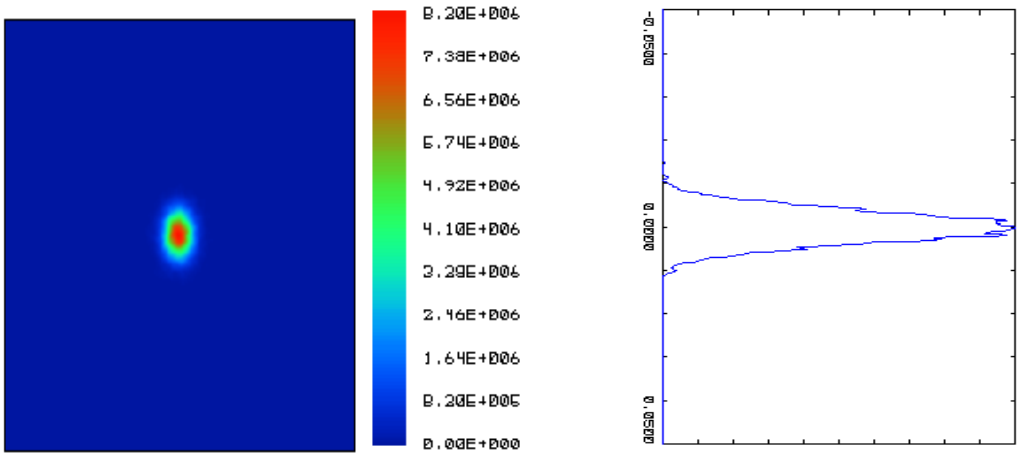

(a) (b)

Figure. 5.5 (a) Detector view of the image produced by the ASCE with simple arrays. (b)The incoherent irradiance profile of the image is shown. The intensity profile is measured in watts/cm^2.

5.2.2 **Simulation of the (ASCE) using micro triplets in the relay array**

The introduction of a micro triplets array in the second MLA2 instead of using a simple micro lenses array gave us the possibility to improve the image registered by the detector. The convenience of using the micro triplets array is that the thickness of the objective is reduced. The configuration of the ASCE objective with the micro triplets is shown in Fig. 5.6 and the detector view is shown in Fig. 5.7. Both simulations were performed in Zemax.

Table 5.2 shows the optical parameters used for the simulation of the ASCE using a micro-triplet relay array as MLA2.

Table 5.2 Optical Parameters of the ASCE with a micro-triplet relay array MLA2 [43].

Corresponding lens	Surface #	Radius of Curvature R_c [μm]	Thickness t [μm]	Refractive Index [n_i]	Pitch [p_i]	Focal length [f_i]
Object	1					
MLA1	2	162	30	1.563840	100	190
	3	-650		1.000000		
MLA2	4	165	10	1.497000	84	
microtriplets	5	165	20	1.784720		
array	6	-164	10	1.497000		
	7	-164		1.000000		
MLA3	8	386	15	1.952500	66	411
	9	-282		1.000000		

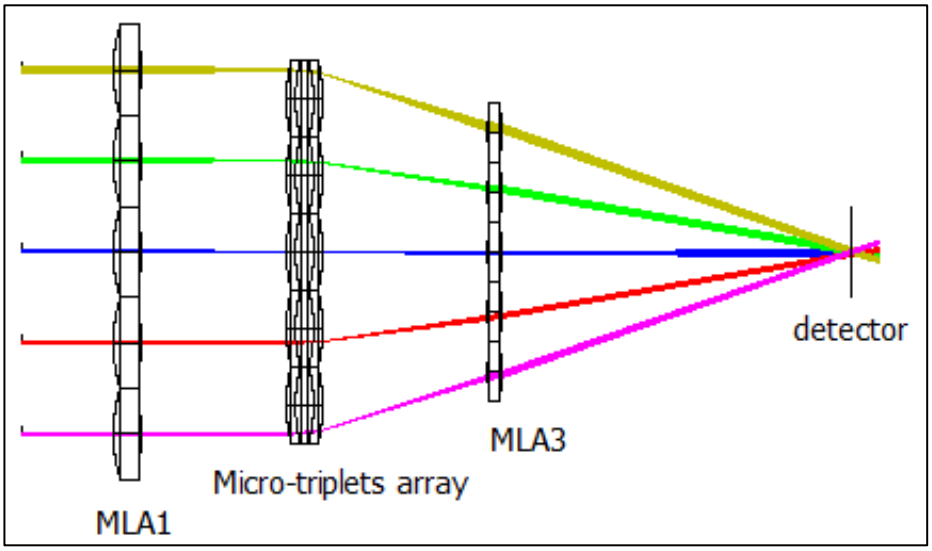

Figure. 5.6 ASCE Simulation with the micro triplets array in MLA2. Raytrace performed with Zemax.

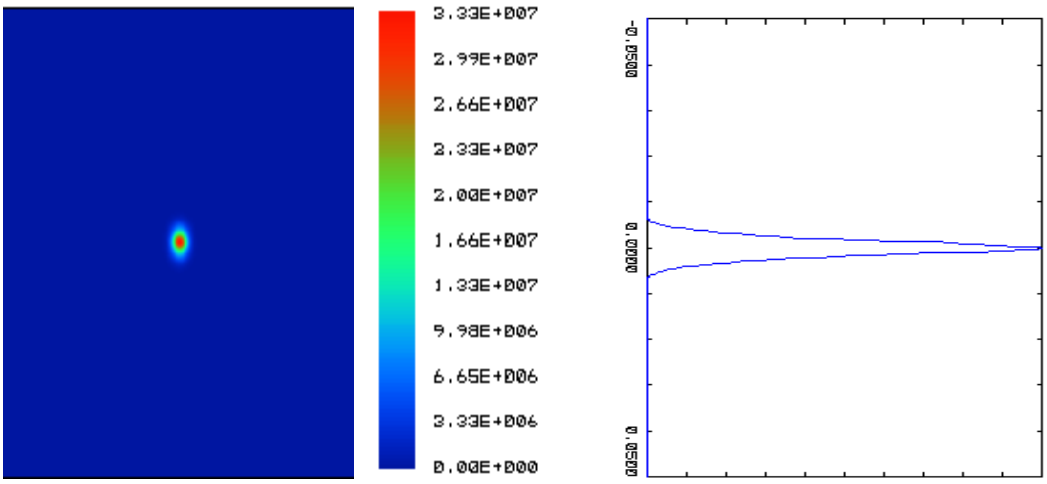

(a) (b)

Figure. 5.7 (a) Detector view of the image produced by the ASCE with a micro triplet array as MLA2. (b)The incoherent irradiance profile of the image is shown. The intensity profile is measured in watts/cm^2.

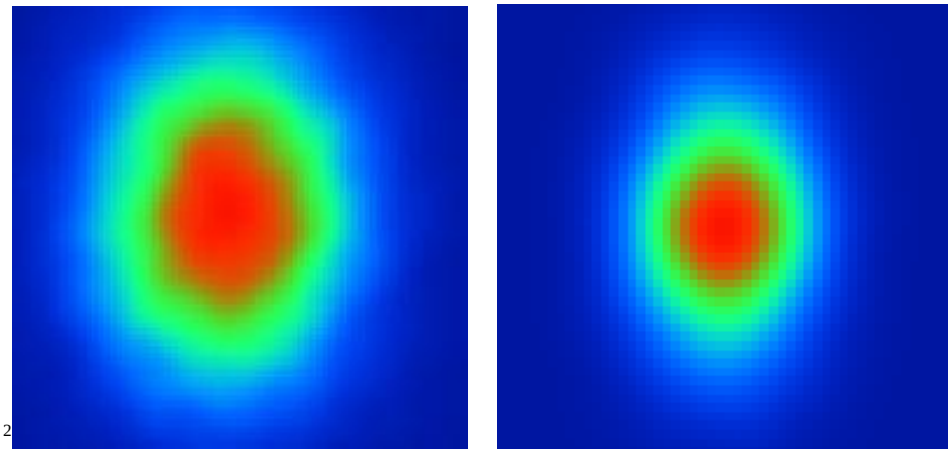

(a) (b)

Figure 5.8 Comparison between the detector views of (a) the image produced by the ASCE with simple arrays and (b) the ASCE with a micro triplet array as MLA2.

In Table 5.3 it is possible to see that the total thickness of the ASCE is reduced by introducing the micro-triplets array as MLA2. The number of channels is lower, and the image quality at the detector is highly improved according to the incoherent irradiance intensity distribution. See (Fig. 5.8)

Table 5.3 Comparison of the ASCE with an ASCE with a micro-triplet array [43].

Design Parameters	ASCE	ASCE with micro-triplets
F# number	2.6	2.6
Number of channels *N*	25 x 25	25 x 25
(for a 500 pixel detector)	250 x 250	250 x 250
Focal length of the system F_s (μm)	835	831

5.3 Design of an Artificial Superposition Compound Eye Objective using an array of micro-tunable lenses. (ASCETL)

After introducing a micro triplet array as relay array, the idea of using an array of liquid mircolenses that change their curvature arose. The optical design of an objective lens, inspired in the superposition refractive compound eye is presented. An array of micro-tunable liquid lenses that function by means of an electrowetting principle is included. The possibilities of changing curvature, optical power and focal length give our device the capability of having different image planes which can result in a zoom operation. A Gabor superlens configuration, with off-axis micro Keplerian telescopes used as "ommatidias", is used for the desired design.

5.3.1 Artificial Superposition Compound Eye Objective with Tunable lenses. *(*ASCETL)

5.3.1.1 Micro-optical arrays

For micro-optical systems, traditional simulation methods cannot be used strictly [45]. The imaging properties of the individual off-axis lens systems have to be considered. In micro-optical systems, (i) diffraction effects, due to the small size of the elements, gain importance, (ii) complete arrays of elements are often used, and (iii) the possibility of having a superlens effect must be considered.

5.3.1.2 System with variable focus

A zoom lens is an image-forming optical system with such properties that an axial movement of certain components will produce a change in the equivalent focal length of the system, while keeping the resultant image fixed with respect to the desired image plane [46].

The option of including an array of micro-tunable lens instead of a conventional MLA3 let us change the focal length and the optical power of each off-axis channel as a function of the change of curvature. The curvature of the lenses of the MLA3 array is modified when we have a voltage change (see Appendix 1).

Micro-doublets, which work by electrowetting were introduced. The complete systems with the variable curvatures in the second surface of the doublets were simulated. The parameters of the ASCETL with v=0 are shown in Table 5.4.

Table 5.4 Parameters of the complete system of the ASCETL including a micro tunable liquid lens array with *F/#* 2.6, object distance s_1=572 μm and image distance $s_{2=}$810 μm. The Radius of curvature for the tunable liquid lens is fixed for the simulation.

Corresponding lens	Surface #	Radius of Curvature R_c [μm]	Thickness t [μm]	Refractive Index [n_i]	Pitch [p_i]
Object	1	∞			
MLA1	2	162.0	30	1.563840	100
	3	-650.0	211	1.000000	
MLA2	4	165.0	20	1.784720	84
	5	-164.0	169	1.000000	
MLA3	6	∞	10	1.529440	66
	7	∞	10	1.337774	
	8	-100.0	442	1.000000	
Image Plane	9	∞	850		

i=1,2,3

We decided to use micro tunable liquid doublets in the MLA3 of the ASCETL system that have a plane first surface, a second variable surface and a third surface with a radius of curvature of -0.1 mm. The goal is that by the change of curvature, optical power, and variation of focal length of the liquid meniscus, a zoom effect would be achieved.

The complete system of the ASCETL only works with specific values of the curvatures of the second surface of the doublets. That is why different doublets that work by electrowetting applying a voltage between 100V to 115V were simulated in order to focus light in the way that it was needed.

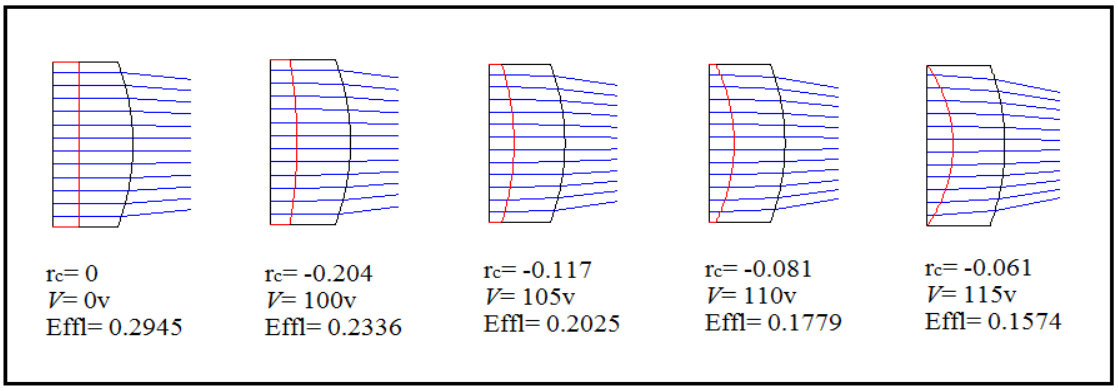

Figure 5.9 Tunable liquid microlens doublets with variable curvature in the contact surface due to electrowetting. Arrays of these units were used in the ASCETL as MLA3.

In Fig.5.9 the effective focal lengths of the doublets with variable curvatures in the contact surface of the meniscus were calculated by means of a simulation with Zemax.

5.3.2 Simulation of the ASCETL with the micro-tunable lenses

The simulation of the complete system was done using the Zemax non-sequential mode. The final design was simulated according to the Gabor configuration and with the array of micro-tunable lenses as MLA3 included.

To achieve the Gabor superlens condition, it is extremely important to calculate the correct pitch difference between the arrays, the position of the microlenses and the focal length variation in the "z" axis (see Fig. 5.2). The source conditions and its' location must also have to be considered. Due to these arrangements, each individual channel functions as an off-axis micro-telescope which works as the *"ommatidia"* of the SCE. A common focus at the image plane is formed by the corresponding units of the entrance pupil. Fig. 5.10- Fig. 5.14 show the results of the simulations of the ASCETL with the micro tunable lenses arrays used as MLA3. All rays were superposed in a common point to form a unique erect image. The spot registered in the detector is also shown.

Fig. 5.10a shows the simulation of the ASCETL with a micro-doublet array with v=0, used as MLA3. The radius of curvature of the contact liquid meniscus is infinite. The lens parameters are the ones presented in Table 5.4. The detector view is shown in Fig. 5.10b.

If a voltage difference is applied to the micro tunable array MLA3 the curvature of the conducting liquid changes and a variation of the focal length is noticed. The spot's size changes with the variation of the focal length. The irradiance intensity registered in the detector is measured in watts/cm^2.

In Figure 5.11a we show the simulation of ASCETL with a micro-doublet array. The voltage proposed to change the meniscus of the conducting liquid was of 100V. The lens parameters are the ones presented in Table 5.5. The detector view is shown in Fig. 5.11b.

Fig. 5.12a shows the simulation of ASCETL with a micro-doublet array. The voltage proposed to change the meniscus of the conducting liquid was of 105V. The lens parameters are the ones presented in Table 5.5. The detector view is shown in Fig. 5.12b.

Fig. 5.13a shows the simulation of ASCETL with a micro-doublet array. The voltage proposed to change the meniscus of the conducting liquid was of 110V. The lens parameters are the ones presented in Table 5.5. The detector view is shown in Fig. 5.13b.

Fig. 5.14a shows the simulation of ASCETL with a micro-doublet array. The voltage proposed to change the meniscus of the conducting liquid was of 115V. The lens parameters are the ones presented in Table 5.5. The detector view is shown in Fig. 5.14b.

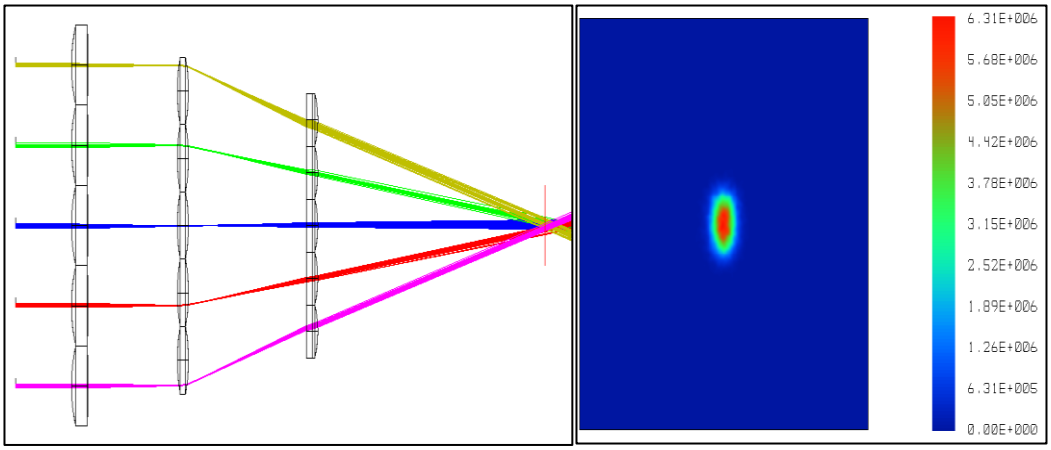

(a) (b)

Figure. 5.10 Simulation of ASCETL with an array of micro tunable liquid lens as MLA3 with v=0 V. a)Raytrace and b) detector view respectively.

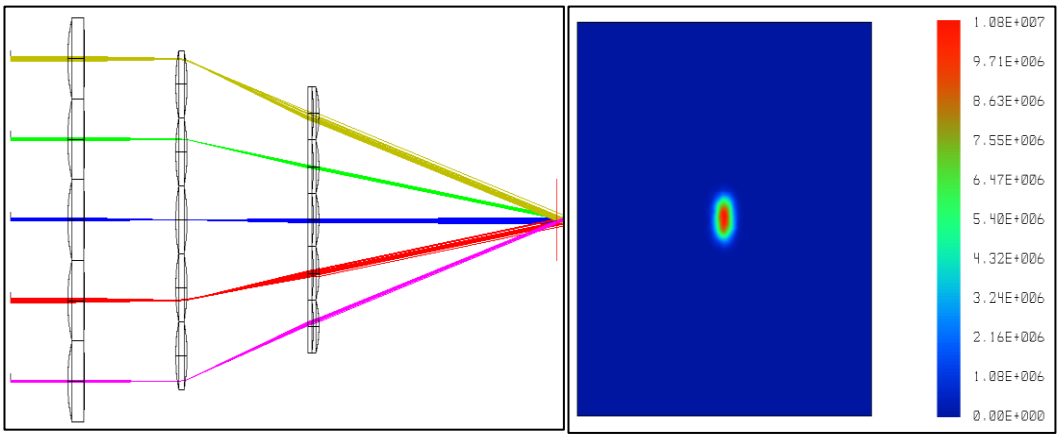

(a) (b)

Figure. 5.11 Simulation of ASCETL with an array of micro tunable liquid lens with v=100 V and a radius of curvature of -0.204 in the middle surface of the third array. A) Raytrace and b) detector view respectively.

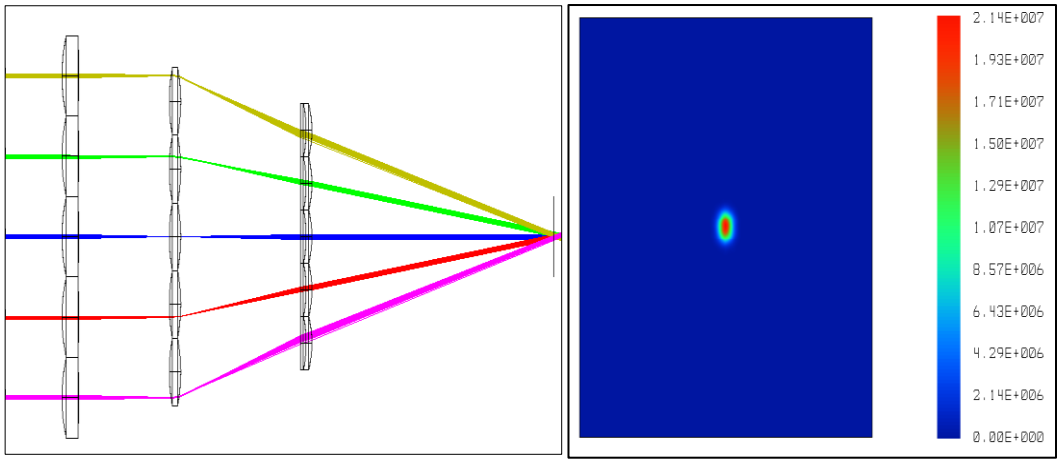

(a) (b)

Figure. 5.12 Simulation of ASCETL with an array of micro tunable liquid lens with a v=105V and a Radius of curvature of -0.117 in the middle surface of the third array. A) Raytrace and b) detector view respectively.

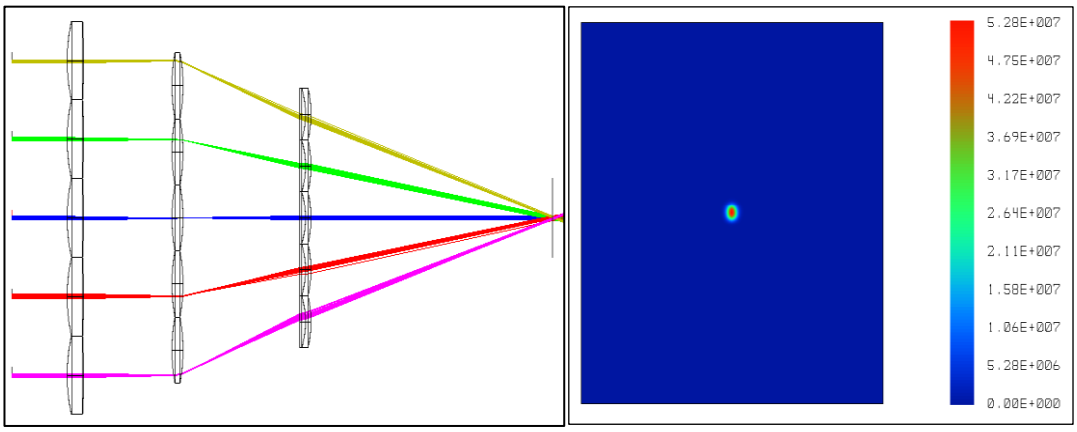

(a) (b)

Figure. 5.13 Simulation of ASCETL with an array of micro tunable liquid lens with v= 110V and a Radius of curvature of -0.081 in the middle surface of the third array. A) Raytrace and b) detector view respectively.

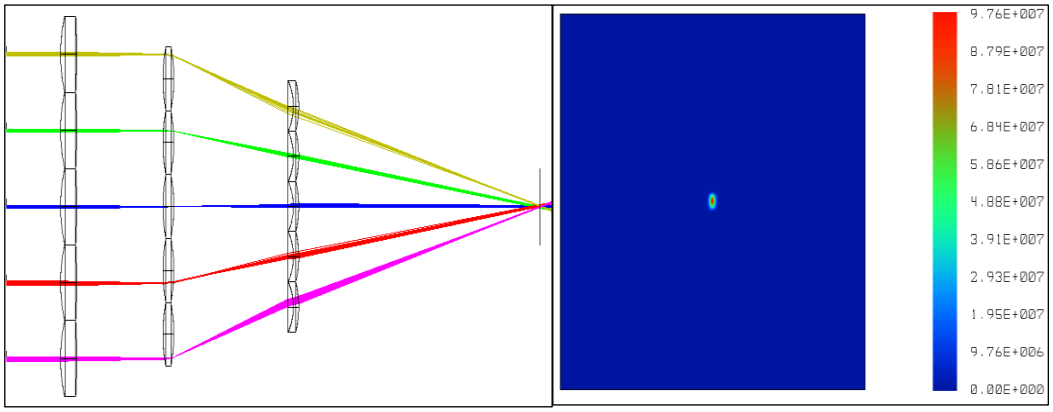

(a) (b)

Figure. 5.14 Simulation of ASCETL with an array of micro tunable liquid lens with v= 115V and a radius of curvature of -0.061 in the middle surface of the third array. A) Raytrace and b) detector view respectively.

Table 5.5 Parameters of the radius of curvature, focal length and Gabor focal length of the complete system with the micro tunable liquid lens used as MLA3. The variations of the parameters are functions of the change of voltage.

Voltage [V]	R_c Radius of Curvature [mm]	f focal length [mm]	F_{G1} *Gabor* focal length [mm]
100	-0.204	0.2324	0.86
105	-0.117	0.2025	0.87
110	-0.081	0.1760	0.88
115	-0.061	0.1543	0.89

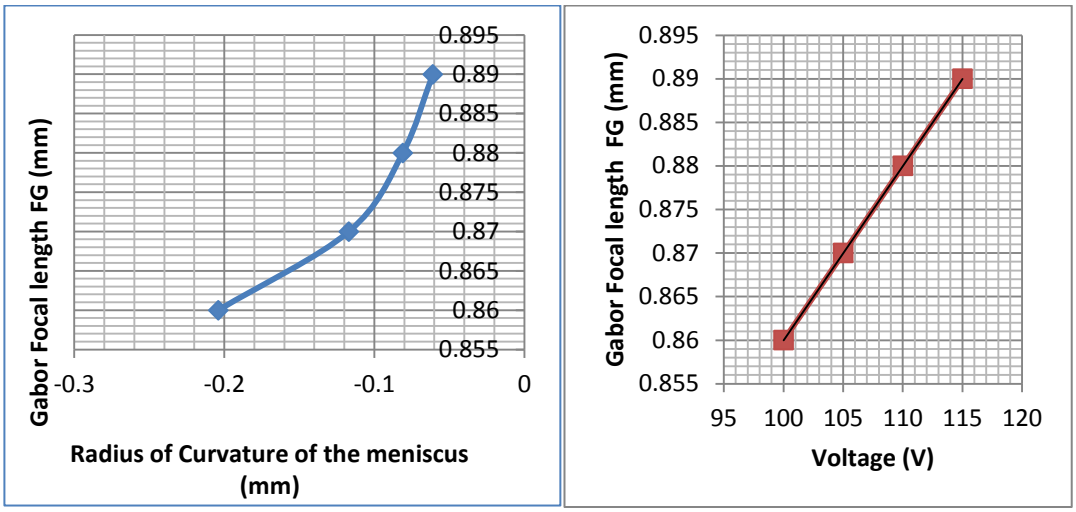

(a) (b)

Figure. 5.15 a) Plot of the Gabor Focal length vs. Radius of curvature of the meniscus of the contact surface of the liquid micro tunable lens. B) Plot of the Gabor focal length vs. the voltage applied to the micro liquid tunable lens.

In Fig. 5.15a it is possible to see how the Gabor Focal length of the complete system changes as a function of the variation of the radius of curvature of the meniscus of the contact surface of the micro liquid tunable lens. When the value of the radius of curvature increases, the focal length also increases. The size of the spot registered by the detector is also different. Fig. 5.15b shows how the Gabor focal length increases linearly when more voltage is applied to the micro tunable lenses array.

5.4 Design of Free-Space Optical Interconnects using two Gabor Superlenses

A design of free space optical interconnects based on multi aperture compound insect eyes by means of two Gabor Superlens is presented [47]. We propose an optical model that uses a set of microlens arrays in a GSL arrangement that performs the function of mixing multiple signals at one point (multiplexation) and a reverted GSL that separates the optical signal in different channels (demultiplexation). We call this pair of GSL a double Gabor Superlens system (DGSL).

The simulations of the double DGSL were performed with two different kinds of sources: coherent and non-coherent light. The DGSL design with coherent light and the diffraction grating, achieves only optical switching, and the DGSL design with the non-coherent source and the grating performs both optical switching and wave division multiplexing (WDM). DGSL optical parameters, ray tracing, simulations, and the optical performance of the signal after propagating through the multiplexer/demultiplexer devices are shown.

5.4.1 Historical Background

Integrated optics is based on the guiding of electromagnetic energy at optical frequencies, it was first proposed by S. E. Miller in 1969 and the two main areas that stimulated it's grow, were microwave engineering and thin-film optics [48]. It was the first integration method based on the electronic model. Light is guided in optical wires made of different materials like polymers, glass and some semiconductors. Waveguiding takes place in areas where the refractive index is higher than in the surrounding medium. The need of active components that manipulate light, include the development of smaller sources, modulators, couplers, detectors, etc. These components have as limitation that the computing speed is limited to electronic speeds, far slower than the possible all optical switching. For these reason passive components are commonly used for high speed applications [49].

The generation and rapid control of light requires that electric currents interact directly or indirectly with the optical energy. The main effort of developing an optical transmitter has been made using optical fibers. In the late 1960s, the attempt to make optical fibers that transmitted images rather than only intensity inspired the interest in inhomogeneous cylindrical lenses. The ability of an extended lens cylinder of imaging and re-imaging an object placed against its end at regular intervals along its

length could be used to convey as much information per unit cross-sectional area as an optical fiber; this device would be an expensive coherent light-guided array**.** Fletcher, Murphy and Young calculated the exact refractive index gradient of an image- transmitting lens cylinder. The relationship that they formulated is [50]:

$$n_r = n_0 sech(\pi r|2f), \tag{5.3}$$

where f is the focal length, n_0 is the axial refractive index and n_{rd} is the refractive index at a radial distance r_d from the axis. (Eq. 5.3) can be expanded in the following expression:

$$n_{rd} = n_0 \left(1 - \frac{1}{2}a_e^2 r_d^2 + \frac{5}{24}a_e^4 r_d^4 - \frac{61}{720}a_e^6 r_d^6 + \cdots + \frac{E_n}{(2n)!}(a_e n)^{2n} \ldots\right), \tag{5.4}$$

where $a_e = \pi/2f$, and E_n are the Euler numbers, If the terms after the r_d^2 term are ignored, the refractive index gradient profile becomes a parabola. This approximation has a connection with biological lens cylinders.

In 1968 a glass less cylinder was produced in Japan. The process consisted in heating a mixture of a thalium-rich flint glass in a molted salt of Potasium Nitrate (KNO_3) at 500^{o}C. In the present, plastic lens cylinders are made by heating a polymerized plastic (diallyl isophtalate) in a bath of a monomer (methylmethacylate), which results in a lens with a similar refractive index profile as the glass lenses. Artificial ommatidia had been fabricated by self-aligned microlenses and waveguides using polymer integrated optics. They consist of a microlens, a spacer, and a waveguide. This method combines: replica molding of elastomer microlenses and self-writing of waveguides in photopolymers [51]. The polymer used is polydimethylsiloxane. The estimated dimensions were around the 300 μm.

There have been some attempts to design free-space modulators, multiprocessors and multiplexors [49,52]. The common features of these designs include micro-lens arrays and diffractive elements. We propose a model that uses lens arrays that will perform multiplexation and demultiplexation of an optical signal and a model that uses a diffractive grating to make a selection of different wavelengths. These designs are inspired in the way that nocturnal insect eyes work. By means of studying the Refractive Superposition Compound eye, we have come to a proposal that will emulate its' behavior by means of having multiple optical channels. The proposed configurations, the optical designs, ray tracing, simulations, and the performance of the signal after propagating through our multiplexer/demultiplexer devices are shown.

5.4.2 Optical Communications

The function of a communication channel is to transport an optical signal from a transmitter to a receiver without distorting it. Optical Communication Systems (OCS) work in a frequency approximately of 100 THz. The potential at bit rates of these systems is about 10 Tb/s. This extremely large value of bandwidth has been a powerful reason for their development. There are two main groups of OCS: guided and unguided. In guided lightwave systems, the optical signal remains spatially confined. They use optical fibers due to their small power loss. The unguided OCS let the optical beam emitted by the transmitter spread in free space. The drawback of these systems is the deterioration of the signal due to scattering from foreign particles [48].

The dimensions of optical systems can be reduced by working on the interconnection between the components. A generic OCS consists of an optical transmitter, a communication channel and an optical receiver. The use of multiple channels over the same OCS gives a way of using the great capacity of bandwidth offered by optics. Each channel is transmitted by modulation of its own carrier. The main ways of transmission of multiple channels are: time-division multiplexing (TDM) and frequency division multiplexing (FDM), also called wave division multiplexing (WDM).

Multiplexers and demultiplexers are very important components in OCS. Multiplexers combine the transmitter outputs and demultiplexers separate them at the receiver end. In FDM, the carrier wave frequencies are separated enough that the optical spectra of modulated channels do not overlap in the frequency domain. The most widely used technologies to accomplish these tasks include diffraction gratings or arrayed-waveguide gratings (AWGs). One of the main categories of FDM systems are the point-to-point links. These systems work: by multiplexing together the output of several transmitters, each operating at its own carrier frequency (or wavelength). The multiplexed signal is launched into the optical fiber for transmission to the other end, where a demultiplexer routes each channel to its own receiver [48-49]. In Fig.5.15 a conventional guided point-to-point interconnects system is shown. Signals from different channels with different wavelengths are mixed in a guided multiplexer, and they propagate in a single common channel which consists of an optical fiber. The signals are recovered and separated in different wavelengths when they reach the demultiplexer.

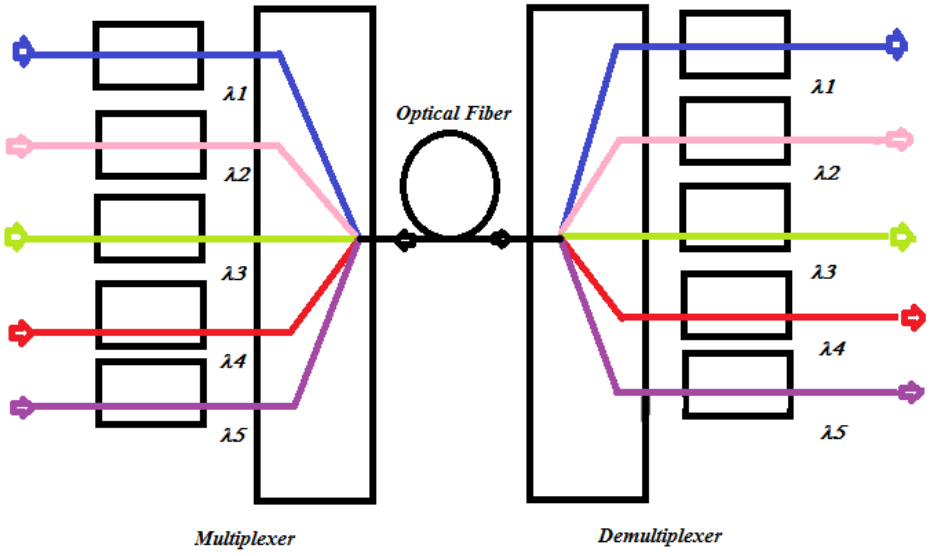

Figure. 5.16: A multichannel point-to-point optical interconnects system using an optical fiber [48]. Five different channels with different wavelengths (λ_1, λ_2, λ_3, λ_4 and λ_5) are multiplexed by a guided OCS and afterwards they are demultiplexed to recover the original signals.

5.4.3 Gratings

A diffraction grating is an arrangement which imposes on an incident wave a periodic variation of amplitude of phase, or both. It is an optical component with a periodic structure, which splits and diffracts light into several beams travelling in different directions. The directions of these beams depend on the spacing of the grating and the wavelength of the light so that the grating acts as the dispersive element. An idealized grating is made up of a set of slits of spacing d_g that must be wider than the wavelength of interest to cause diffraction, and with a plane wave of wavelength λ with normal incidence, each slit in the grating acts as a quasi point-source from which light propagates in all directions. After light interacts with the grating, the diffracted light is composed of the sum of interfering wave components emanating from each slit. At any given point in space through which diffracted light may pass, the path length to each slit in the grating will vary [53].

The light that corresponds to direct transmission is called the zero order, and is denoted $m = 0$. The other maxima occur at angles which are represented by non-zero integers m which can be positive or negative, resulting in diffracted orders on both sides of the zero order beam.

The grating equation for a transmission grating is [54]:

$$n_2 \sin\theta_2 = n_1 \sin\theta_1 + m\frac{\lambda}{\Lambda}, \quad (5.5)$$

where n_1 is the refractive index on the left of the grating and n_2 is the refractive index on the right, θ_1 is the incident angle and θ_2 is the exiting angle of the light leaving the grating, λ is the wavelength, Λ is the period of the grating, and m is the grating order.

5.4.4 Wave Division Multiplexing (WDM)

It is a technique by which two or more optical signals having different wavelengths may be simultaneously transmitted in the same direction over one optical fiber, and then be separated by wavelength at the distant end [48].

5.4.5 Free Space Optical Interconnects

The first step towards the design of the GSL was to establish the basic parameters of the Keplerian microtelescopes that perform the function of "artificial ommatidias" [55]. After the first order design was finished, the microtelescopes consisted of three refractive elements. Table 5.6 shows the lens parameters of the microtelescopes.

Table 5.6 Lens parameters of the Emiter micro Keplerian telescopes used for optical interconnects.

Surface number #	Radius of curvature R_c (μm)	Lens thickness t (μm)	Refractive Index n
L_1 1	162	30	1.56384
L_1 2	-650	190	
L_2 3	165	20	1.78472
L_2 4	-164	150	
L_3 5	386	15	1.95250
L_3 6	-242	120	

The lens parameters of the inverted Micro Keplerian telescopes are shown in Table 5.7 The simulations and optimization of the micro telescopes were performed with the sequential mode of Zemax©.

Table 5.7 Lens parameters of the inverted Micro Keplerian telescopes used as Receiver.

Surface number #		Radius of curvature R_c (μm)	Lens thickness t (μm)	Refractive Index n
L_4	1	242	15	1.95250
L_4	2	-386	120	
L_5	3	164	20	1.78472
L_5	4	-165	150	
L_6	5	650	30	1.56384
L_6	6	-162	190	

The free-space interconnects designs were made using equations (5.1) and (5.2). The multiplexer/demultiplexer system consists of a double Gabor Superlens configuration. L_1, L_2, L_3, L_4, L_5 and L_6 are the microlenses of each microlens array MLA1, MLA2, MLA3, MLA4, MLA5 and MLA6 respectively.

In Fig. 5.16 a double GSL, achieving multiplexing and demultiplexing is shown, after the multiple beams exit the microlens array MLA3, all the beams focus in a single point at the back focal point F_s. So, the multiplexer function is achieved. The inverted GSL composed of microlens arrays: MLA4, MLA5 and ML6 demultiplexes the light beams and divide the optical signal.

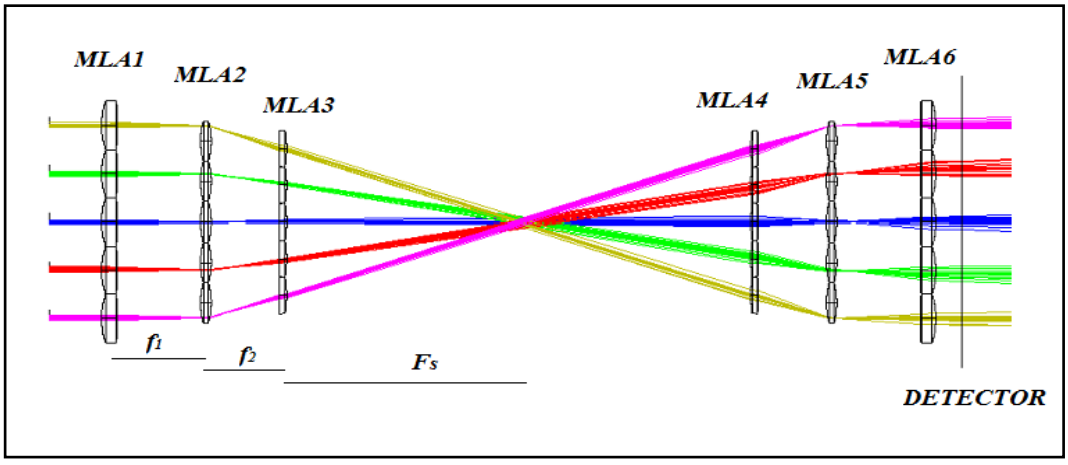

Figure. 5.17 View of the configuration of the multiplexer/demultiplexer using a double Gabor superlens (DGSL). Light comes from different sources and six microlens arrays are used.

The simulation of the DGSL was performed in the non-sequential mode of Zemax©. Four cases were simulated:

5.4.6.1 DGSL with coherent sources
5.4.6.2 DGSL with coherent sources and a diffraction grating,
5.4.6.3 DGSL with an incoherent source, and
5.4.6.4 DGSL with an incoherent source and a diffraction grating.

In Table 5.8 it is possible to see the parameters of the diffraction grating used in the simulations to perform WDM.

Table 5.8 Parameters of the diffraction grating used as diffractive element.

Design parameters	
Material	BK7
Diameter d_g (μm)	100
Thickness t (μm)	5
Lines/micron	0.21
Diff. order m	1

5.4.6 Results

5.4.6.1 DGSL with coherent sources

In Table 5.9 it is possible to see the values taken by the parameters used for the design of the GSL demultiplexer with independent coherent sources for each channel.

Table 5.9 Parameters of the double Gabor Superlens demultiplexer used with Gaussian beams.

Design Parameters	MLA1	MLA2	MLA3	MLA4	MLA5	MLA6
f-number *F#*	1.9	1.78	2	1.78	1.9	1.9
Microlens pitch p_i (μm)	100	84	76	76	84	100
Radius of curvature Rc_{1i} (μm)	162	165	386	242	164	650
R5.4.6adius of curvature Rc_{2i} (μm)	-650	-164	-242	-386	-165	-162
Thickness t_i (μm)	30	20	15	15	20	30
Refractive index n_i	1.56384	1.78472	1.95250	1.95250	1.78472	1.56384
Focal length f (μm)	190	150	150	150	150	190
Global back focal length F_S (μm)	-	-	460	460	-	-

i= 1,2,3,4,5 and 6

When many Gaussian beams of the same wavelength pass through the first three arrays of the GSL, a multiplexed signal is achieved. Afterwards, the signal propagates through the second GSL which divides the signal in multiple beams See (Fig. 5.17). It is very important to consider the size of the original Gaussian beam in comparison with the pitches of the microlenses. A better performance is achieved when the diameter of the beam does not expand considerably after the multiple refractions.

The diameter of the signal at the output of the demultiplexer will be larger in comparison with the input signal. This happens as a cause of the behavior of the propagation of the Gaussian beams. In (Fig.5.18), five laser sources, processed by DGSL are shown. Each one is parallel to the optical axis and propagates in a different channel, the input signals are recovered in the image plane. Each signal is recovered in a different corresponding channel.

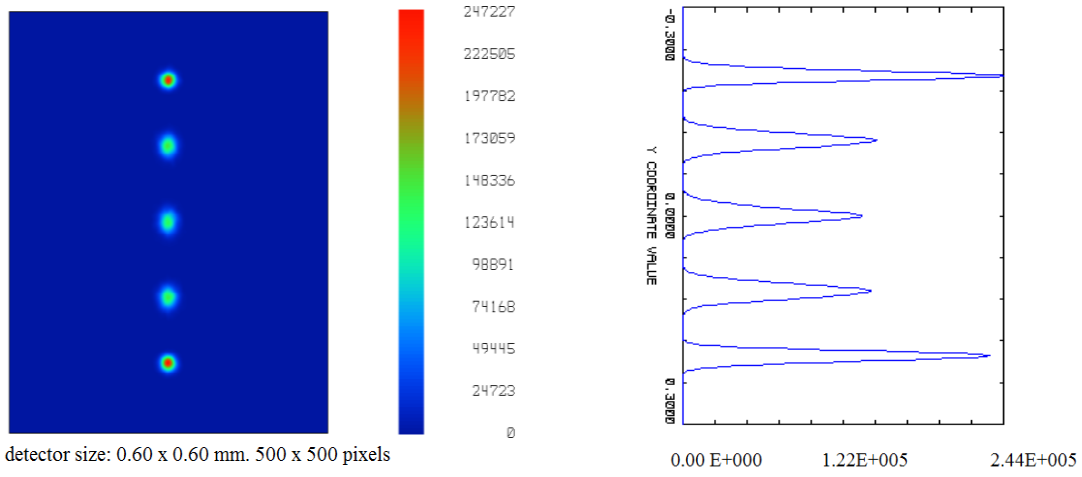

(a) (b)

Figure. 5.18. (a)The five recovered Gaussian beams, processed by a DGSL, captured at the detector plane. (b) The incoherent irradiance profile of the five spots recovered in each channel is shown. The intensity profile is measured in watts/cm^2 for both figures.

5.4.6.2 DGSL with coherent sources and a diffraction grating

Fig. 5.19 shows a DGSL with a diffraction grating placed at the back focus F_s of the GSL. If the grating works with a diffraction order 1, each channel is moved to the following upward channel to recover the image, while for diffraction order -1, the signals are moved downwards.

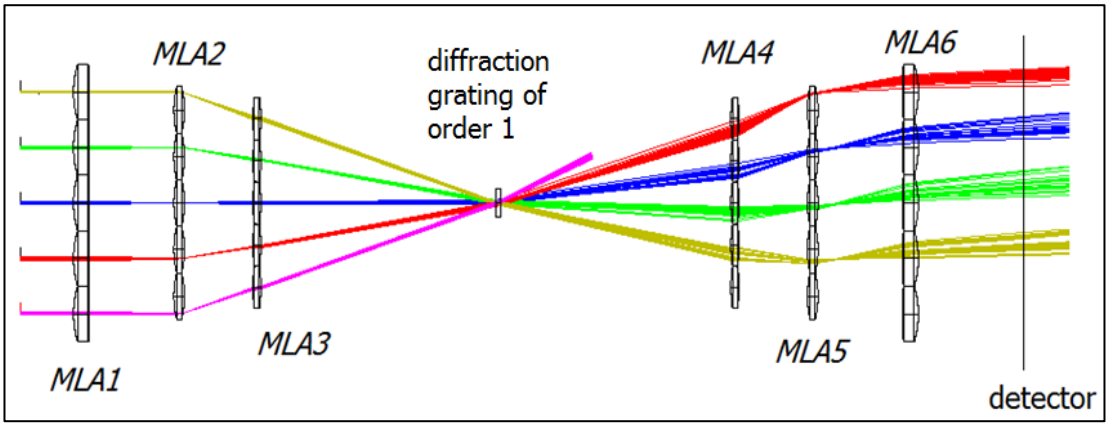

Figure. 5.19 Double Gabor Superlens demultiplexer processing Gaussian beams and using a diffraction grating. A switching action is performed. The information recovered at the image plane is moved to the next upward optical channel.

While Fig. 5.19 shows the raytrace of the proposed system, Fig. 5.20 shows the detector view where the optical switching of the demultiplexed signal could be seen.

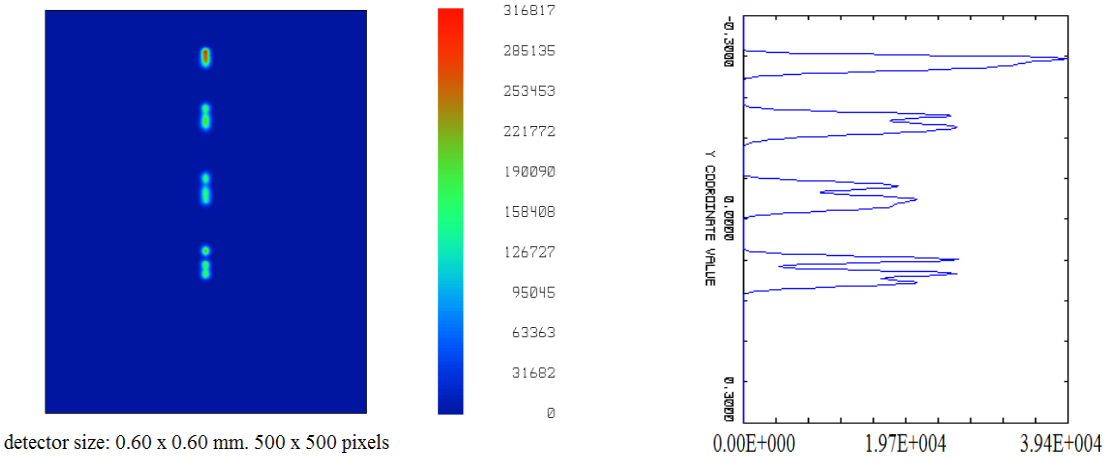

(a) (b)

Figure 5.20 (a) The four spots recovered by the detector. The DGSL system used a diffraction grating of order 1 (b) The irradiance profile of the four recovered spots. The intensity profile is measured in watts/cm^2 for both figures. The information of the lower source is lost due to the switching function performed by the DGSL system with the diffraction grating of order 1.

5.4.6.3 DGSL with an incoherent source

Fig. 5.21 shows a DGSL processing white light. The lens parameters are shown in Table 5.10. A plane wave coming from infinite reaches the first GSL and it is focused at *Fs*. The second GSL demultiplexes the optical signal.

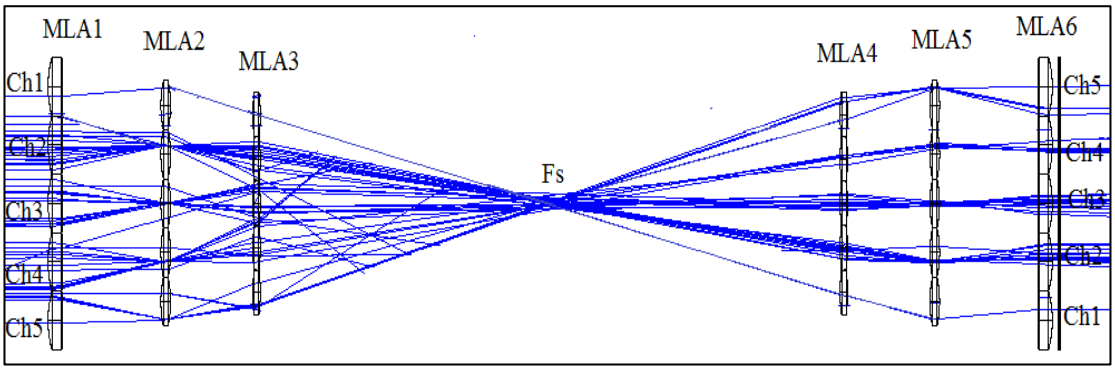

Figure 5.21 Ray tracing of the DGSL system with an incoherent source. The white light is collected by the microlenses of MLA1. The light signal coming from the source is referred as channels: Ch1, Ch2, Ch3, Ch4 and Ch5).

Table 5.10 Parameters of the double Gabor Superlens demultiplexer used with an incoherent source.

Design Parameters	MLA1	MLA2	MLA3	MLA4	MLA5	MLA6
f-number *F#*	2.3	2.26	2.5	2.5	2.26	2.3
Microlens pitch p_i (μm)	100	84	76	76	84	100
Radius of curvature Rc_{1i} (μm)	162	165	386	242	164	650
Radius of curvature Rc_{2i} (μm)	-650	-164	-242	-386	-165	-162
Lens thickness t_i (μm)	30	20	15	15	20	30
Refractive index n_i	1.56384	1.78472	1.95250	1.95250	1.78472	1.56384
Focal length f (μm)	230	190	190	190	190	230
Global focal length F_S (μm)	-	-	580	580	-	

i= 1,2,3,4,5 and 6

In the detector plane, it could be seen that each separated beam is recovered in a different channel. This is shown in Fig. 5.22.

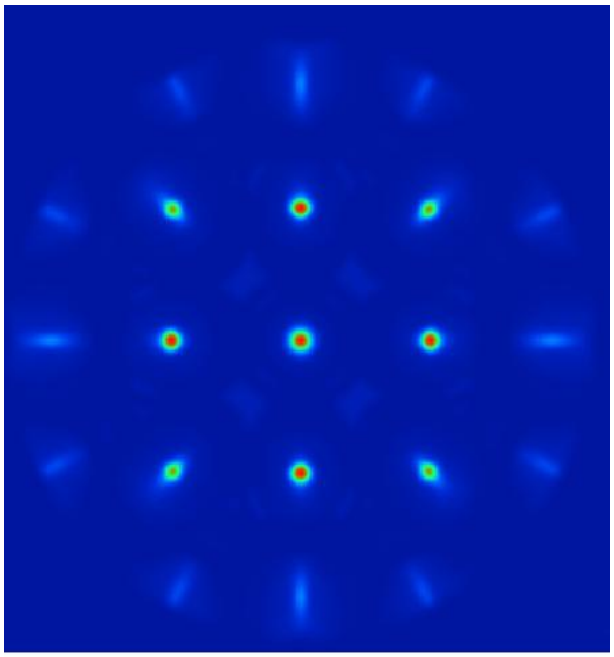

Figure 5.22 Demultiplexing function performed by the DGSL system with an incoherent source. The simulation was made using the microlens arrays in a 2D matrix without a diffraction grating.

5.4.6.4 DGSL with an incoherent source and a diffraction grating.

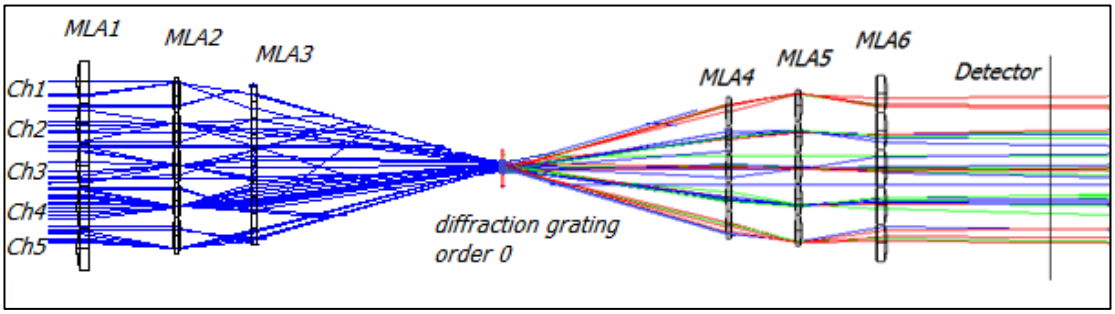

Figure 5.23 DGSL processing white light with a diffraction grating of order 0 at F_s. The different wavelengths are separated due to the diffraction grating.

In Fig. 5.23 a DGSL processing white light is shown and a diffraction grating is placed at the back focal length F_s of the first GSL. When the diffraction order of the grating is zero, it could be seen that the recovered signals in the detector are slightly modified.

In Fig. 5.24 the recovered signals processed by the DGSL in the detector plane are shown. A diffraction grating with zero order is used.

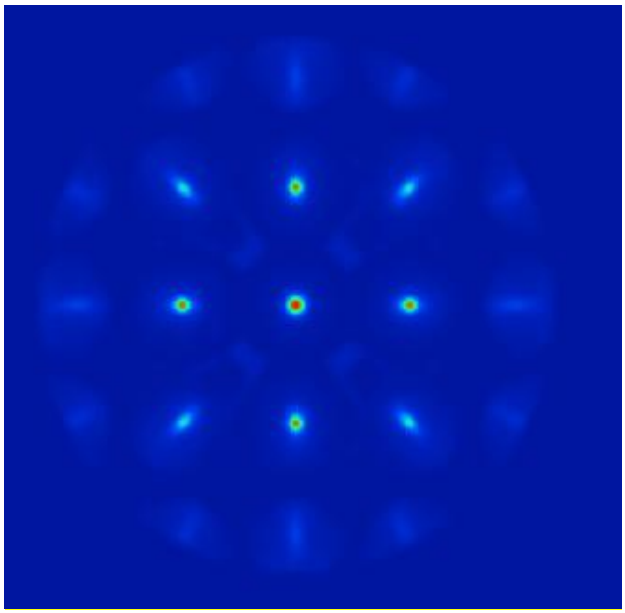

Figure 5.24 Demultiplexed optical signal by the DGSL of Figure 5.22 (grating with 0 order).

Fig. 5.25 shows how a DGSL processing white light and using a diffraction grating achieves WDM. The recovery of the signal at the image plane is displaced. A switching function is performed.

Fig. 5.26a shows the detector view of the system presented in Figure 5.25 with a diffractive grating of order 1. One channel is move upward due to the switching action. Fig. 5.26b shows the detector view of the system presented in Figure 5.25 with a diffractive grating of order -1. One channel is move downward due to the switching action.

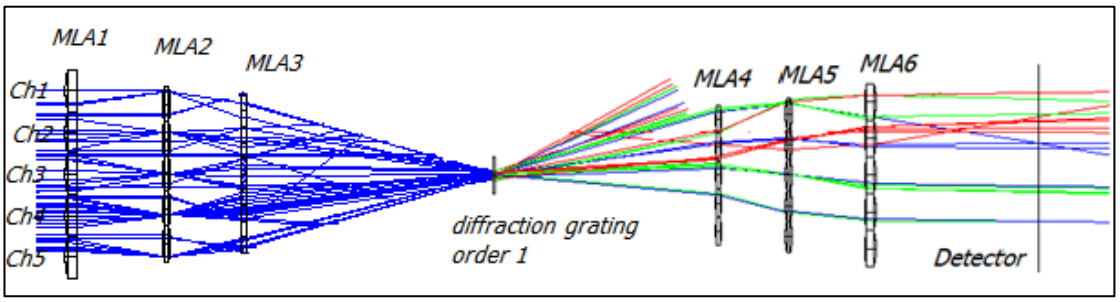

Figure 5.25 DGSL using an incoherent source and a diffraction grating with diffraction order 1. The different colors represent the different wavelengths divided by means of the diffraction grating of order 1. WDM is performed because the longer wavelengths tend to go to the lower channels and the shorter to the upper channels of the demultiplexer. The grating displaces the signal of the lower channel upwards, and if another channel is placed in that position it could also be recovered.

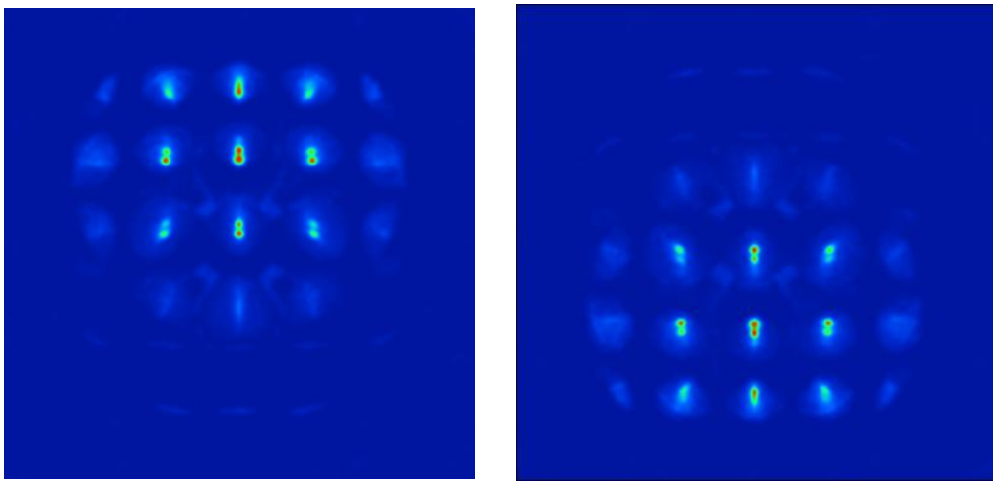

(a) (b)

Figure 5.26 (a) Detector view of the demultiplexed optical signal using a DGSL and a diffraction grating with diffraction order 1. (b) Detector view of the demultiplexed signal using a grating with diffraction order -1. It could be seen that the switching function is performed by analyzing how the image is moved depending of the grating's order. The information of one channel is lost.

6 Conclusions

Scaling limits in conventional optical systems are a reason to look for different ways to achieve miniaturization. The result of this action would be to have more compact devices with an acceptable image quality that could be used in many applications.
Nature has solved the problem of miniaturization of visual systems in living organisms by means of multi aperture optics. Compound eyes are formed by many hexagonal lenslets arranged in a convex surface. These systems vary according to the animal's needs.
Apposition compound eyes are present mostly in diurnal insects that do not require great sensitivity. Nocturnal insects or arthropods that live in environments with a limited amount of light have usually superposition compound eyes, which are more light sensitive than apposition compound eyes.
The design of an AACE based on previous models, enabled us to apply the segmentation of the field of view to image formation. The proposal presented in Chapter 4 resulted in a thickness reduction of the objective's length. By means of performing an optimization of Micro Cylindrical doublets MCD, with the calculation of the coefficients of asphericization, the image quality was improved. The Spot size on axis was reduced to less than 20 microns. The Spherical aberration also reduced its value from -8 to cero on the edge of the entrance pupil thanks to the asphericization of the doublets.
The complete AACE2 was simulated with a 3D configuration that used a sampling frequency of 59.26cycles/rad for each individual channel. The simulations were performed in the non-sequential mode of Zemax. The AACE is limited to a low spatial resolution and limited applications due to the image quality.

The design of an Artificial Superposition Compound Eye ASCE was performed using MKT as the basic units of individual channels. The global system was the sum of many off-axis micro telescopes. The Gabor Superlens configuration was used to achieve the working principle of the objective as a natural superposition compound eye. The simulation of a complete system was done using the non-sequential mode of Zemax. A second design for an improved imaging system was simulated with a micro triplets array instead of the simple MLA2. The total focal length of the objective could be reduced by means of this modification, and the image quality in the detector is highly improved due to the reduction of the spot size.

To develop a more versatile micro imaging system, a zoom effect is valuable. To be able to introduce this function, an array of micro tunable liquid lens that work by electrowetting was included as MLA3. An ASCETL imaging system was simulated. It has the property that by changing the radius of curvature of the micro tunable lenses, the optical power and the Global focal length of the system is modified. The image size is different and it is best focused in different planes. The Gabor global focus is function of the voltage applied to the micro tunable lenses. This property could result in future applications where zoom properties could be needed. We still have the drawback that the microlens further away from the optical axis could introduce aberrations that will have to be corrected otherwise.

GSL is a very useful configuration used to implement an artificial model of a multi aperture refractive superposition compound eye. It is also possible to use a GSL to achieve multiplexation of optical signals, and an inverted GSL is able to achieve demultiplexing.

Two free-space optical interconnects systems called DGSL were presented. The first superimpose the optical signal in a Global focus performing a circulator function, and the second GSL performs demultiplexing.

The introduction of a diffraction grating makes the DGSL more powerful, because an optical switching function is achieved for the coherent sources by changing the diffraction order of the grating. For the non-coherent sources, switching and wave division multiplexing (WDM) are achieved with the introduction of the grating.

Applications of the presented devices could be implemented in communications and in the development of free-space interconnects and MEMS and MOEMs. It is expected that the quality of the recovered data could still be improved, by means of an optical optimization. Maybe the dream of the optical computer is not so far away.

Bibliography

[1] T. Hayes, "Next-Generation Cell Phone Cameras," OPN Optics and Photonics News, Vol.23 No. 2 (17-21) OSA, (USA 2012)

[2] M.F. Land and D. E. Nilsson, *Animal Eyes*, Oxford Animal Biology Series (Oxford University Press, Oxford (2002).

[3] L.P. Lee, and R. Szema, "Inspirations from biological optics for advanced photonics systems," Science 310 (5751), 1148-1150 (2005).

[4] M.F. Land, "Compound eyes: old and new optical mechanisms," Nature **287**, 681-686 (1980).

[5] www.flicker.com/photos consulted on August 31,2012

[6] www.earthlife.net/insects/anat-head.htm consulted on August 31,2012

[7] J.S. Sanders and C. E. Halford, "Design and analysis of apposition compound eye optical sensors," Opt. Eng. 34, 222-235 (1995).

[8] www.Ih3.ggpht.com consulted on July 2, 2013

[9] R. Navarro and N. Franceschini, "On image quality of microlens arrays in diurnal superposition eyes," Pure Appl. Opt. **7**, 69-78 (1998).

[10] K. Vogt, Z. Naturforsch. **30c**, 691 (1975).

[11] M.F. Land, "The Optics of Invertebrate Eyes," Tutorials in Optics (OSA), 1-14 (1992).

[12] www.wired.com/science/discoveries/news/2008/03/shrimp_vision consulted on August 31,2012

[13] N. F. Borrelli, *Microoptics Technology, Fabrication and Applications of Lens arrays and devices*, Dekker, (N.Y., USA 1999)

[14] M. Kufner and S. Kufner, *Micro-optics and Lithography*, Vubpress, (Brussels, Belgium 1997).

[15] Dawes' limit. http://en.wikipedia.org/wiki/Dawes'_ limit consulted on August 31,2012

[16] R. Voelkel, M. Eisner and K.J. Weible, "Miniaturization of Imaging Systems," MST/MEMS for Production Engineering

[17] www.suss-microoptics.com consulted on August 31,2012

[18] M. Katz, *Introduction to Geometrical Optics*, World Scientific Publishing, (USA 2002).

[19] A. Garza-Rivera: Master Dissertation, “Diseno de un Objetivo Ultradelgado Miniaturizado del Tipo Ojo Compuesto de Aposicion Artificial”, Instituto Nacional de Astrofisica, Optica y Electronica INAOE (2009).

[20] W. Smith, *Modern Optical Engineering*, McGraw Hill , (USA 2010).

[21] A. Brueckner, “Microoptical Multi Aperture Imaging Systems,” Diplomarbeit, Friedrich-Schiller-Universitaet Jena (2011).

[22] M.F. Land, Tutorials in Optics, OSA, Rochester USA 1-14 (1998).

[23] J. Duparré, P. Dannberg, P. Schreiber, A. Bräuer and A. Tünnermann, “Artificial Apposition Compound Eye fabricated by micro-optics technology”, Appl. Opt. 43, (2004)

[24] J. Duparré, P. Schreiber, and R. Völkel, “Theoretical analysis of an artificial superposition compound eye for application in ultra-flat digital image acquisition devices,” Proc. Of Optical Design and Engineering vol. 5249 ed. L Mazurany, P J Rogers and R Wartmann (Bellingham, WA: SPIE) (408-418) (2003).

[25] J. Duparré, P. Schreiber, P. Dannberg, T. Scharf, P. Pelli, R. Völkel, H-P. Herzig, and A. Bräuer, “Artificial compound eyes-different concepts and their application to ultra-flat image acquisition sensors,” Proc. Of MOEMS and Miniaturized Systems IV Vol. 5346 ed A El-Fatatry (Bellingham, WA:SPIE) (89-100) (2004).

[26] J. Duparré, P. Schreiber, A. Matthes, E. Pshenay-Severin, A. Bräuer, A. Tünnermann, R. Völkel, M. Eisner, and T. Scharf, “Microoptical telescope compound eye,” Opt. Exp. **13** (889-903) (2005).

[27] J. Duparré, and F. Wippermann, “Micro-optical artificial compound eyes,” Bioinspiration & Biomimetics 1 (R1-R16) (2006).

[28] M. Kawazu, and Y. Ogura, “Application of gradient-index fiber arrays to copying machines,” Appl. Opt. 19 (1105-1112) (1980).

[29] J. Tanida, K. Kumagai, K. Yamada, and S. Miyatake, K.Ishida, T. Morimoto, N. Kondou, D. Miyazaki, and Y. Ichioka, “ Thin observation module by bound optics (TOMBO): Concept and experimental verification”, Appl. Opt. **40** (1806-1813) (2001).

[30] R. Horisaki, Y. Nakao, T. Toyoda, and J. Tanida, Opt. Rev. **16** (241-243) (2009).

[31] A. Garza-Rivera, and F.J. Renero-Carrillo, “Design of Artificial Apposition Compound Eye with Cylindrical Micro-Doublets.” Opt. Rev. **18** (1-3) (2011).

[32] T. Suzuki, S. Yonezawa, “System of Simultaneous Nonlinear Inequalities and Automatic Lens-Design Method” J. Opt. S. Am. 56, 677-683 (1966).

[33] D. Malacara *Optical Shop Testing*, Third Edition, Wiley, New Jersey, U.S.A (2007)

[34] F.J. Renero-Carrillo and A. Garza-Rivera, "Artificial Apposition Compound Eye using Aspherical Cylindrical Micro-Doublets." Proc. Of SPIE 22nd. Congress of ICO Vol. 8011 80119M-2 (2011).

[35] D. Gabor 1940 UK *Patent* 541 753

[36] C. Hembd-Sölner, R.F. Stevens, and M.C. Hutley, "Imaging properties of the Gabor superlens," J. Opt. A: Pure Appl. Opt., UK 94-102 (1999).

[37] K. Stollberg, A. Brückner, J. Duparré, P. Dannberg, A. Bräuer, and A. Tünnermann, "The Gabor superlens as an alternative wafer level camera approach inspired by superposition compound eyes of nocturnal insects," Opt. Exp. **17** (15747-15759) (2009).

[38] K. Stollberg, "Gabor-Superlinse-Miniaturisierte Abbildunsoptik nach dem Vorbild natuerlicher Superpositionsaugen," Diplomarbeit, Friederich-Schiller-Universitaet. Jena (2009).

[39] J. Meyer, A. Brückner, R. Leitel, P. Dannberg, A. Bräuer, and A. Tünnermann, "Optical Cluster Eye fabricated on wafer-level," Opt. Express **19**, 17506-17519 (2011).

[40] Völkel, R. and Wallstab, S. Flachbauendes Bilderfassungssystem Patent DE 199 17 890A 1

[41] T. Nakamura, R. Horisaki and J. Tanida, "Computational superposition compound eye imaging for extended depth-of-field and field-of-view," Opt. Exp. 20 (27482-27495)(2012)

[42] R. Horisaki, S. Irie, Y. Ogura, and J. Tanida, "Three-dimensional information acquisition using a compound imaging system," Opt. Rev. 14, 347-350 (2007).

[43] A. Garza-Rivera, and F.J. Renero-Carrillo, "Design of an ultra-thin objective lens based on superposition compound eye", Proc. Of SPIE Vol. 7930, 793010 (2011)

[44] "Zemax," http://www.zemax.com/

[45] N. Lindlein, "Simulation of micro-optical systems including microlens arrays," J. Opt. A, Pure Appl. Opt**. 4**(4), S1-S9 (2002)

[46] A.D. Clark, "Zoom lenses," Monographs in Applied Optics No.7. London, U.K. (1973)

[47] S. Exner, "Die Physiologie der Facettierten Augen von Krebsen und Insecten," (Leipzig: Deuticke) (1891).

[48] G. P. Agrawal, *Fiber-Optic Communication Systems*, John Wiley & Sons, USA, (1992).

[49] M. Menard, F. Thomas-Dupuis and A. G. Kirk, "One-dimensional to two-dimensional channel formatting with micro-optics for wavelength division multiplexing networks," Applied Optics, Vol.45, No. 1 (2006).

[50] A. Fletcher, T. Murphy and A. Young, *Proc. Royal Soc.* **A223**, 216-225 (1954).

[51] J. Kim, K. H. Jeong, and L.P. Lee, "Artificial ommatidia by self-aligned microlenses and waveguides," Opt. Lett. **30**, 5-7 (2005).

[52] T. Tamir, *Topics in Applied Physics, Integrated Optics*, Springer-Verlag, Berlin Heidelberg New York (1979).

[53] Smith, W. *Modern Optical Engineering*, McGraw Hill, (USA 2010).

[54] Goodman, J., *Introduction to Fourier Optics*, Third Edition, USA (2005)

[55] A. Garza-Rivera and F.J. Renero-Carrillo,"Design of Optical Interconnects inspired in multi-aperture optics based in compound insect eyes," SPIE Proceedings. Photonics Europe (2012).

[56] J.H. Sun, B.R, Hsueh, Y.C. Fang, J. MacDonald, and C.C. Hu, "Optical design and multiobjective optimization of miniature zoom optics with liquid lens element." Applied Optics vol. 48 n. 9 (1741-1757) (2009).

[57] S. Kuiper, "Electrowetting-based liquid lens for endoscopy", Proc. Of SPIE Vol.7930, 793008-1 (2011)

[58] S. Kuiper, and B.H.W. Hendriks, "Variable-focus liquid lens for miniature cameras," Applied Physics letters, Vol. 85. No. 7, 1128-1130 (2004).

[59] C. Yang, C.G. Tsai, and J.A. Yeh, "Dielectrically Tunable Liquid Microlens," ODF´10 Yokohama. Technical Digest 415-416 (2010).

[60] B. Berge and J. Peseux, "Variable-focus liquid lens controlled by an external voltage: an application of electrowetting", Eur. Phys. J.E. 3, 159-163 (2000).

[61] T. Tkaczyk, "Field guide to Microscopy," SPIE, Bellingham, WA, USA (2010).

Appendix

A Tunable lens

Several ways to achieve tunable lenses are discussed in literature [56-60]. We based our work in *Kuiper's*, who showed that variation of focal length is a function of the radius of curvature of the meniscus of a liquid lens that works by means of electro wetting, and of the refractive indexes of a conducting and an insulating liquid that conform it [57]. Fig. A1a shows a solid model of a tunable liquid lens seen from the outside. In Fig. A1b it is possible to see the main parameters of a liquid tunable lens.

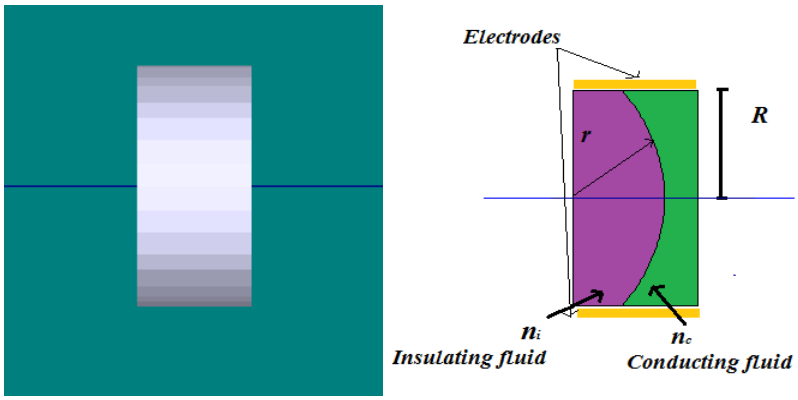

(a) (b)

Figure. A.1 a) Solid model of the tunable lens. B) Parameters of a tunable lens that works by electrowetting are shown: n_c is the refractive index of the conducting liquid, n_i is the refractive index of the insulating liquid, R_c is the radius of curvature and R is the cylinder radius.

The relationship is described by:

$$O = \frac{1}{f} = \frac{n_c - n_i}{R_c}, \qquad \text{(A.1)}$$

where O is the optical power, f is the focal length, n_c is the refractive index of the conducting liquid, n_i is the refractive index of the insulating liquid, and R_c is the lens meniscus radius.

An electromechanical force changes R_c, so a change in the contact angle θ of the conducting liquid with the wall can be described by:

$$\cos\theta = cos\theta_0 + \frac{1}{2}\frac{\varepsilon}{t.\gamma_{ci}}V^2, \qquad \text{(A.2)}$$

for $0° < \theta_0 < 180°$

where θ_0 is the contact angle in the off-state, ε the dielectric constant of the insulator, t is the thickness, γ_{ci} the interfacial tension between conducting and insulating liquid, and V the applied voltage.

The relationship between the meniscus radius R_c, the cylinder radius R, and the contact angle θ can be calculated with:

$$r_c = \frac{-R}{\cos\theta} \ , \qquad \text{(A.3)}$$

so, to establish a relationship between optical power and voltage:

$$O = O_0 + [\frac{(n_i - n_c)}{R} . \frac{1}{2} . \frac{\varepsilon}{t.\gamma_{ci}} . V^2] \ , \qquad \text{(A.4)}$$

where O_0 is the optical power calculated at the off-state contact angle.

B Calculation of the optical power of the micro-tunable lens array.

In order to design the ASCETL with the characteristic of achieving zoom by means of variable focal length, we needed to implement in the third micro lens array, micro-tunable lens that would modify their optical power depending of the variation of the radius of curvature. A change in the curvature of the conducting liquid meniscus of the micro tunable lens was produced by means of a voltage variation.

Eq. (A.4) was used to establish a relationship between the voltage change and the optical power. The simulations of the ASCETL were made using Zemax. For the third array of liquid tunable micro lenses the values of the refractive indexes are: n_c=1.33000 for the conducting liquid, and n_i=1.52944 for the insulation fluid. *Kuiper* [57] worked with slightly salted water as conducting fluid, and a phenylated siloxane as insulating liquid, so there is a change in the values that he used experimentally to prove the performance of the system. Fig. A.1b shows the tunable lens parameters used to calculate the change of curvature. The value of the cylinder radius is R=33 μm which corresponds to a lens pitch p_3=66 μm., a lens thickness of d=20 μm., a dielectric constant of the insulator of ε =(2.78901.10^{-11}) Fm^{-1} , γ_{ci}=0.040 Nm^{-1} which is the interfacial tension between conducting and insulating liquid, and θ_o= 3.14 rad for the contact angle in the off-state. Fig. B.1 shows a plot of optical power versus voltage. The voltage ranges from 0 to 120 V.

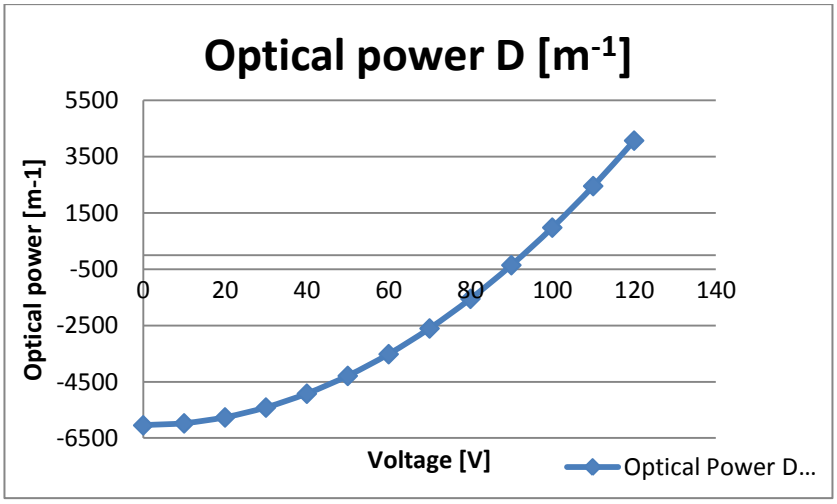

Figure B.1 Plot of the optical power versus voltage for the micro tunable lens according to Eq. (A.4). The voltage variation is between 0 to 120 volts, and the range of the optical power varies from -6043 to 4070 m^{-1}.

The change in the contact angle, between the two fluids, as a result of applying different voltages, gives us different values of the optical power and then a variation in the focal length of the tunable lenses and of the Gabor Focal length of the system. This is a result of the different values of the radius of curvature of the meniscus according to the different voltages applied. The radius of curvature has to be calculated using Eq. (A.2).

Table B.1 Value of the radius of curvature, optical power and focal length of the micro tunable liquid lens as functions of the change of voltage.

Voltage [V]	R_c Radius of Curvature [mm]	O Optical power [mm^{-1}]	f focal length [mm]
0	0.033	-6.040	-0.166
10	0.034	-5.973	-0.167
20	0.035	-5.760	-0.174
30	0.037	-5.411	-0.185
40	0.041	-4.920	-0.203
50	0.047	-4.487	-0.233
60	0.057	-3.520	-0.284
70	0.077	-2.602	-0.384
80	0.129	-1.550	-0.646
90	0.562	-0.355	-2.818
100	-0.204	0.980	1.021
110	-0.081	2.454	0.407
120	-0.050	4.070	0.246

C Design of the Micro tunable doublets used in the MLA3

"Kuiper" proposed in his work [57] a tunable lens that was intended to work in an endoscope. Both surfaces were plane. To design micro tunable doublets that could be used in the ASCETL system, we began with a lens which first and third surfaces were plane.

Figure C1 shows five different lenses which first and third surfaces are plane. A voltage was applied to change the radius of curvature of the second surface. For values lower than 90 volts, the radius of curvature was positive and for higher than 90 volts the radius of curvature was negative. From 0 to 90 V the micro tunable doublets were negative lenses and they could not focus light.

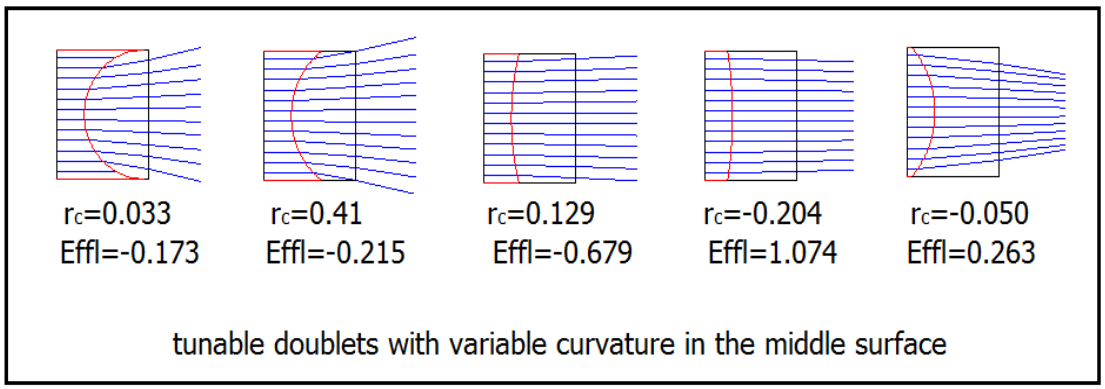

Figure. C.1 Shows tunable doublets with plane first and third surfaces. The second surface changes according to a voltage variation. The values of the radius of curvature r_c and effective focal length *Effl* are shown.

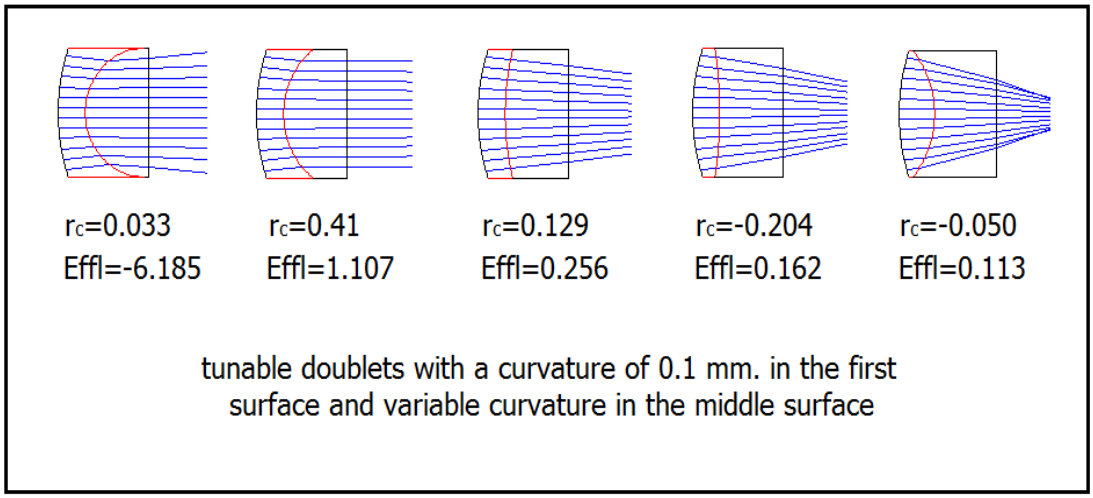

Figure. C.2 Shows tunable doublets with the first surface with a radius of curvature of 0.1mm, the third surface is plane. The second surface changes according to a voltage variation. The values of the radius of curvature r_c and effective focal length *Effl* are shown.

Figure C2 shows five different doublets which first surface has a radius of curvature of 0.1mm and the third surface is plane. A voltage was applied to change the radius of curvature of the contact meniscus. For values lower than 90 volts, the radius of curvature was positive and for higher than 90 volts the radius of curvature was negative. For the first two doublets the *Effl* was longer in comparison with the doublets with two plane surfaces. For the other three doublets the effective focal length was reduced and the doublets focused light more rapidly.

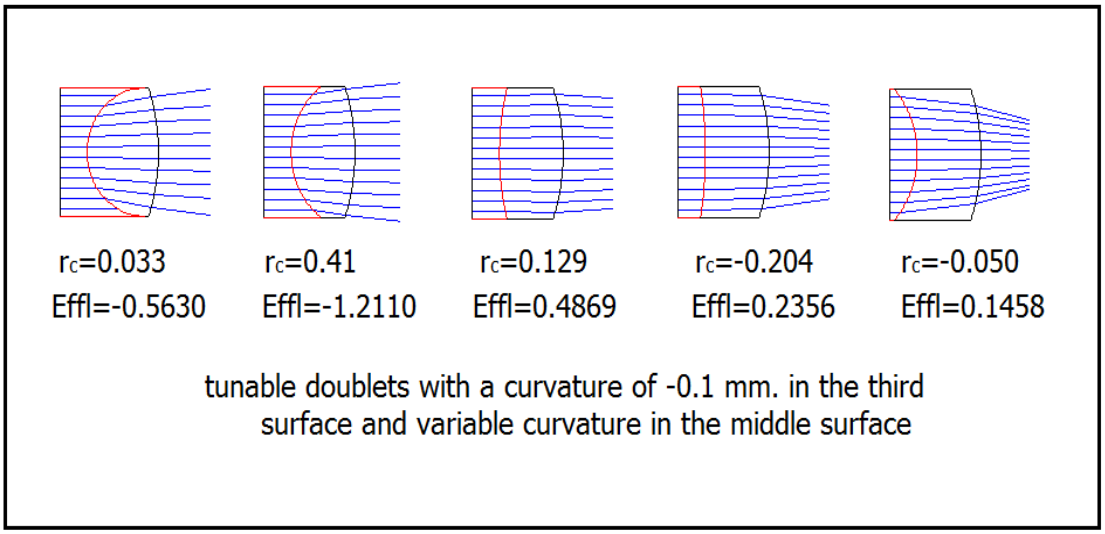

Figure. C.3 Shows tunable doublets with plane first surface and with the third surface with a radius of curvature of -0.1mm.The second surface changes according to a voltage variation. The values of the radius of curvature r_c and effective focal length *Effl* are shown.

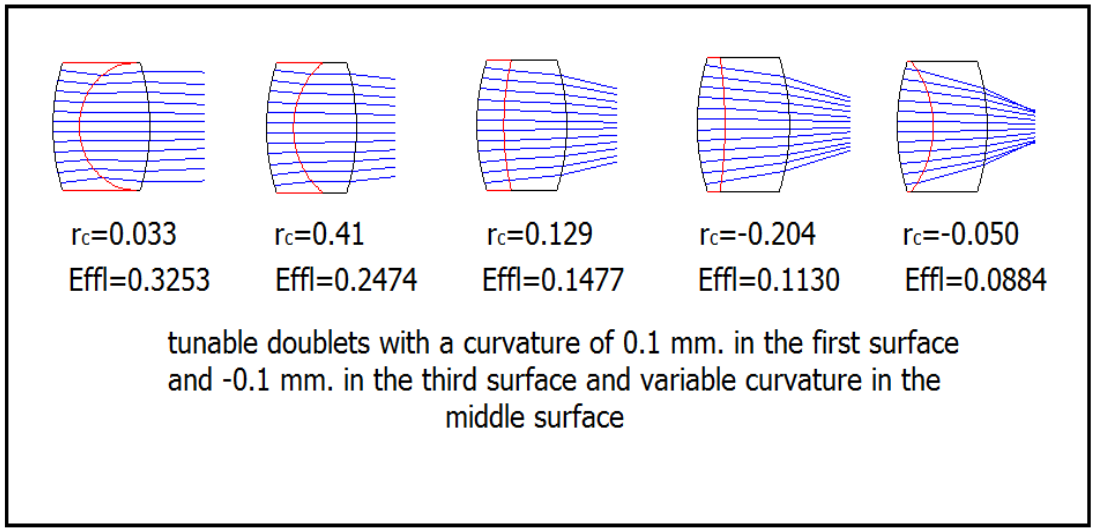

Figure. C.4 Shows tunable doublets with a first surface with a radius of curvature of 0.1 mm and with the third surface with a radius of curvature of -0.1mm.The second surface changes according to a voltage variation. The values of the radius of curvature r_c and effective focal length *Effl* are shown.

Figure C3 shows five different doublets which first surface is plane and the third surface has a radius of curvature of -0.1mm. A voltage was applied to change the radius of curvature of the contact meniscus. For values lower than 90 volts, the radius of curvature was positive and for higher than 90 volts the radius of curvature was negative. The *Effl* is not so reduced as by the doublets presented in Figure C2, but the chromatic aberration was a lot less than for the other doublets. The variations in the curvature did not have such an extremely high impact in the thickness of the doublets.

Figure C4 shows five different doublets which first surface has a radius of curvature of 0.1mm and the third surface has a radius of curvature of -0.1mm. A voltage was applied to change the radius of curvature of the contact meniscus. For values lower than 90 volts, the radius of curvature was positive and for higher than 90 volts the radius of curvature was negative. The *Effl* is reduced in comparison to the doublets presented in Figure C1, C2 and C3. The variations in the curvature have an extremely high impact in the thickness of the doublets.

D Coherent and Incoherent Sources

An ideal light wave that extends in space and has only one wavelength λ (or frequency ν) is said to be monochromatic. If the range of wavelengths λ or frequencies ν is very small, the wave is quasi-monochromatic. The packet of these waves is called a wave group. The intensity of this kind of light can be calculated as a simple addition of intensities from different waves: there is not phase relationship between them or the phase changes are very fast.

Multiple waves are coherent or partially coherent if they have a common phase relation dependence. A source of a coherent wave is a laser where waves must be in resonance and therefore in phase. The average length of the wave group is called the coherence length, while the time required to pass this length is called coherence time.

Spatial coherence is related to the coherence of light with regard to the extent of the light source. Light is partially coherent if its coherence is limited by the source bandwidth, dimension, temperature, or other effects.

Interference is a process of superposition of two coherent or partially coherent waves. The result of interference is a periodic intensity change in space, which creates fringes on a screen. The contrast of the fringes depends on the extent of the source and it is related to spatial coherence. The intensity of fringes depends on the Optical path length and the temporal coherence of the source [61].

Coherence length could be defined as:

$$l_c = \frac{\lambda^2}{\Delta\lambda}, \qquad \text{(D.1)}$$

where l_c is the coherence length, λ wavelength and Δλ is the bandwidth.

The relationship between coherence length and coherence time could be seen in the following equation:

$$\Delta\nu = \frac{1}{t_c} = \frac{Ve}{l_c}, \qquad \text{(D.2)}$$

Where Δν is the frequency variation, t_c is the temporal coherence and *Ve* is the wave velocity.

Index of Tables

Table of Figures

Abbreviations and Symbols

ACE	Apposition compound eye
AACE	Artificial apposition compound eye
ALSIE	Automatic Lens design by Solving InEqualities
AMCD	Aspherical micro-cylindrical doublets
ASCE	Artificial superposition compound eye
AWG	Arrayed-waveguided grating
CMOS	Complementary metal-oxide semiconductor
FDM	Frequency division multiplexing
FOV	Field of view
FWHM	Full width at half maximum
GRIN	Gradient refractive index
GSL	Gabor Superlens
LED	Light-emitting diode
MAO	Multi aperture optical imaging system
MCD	Micro-Cylindrical doublets
MEMS	Micro-Electro-Mechanical Systems
MOEMS	Micro-Opto-Electro-Mechanical Systems
MLA	Microlens array
OCS	Optical communication system
OSLO	Optics Software for Layout and Optimization
SCE	Superposition compound eye
SCED1	Superposition compound eye demultiplexer 1
SCED2	Superposition compound eye demultiplexer 2
SW	Space-bandwith-product
TDM	Time division multiplexing
WDM	Wave division multiplexing

α	Deflection angle
a	Subimage size
A_F	Image field size
A_P	Area of one pixel
C	Centre of curvature
d	Pinhole diameter
d_g	Distance between the slits in a grating
D_{eff}	Effective pupil aperture stop
D	Microlens diameter
D_t	Length of a simple telescope
Λ	Period of a grating
$\Delta\Phi$	Interommatidial angle
$\Delta\Phi_{eff}$	Effective sampling angle
$\Delta\Phi_{nat}$	Effective sampling angle of the natural compound eye
$\Delta\Phi_{px}$	Interpixel angle
$\Delta\phi$	Inter rhabdom angle
$\Delta\varphi$	Acceptance angle
$\Delta\varphi_{nat}$	Acceptance angle of the natural compound eye
$\Delta\rho$	Geometrical contribution of the acceptance angle
ΔP	Pitch difference
Δt	Travel time of light
Δx, Δy	Lateral dimensions of the image field
E_n	Euler numbers
e_p	Wall thickness
ε	Dielectric constant
F	Stop number
f	Focal length
f_1	Back focal length of the first lens or first microlens array

f_2	Front focal length of the second lens or second microlens array
fe	Focal length of the eyelens
$Fe,_f$	Effective front focal length
f_{glass}	Focal length in glass
fo	Focal length of the objective
Fs	Back focal length of the GSL system
γ_{ci}	Interfacial tension
h	Lens sag
h_i	Aspherical coefficients
I	Image size
I_1	Distance from the input lens to the beam waist
I_2	Distance from the beam waist to the output lens.
J	j-level of an etched grating
K	Conic constant
K_x , K_y	Number of optical channels in x,y dimensions of an array
L	Rhabdom's length
l_c	Coherence length
λ	Wavelength
$\Delta\lambda$	Bandwidth
M	Angular magnification
m	Grating order
N	Number of microlenses in one dimension
N_L	Corresponding MCD unit
n	Refractive index of the glass
n_0	Axial refractive index
n_c	Refractive index of the conducting liquid
n_i	Refractive index of the insulating liquid
n_{rd}	Refractive index at a radial distance

n_t	Refractive index of the first and third part of the micro-triplet
n_{tl}	Refractive index of the middle part of the micro-triplet
n_x , n_y	Number of pixels along x,y dimensions of a partial image
N_x , N_y	Number of pixels along x,y dimensions of the image
ν	frequency
$\Delta\nu$	frequency variation
ν_{co}	Cut-off frequency
ν_s	Sampling frequency according to the Nyquist criterion
O	Optical power
O_0	Off-state optical power
O_b	Object size
p_k	Pixel pitch
p_{min}	Minimum grating period
P_L	Pitch of the microlenses
p_{px}	Pixel pitch of image sensor
P_p	Pinhole pitch
r	Lens radius
R	Radius of the cylinder
R_c	Radius of curvature of a lens
R_{eye}	Radius of curvature of a natural compound eye
R_p	Resolving power
r_s	Resolution
r_d	Radial distance from the axis
S	System length
S_c	Scaling factor
s_{e1}	Front focal length of the erector lens
s_{e2}	Back focal length of the erector lens
s_i	Image distance

s_o	Object distance
s_r	Rhabdom's separation distance
$t,\ T$	Thickness
t_c	temporal coherence
θ	Contact angle of the conducting liquid with the wall
θ_0	Off-state contact angle
V	Voltage
Ve	Wave velocity
Vol	System volume
W	System weight
W_D	Detector width
ω	Angle subtended by the object
ω'	Angle subtended by the image
ω_0'	Beam waist
ω_{in}	Input beam radius
ω_{out}	Output beam radius
ξ	Lateral aberrations
X_N	Position of the *N* pinhole measured from the left side
Y_N	Position of the *N* pinhole measured from the right side

Publications by the Author

Papers

*Anel Garza-Rivera and Francisco-J Renero-Carrillo, ***"Design of Artificial Apposition Compound Eye with Cylindrical Micro-Doublets"***, Optical Review, Vol. 18, No. 1 (2011) 184-186.

*Anel Garza-Rivera, Francisco-Javier Renero-Carrillo and Carlos-G. Trevino-Palacios, ***"Design of Free-Space Optical Interconnects using two Gabor Superlenses"*** ,Optical Review, accepted after minor corrections (enviado en junio 2013)

Proceedings

*Anel Garza-Rivera and Francisco-J Renero-Carrillo, **"Design of Artificial Apposition Compound Eye with Cylindrical Micro-Doublets",** Optics-photonics Design & Fabrication' 10, Yokohama, Japan (2010) 465-466.

*Anel Garza-Rivera and Francisco-J Renero-Carrillo, **"Design of an ultra-thin objective lens based on superposition compound eye"**, MOEMS and Miniaturized Systems X, Proceeding of SPIE Vol. 7930-10. Photonics West USA (2011).

*Anel Garza-Rivera, Juan Martinez-Carranza, J.E. Gomez-Correa, Carlos-G. Trevino-Palacios, and Francisco-Javier Renero-Carrillo, **"Propagation of multiple laser beams through an ultra-thin objective lens based on superposition compound eye",** CIOMP-OSA International Summer Session Lasers and Their Applications, Changchun, China (2011).

*Renero-Carrillo Francisco-J and Garza-Rivera Anel, **"Aspherical cylindrical micro-doublets for artificial apposition compound eye"**, (Paper 2284780) 22nd.General Congress of the International Commission for Optics (ICO-22), Puebla, Mexico (2011) 227

*Anel Garza-Rivera, Carlos-G. Trevino-Palacios and Francisco-Javier Renero-Carrillo, "**Design of optical interconnects inspired in multi-aperture optics based in compound insect eyes",** MOEMS and Miniaturized Systems X, Proceeding of SPIE Vol. Photonics Europe, Brussels, Belgium (2012).

Outreach

*Anel Garza-Rivera y Francisco-Javier Renero-Carrillo, **"Son los ojos de los insectos una nueva alternativa para encontrar nuevas aplicaciones en la**

Fotónica?”, Boletín de la Sociedad Mexicana de Física, Vol. 25 No. 3, jul.-sep. (2011) 165-169.

“Diseño de Sistemas Opticos de Multi-apertura basados en los Ojos Compuestos de Aposición y Superposición”

Anel Garza-Rivera
INAOE, Tonanzintla, Puebla, México

Francisco-Javier Renero-Carrillo
INAOE, Tonanzintla, Puebla, México

Diciembre 12, 2013

1. Resumen

El diseño de micro sistemas ópticos de multi apertura, inspirados en los ojos compuestos de insectos y artrópodos, es el objetivo principal de este trabajo. Se presentan los diseños de arreglos de microlentes sencillas, micro dobletes y micro tripletes. El uso de micro elementos ópticos, asi como el principio de funcionamiento de los ojos compuestos naturales de Aposición y Superposición, han permitido la existencia de sus contrapartes artificiales. Se explican los diseños de un ojo compuesto de Aposición Artificial AACE, de un ojo compuesto de Superposición Artificial ASCE, y de un Ojo Compuesto de Multi Apertura con microlentes sintonizables ASCETL. Estos micro modelos ópticos son usados para desarrollar aplicaciones en sistemas formadores de imágenes. Los disenos de un multiplexor y demultiplexor no guiados, asi como de un circulador y un divisor de longitud de onda WDM con aplicaciones en comunicaciones ópticas, son descritos. Los antecedentes biológicos, las ecuaciones, simulaciones, desempeño óptico y algunas aplicaciones se muestran también en este trabajo.

2. Introducción

La imágenes con cámara fotográfica en los teléfonos inteligentes, ha sido un producto que ha revolucionado al mercado de una manera considerable. El pronóstico para los próximos años es que la demanda aumente de 1,340 a 2,393 millones de unidades por año [1]. Este módulo ha sido miniaturizado para poder ser incluido en el teléfono, pero los siguientes avances tecnológicos han sido necesarios para poder desarrollar este producto:

1. Un sensor lo suficientemente pequeño para caber en un espacio muy reducido, pero con una sensitividad lo suficientemente buena para poder producir imágenes con una calidad aceptable.
2. Un sistema óptico funcional para poder manipular la imagen.
3. Tecnologías de oblea y de empaque, que permitan la construcción y ensamblaje de los módulos de cámara y que sean compatibles con la producción masiva de semiconductores, y

4. Un sistema de flash que provea iluminación adicional y que mejore la calidad de la imagen.

Casi todos los consumidores han adoptado la fotografía a través de sus teléfonos, como resultado de la aplicaciones móviles y de la demanda producida para capturar y compartir imágenes directamente del dispositivo al Facebook o al correo electrónico.

La óptica sigue siendo la clave para desarrollar estos productos. Aunque la calidad de las imágenes ha mejorado mucho gracias a los sensores y a las lentes, los diseñadores de tecnología móvil estan cada vez mas deseosos de reducir las dimensiones de sus productos. El mayor reto sigue siendo, la colocación de un módulo de cámara con tecnología efectiva en un dispositivo móvil. Este problema, ha dado lugar a muchas imágenes como son: una mejor tecnología en semiconductores complementarios metal-oxido (CMOS), lentes líquidas sintonizables, óptica de oblea de multi apertura que tenga un buen desempeño, y la incorporación de un flash LED de pequeñas dimensiones con buena estabilidad mecánica y larga durabilidad. La idea de incorporar arreglos de microlentes que asemejen las estructuras de los ojos compuestos de insectos, permite reemplazar lentes individuales con arreglos o multilentes que permitan hacer mucho mas delgado al módulo. De esta manera se evitan los desalineamientos de múltiples elementos ópticos. Otra ventaja es que se tendrían módulos de cámaras con un campo de visión mucho mas amplio para cada imagen.
Este trabajo de tesis presenta en el capitulo 2, la introduccion a la morfología y fisiología de los ojos naturales de los insectos. En el capitulo 3 se presentan algunos conceptos generales sobre microlentes y arreglos de microlentes, asi como ecuaciones. En el capitulo 4 se muestra el ojo compuesto de aposición artificial, y en el capitulo 5 el ojo compuesto de superposición artificial con diferentes variantes y aplicaciones.

Conforme fuimos avanzando en esta investigación, desarrollamos diferentes aplicaciones como son las de las lentes líquidas sintonizables para lograr zoom, y los dispositivos ópticos no guiados como los multiplexores, demultiplexores, switches y divisores de longitud de onda muy usados en comunicaciones ópticas.

3. La Optica de los Ojos Compuestos (Antecedentes)

El ojo es un órgano de vision espacial, en el cual diferentes fotoreceptores observan diferentes direcciones en el espacio y registran variaciones en los niveles de intensidad. Todos los animales comparten un tipo similar de pigmento visual, pero la manera en la cual los órganos se especializan en manejar grandes cantidades del mismo y en hacer la transducción de la información en señales eléctricas, no es la misma. Hay diferentes soluciones para los problemas de sensitividad y de velocidad de las células visuales receptoras. El resultado de la evolución de los órganos visuales desde un organismo extremadamente sencillo, ha dado lugar a una cantidad considerable de tipos de ojos. Estos ojos naturales, presentan diferentes estructuras y componentes formados por células especializadas en diferentes combinaciones con la finalidad de adquirir informacion sobre el medio que rodea a los organismos de los cuales forman parte.

La clasificación más común del tipo de ojos encontrados en animales multicelulares son del tipo refractivo y reflectivo. Los tipos principales son: (a) ojo de orificio, (b) ojo compuesto basico, (c) ojos acuáticos, (d) ojos refractivos de apertura única, (e) ojos compuestos de aposición, (f) ojos compuestos de superposición, (g) ojos reflectivos de apertura única, y (h) ojos compuestos de superposicion reflectivos. La Fig. 1 muestra un esquema de los diferentes tipos de ojos.

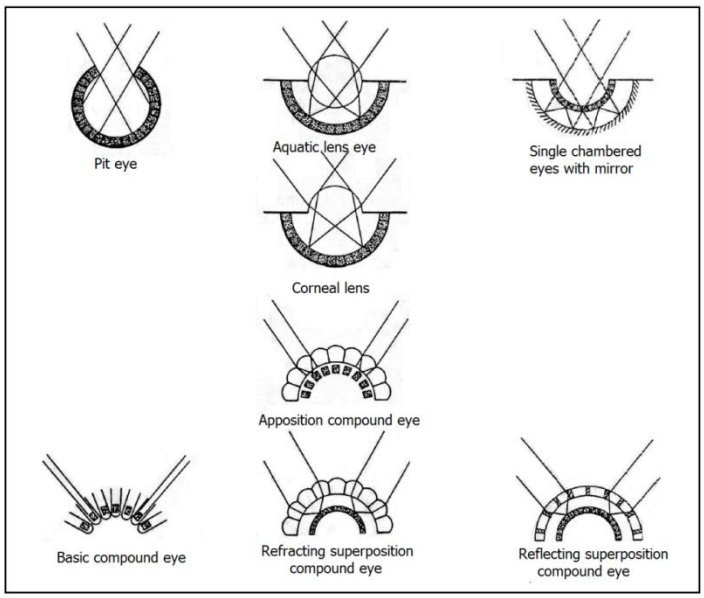

Fig. 1: Clasificación de los diferentes tipos de ojos en animales multicelulares.

Los ojos compuestos emplean un gran número de subsistemas ópticos extremadamente pequeños. La totalidad del sistema óptico esta formado por unidades independientes que actuan en conjunto para realizar la formación de la imagen. Cada tipo de ojo compuesto presenta diferentes mecanismos. La estructura de los ojos compuestos, esta relacionada con el procesamiento de la información que el sistema nervioso del pequeño ser vivo pueda realizar sin sobresaturar su capacidad dependiendo de su tamano y consumo de energia. El hecho de que las unidades independientes llamadas “ommatidias”, esten colocadas en una base curva, permite al ojo tener un gran campo de vision (FOV). Esta configuración permite al ojo conservar un volumen pequeño y la capacidad de informacion del ojo completo es incrementada para cumplir con los requerimentos del animal. Por lo tanto, el mayor volumen del cerebro esta disponible para procesamiento de señales y otras funciones biológicas.

Los dos grupos principales en los que se clasifican los ojos compuestos son ojos compuestos de aposición y ojos compuestos de superposición. Estos tipos de ojos han sido una inspiración para contrapartes artificiales para tratar de dar sus beneficios a sistemas formadores de imágenes miniaturizados y ser implementados en nuevas aplicaciones como pueden ser concentradores de energía, comunicaciones, celdas fotovoltáicas, etc.

Los ojos compuestos de aposición se encuentran por lo regular en insectos diurnos y necesitan una gran cantidad de luz para poder resolver un objeto, ya que su sensitividad esta muy limitada. Se cree comunmente que los ojos compuestos forman multiples imágenes, pero aunque cada microlente forme una pequeña imagen, esa no es la manera en la que ve un insecto. La imagen final formada en la retina, es un mosaico de diferentes pequenas imágenes colocadas una junto a la otra, de manera que cada una parece ser una pieza especifica del rompecabezas. La Fig. 2 muestra el mecanismo de formacion de imágenes de un ojo de aposición natural.

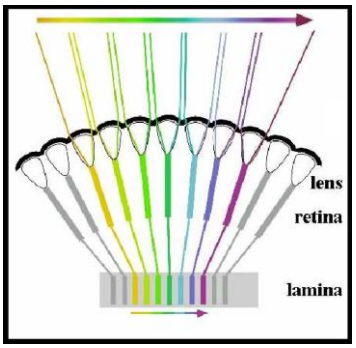

Fig. 2. Mecanismo de formacion de imágenes de un ojo de aposición natural.

Los ojos compuestos de superposición también son estructuras convexas con facetas con dimensiones similares. Se parecen mucho en el exterior a los ojos de aposición, pero internamente presentan grandes diferencias. La retina es una sola pieza y se encuentra colocada muy profundamente en el ojo. Este tipo de ojo tiene una zona llamada "zona clara" que se encuentra entre la retina y las estructuras ópticas detrás de la córnea. La imagen producida, es una imagen erecta, profunda que se encuentra en las vecindades de la retina. Los elementos ópticos son pequeños telescopios refractores o reflectores, según sea el caso. En la Fig. 3 se observa la formación de imágenes de este tipo de ojo.

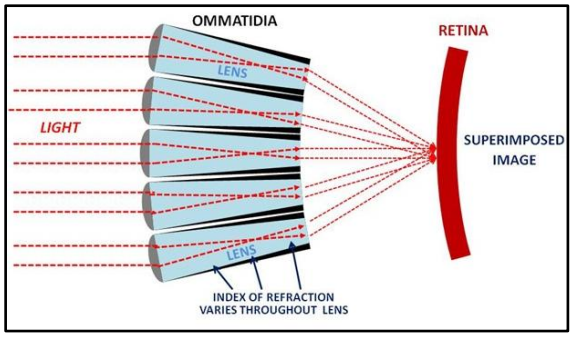

Fig.3: Formación de imágenes del ojo compuesto de superposición refractivo.

4. Ojo Compuesto de Aposición Artificial AACE

Este es un sistema óptico no convencional que usa micro dobletes cilíndricos (CMD) como unidades fundamentales que hacen las veces de "ommatidias", los cuales se encuentran colocados en una configuración que asemeja un ojo compuesto de aposición. En este trabajo se muestran varios diseños de un objetivo ultra delgado inspirado en los ojos de mosca. Los diferentes diseños pueden dar opción a crear nuevas tecnologías que procesan la información de una manera diferente a la usual, pero al mismo tiempo de una manera muy efectiva. Este proceso se lleva a cabo mediante el muestreo de un objeto con un arreglo de microlentes que tienen un valor determinado de angulo de aceptación. El procesamiento de la señal óptica permite tener imágenes parciales que finalmente forman parte de una imagen global. El objetivo tiene las ventajas de tener un tamaño reducido, un gran campo de visión, y produce una calidad de imagen aceptable en comparación con los sistemas previamente diseñados. Los parametros de diseño del ojo compuesto de aposición artifical (AACE) y el desempeño óptico de los (MDC), asi como del

sistema completo se muestran en esta tesis. La Fig. 4 muestra como funciona el sistema propuesto por nosotros.

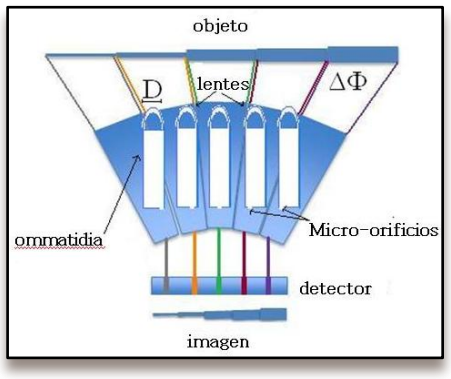

Fig.4: Diagrama de muestreo del objeto y formación de la imagen de un ojo de aposición, donde ΔΦ es el angulo interommatidial y D es el diametro de las microlentes.

Los diseños que se presentan estan compuestos por varias unidades de CMD. El grosor máximo del sistema no excede las 350 μm. La estructura del objetivo consiste en un arreglo de microlentes plásticas, colocadas sobre un substrato de vidrio. Se deben de incluir paredes opacas entre los diversos canales, y en el otro extremo se coloca una placa metálica con micro-orificios en una posición específica. La imagen es registrada en un CCD colocado justo despues del arreglo de micro-orificios. La tabla 1 presenta tres diferentes opciones con sus respectivos parametros de diseño.

Tabla 1 Parámetros de los objetivos de camara del tipo ojo de aposición AACE [31].

Parametros de diseno	AACE1	AACE2	AACE3
Numero f F#	3.3	3.3	3.3
Numero de canales N	25 x 25	30 x 30	30 x 30
(para un detector con 5000 pixels)	250 x 250	300 x 300	300 x 300
Diametro de apertura D (μm)	70	65.5	68.5
Radio de Curvatura R (μm)	102.4	94.5	119.4
Focal length f (μm)	340	320	320
Pitch de los microlentes P_L (μm)	100	84	84
Diametro de los micro-orificios d (μm)	2.8	2.7	2.7
Indice de refraccion de los microlentes (n_1)	1.4370	1.4370	1.5638
Indice de refraccion de los canales (n_2)	1.5168	1.5168	1.5168
Campo de vision FOV (deg)	19	14.71	14.71
Espesor de las paredes opacas w_{th} (μm)	30	18.5	15.5
Angulo Interommatidial ΔΦ (rad)	0.4718	0.4834	0.4834
Angulo de aceptacion Δφ (rad)	0.673	0.937	0.937
Frecuencia de muestreo ν_s (cycle/rad)	44.27	59.26	59.26

5. Ojo Compuesto de Superposición Artificial ASCE y ASCETL

Los ojos de superposición presentan una mayor sensitividad y tambien una optica mucho mas compleja que los de aposición. Para el diseño de un ojo compuesto de superposición artificial se hicieron diseños ópticos de unos “micro telescopios tipo Kepler” MKT que hacen la función de “ommatidias” o canales independientes. Se utilizó el programa de diseño OSLO, se realizaron las simulaciones y se optimizaron los parámetros de las microlentes para minimizar las aberraciones. Al contar con el diseño preliminar, se utilizó una configuración llamada “Superlente de Gabor” (GSL), la cual establece una relación específica entre los diámetros de las microlentes y las distancias focales de los arreglos donde se encuentran colocadas. La GSL tiene como objetivo, desviar la luz de manera que se enfoque en un solo punto despues de pasar por una serie de arreglos de microlentes logrando aumentar considerablemente la resolución de la imagen formada.

El diseño y la simulación del sistema completo se hizo con el modo no secuencial del programa Zemax. Los diseños propuestos fueron analizados de acuerdo al tamaño y calidad de mancha producida en el detector. La intensidad de la irradiandia medida en watts/cm^2 permitió tener una idea mas clara de la distribución de energía en éstos sistemas.

Para sistemas formadores de imágenes, se hicieron los diseños de un ojo compuesto de superposición artificial con tres arreglos de microlentes sencillas, otro diseño con la configuracion de Gabor y con unos microtripletes en el arreglo de enmedio. Posteriormente, con el fin de lograr un efecto zoom, se diseño un arreglo de microdobletes líquidos sintonizables en el ultimo arreglo de microlentes. Estos dobletes tienen la capacidad de modificar su curvatura al aplicar una diferencia de potencial, lo cual permite cambiar la distancia focal del sistema. Este diseño fue llamado ojo compuesto de superposición artificial con microlentes tunables (ASCETL).

La aplicación práctica de estos sistemas formadores de imágenes, es que las dimensiones de los módulos de cámaras para diversos dispositivos pueden ser todavía mucho mas reducidas, cuentan con una calidad aceptable de imagen, y con la integración de la funcion de zoom, se puede lograr una mejor captura del objeto que se pretende observar. El zoom mecánico añade

muchas complicaciones, por lo cual el zoom óptico presenta una buena alternativa a la miniaturización. En la Fig. 5(a) se muestra un ASCETL capaz de lograr un zoom óptico. En la Fig.5 (b) se observa la mancha registrada en el detector.

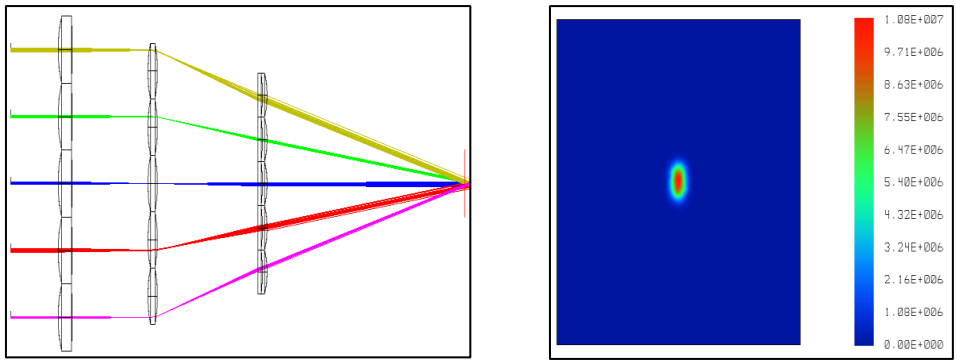

Fig.5: (a) Diseño de un ASCETL con la configuracion de Gabor y con micro'dobletes sintonizables en el tercer arreglo de microlentes (b) Imagen registrada en el detector. La intensidad de la irradiancia esta dada en watts/cm^2.

6. Interconectores opticos no guiados basados en el ojo compuesto de Superposición.

El principio de funcionamiento para la formación de imágenes del ojo de superposición y de la Superlente de Gabor puede tener otras aplicaciones prácticas como lo es el campo de las comunicaciones ópticas. Al realizar los diseños de sistemas ópticos con fuentes coherentes e incoherentes, se planteó la idea de utilizar una segunda SGL revertida, la cual tendría la función de poder recuperar la señal óptica previamente mezclada en una única imagen, en canales independientes. Al desarrollar estas posibilidades se llegó a la aplicación en diversos dispositivos utilizados en el area de comunicaciones como son: multiplexores y demultiplexores. Para lograr una función mas práctica, se introdujo una rejilla de difracción y gracias a esto se logro el diseño de los switches o circuladores y los multiplexores de division de longitud de onda WDM.

Las simulaciones se hicieron en el modo no secuencial de Zemax y el desempeño del sistema se analizó de acuerdo a la distribucion espacial y el registro de intensidad en el detector.La Fig. 6 muestra la configuración básica para un multiplexor y un demultiplexor de señales ópticas utilizando la configuracion de Gabor.

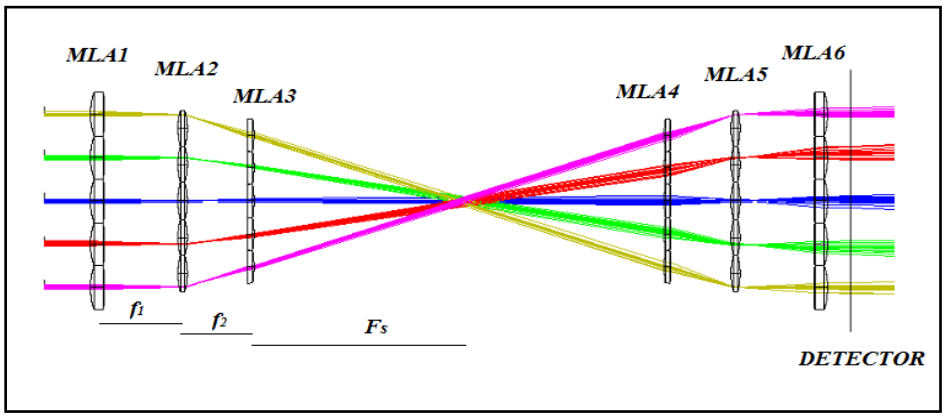

Fig. 6 Multiplexor y demultiplexor a partir de la configuración de superlente de Gabor.

7. Conclusiones

La Biomimetica se ha convertido en una herramienta muy útil para científicos e ingenieros que quieren aplicar los modelos naturales en el desarrollo de nuevas tecnologías.

El uso de los dispositivos miniaturizados ha ido en aumento gracias a la reducción de las dimensiones de los teléfonos celulares y tablets. El módulo de cámara de los teléfonos inteligentes ha causado un cambio en la manera que tenemos de procesar la información. Se espera que la demanda de los consumidores de estos dispositivos siga en aumento en las próximas décadas.

Los ojos compuestos de insectos logran un procesamiento eficiente de la información que rodea a un organismo pequeño sin saturar su sistema nervioso, eficientando volumen y energía. Gracias a este principio, el modelo de los ojos compuestos es útil para mejorar los dispositivos que requieren disminución de tamaño y ahorro de energía.

Los ojos compuestos de aposición tienen muy poca sensitividad, pero permiten lograr una imágen con resolución aceptable y gran campo de visión. El dispositivo AACE permite reducir el espesor del sistema formador de imágenes con respecto a lo previamente diseñado por Duparre y Tanida .

Los ojos compuestos de superposición tienen mejor sensitividad y resolución que los de aposición. El ASCE utiliza el modelo de lente de Gabor, y con la introducción de un arreglo de

microtripletes, se puede mejorar considerablemente la calidad de la imagen producida por el sistema óptico.

La introducción de unos dobletes sintonizables para lograr el modelo de ASCETL, permite cambiar la distancia focal del sistema y lograr un zoom óptico.

Los dispositivos como multiplexores, demultiplexores, switches y multiplexores de division de frente de onda pueden utilizarse para remplazar interconectores guiados con fibra optica. El desempeño de un sistema en comparación al otro puede ser estudiado experimentalmente.

Todos los diseños aquí propuestos pueden ser fabricados con la tecnología actual . En México no se han realizado ninguno de estos prototipos, y cabe mencionar que las aplicaciones de estos sistemas ópticos no convencionales tienen un gran campo no explotado, ya que los ojos compuestos de superposición reflectivos no fueron estudiados en esta tesis. Sus aplicaciones pueden ser muy importantes en otra parte del espectro electromagnético fuera del rango del visible. Otra aplicación pendiente esta en el campo de las celdas fotovoltáicas, las cuales pueden ser miniaturizadas para aumentar la eficiencia de energía producida y volumen.